Systems Biology of Endothelial Mechano-activated Pathways

by

Andrew Jia-An Koo

B.A., Washington University in St. Louis (2006)

Submitted to the Department of Biological Engineering in partial fulfillment of the requirements for the degree of

Doctor of Philosophy

at the

MASSACHUSETS INSTITUTE OF TECHNOLOGY

December 2012

Signature of Author.....
Department of Biological Engineering
Dec 12th, 2012

Certified by.....
C. Forbes Dewey, Jr.
Professor of Mechanical & Biological Engineering
Thesis Supervisor

Certified by.....
Guillermo García-Cardeña
Associate Professor of Pathology
Harvard Medical School
Thesis Supervisor

Accepted by.....
Forest White
Associate Professor of Biological Engineering
Chair, Biological Engineering Graduate Program Committee

This doctoral thesis has been examined by a Committee of the Department of Biological Engineering as follows:

Professor Alan J. Grodzinsky.....
Professor of Biological, Electrical, and Mechanical Engineering
Massachusetts Institute of Technology
Committee Chair

Professor C. Forbes Dewey, Jr.....
Professor of Biological and Mechanical Engineering
Massachusetts Institute of Technology
Thesis Supervisor

Professor Guillermo García-Cardeña.....
Associate Professor of Pathology
Harvard Medical School
Thesis Supervisor

Thesis Defense Date: November 20th, 2012.

To my dear parents

Systems Biology of the Endothelial Mechano-activated Pathways

Multiple signaling pathways are employed by endothelial cells to differentially respond to distinct hemodynamic environments and acquire functional phenotypes, including regulation of inflammation, angiogenesis, blood coagulation, and the vascular tone. In order to understand how these pathways interact, this thesis applies a systems biology approach through a two-step process. First, we constructed an integrated mathematical model for shear-stress-induced nitric oxide (NO) production to assemble the current understanding of this signaling system. Second, we conducted experiments to define how shear stress dynamically modulates the expression of components of the endothelial glycocalyx, a mechanosensor that regulates shear-stress-dependent NO production.

Nitric oxide produced by vascular endothelial cells is an anti-inflammatory mediator and a potent vasodilator. In order to understand the rich diversity of responses observed experimentally in endothelial cells exposed to shear stress, we assembled four quantitative molecular pathways previously defined for shear-stress-induced NO production. In these pathways, endothelial nitric oxide synthase (eNOS) is activated (a) via calcium release, (b) via phosphorylation reactions, and (c) via enhanced protein expression. To these pathways we added (d) an additional pathway describing the actual NO production from the interactions of eNOS with its various protein partners. These pathways were then combined and simulated. The integrated model is able to describe the experimentally observed change in NO production with time following the application of fluid shear stress, and to predict the specific effects to the system following interventional pharmacological or genetic changes. Importantly, this model reflects the up-to-date understanding of the NO system and provides a platform to aggregate information in an additive way.

The endothelial glycocalyx is a glycosaminoglycan layer located on the apical surface of vascular endothelial cells. Previous studies have documented a strong correlation between the glycocalyx expression, local hemodynamic environment, and atheroprotection. Based on these observations, we hypothesized that the expression of components of the endothelial glycocalyx is differentially regulated by distinct hemodynamic environments. In order to test this hypothesis, human endothelial cells were exposed to shear stress waveforms characteristic of atherosclerosis-resistant or atherosclerosis-susceptible regions of the human carotid, and the expression of several components of the glycocalyx was then assessed. Interestingly, we found that heparan sulfate expression is higher and evenly distributed on the apical surface of endothelial cells exposed to the atheroprotective waveform, and is irregularly present in cells exposed to the atheroprone waveform. Furthermore, the expression of a heparan sulfate proteoglycan, syndecan-1, is also differentially regulated by the two waveforms, and its suppression mutes the atheroprotective-flow-induced cell surface expression of heparan sulfate. Collectively, these data links distinct hemodynamic environments to the differential expression of critical components of the endothelial glycocalyx.

Taken together, these projects present in this doctoral thesis increase our understanding of endothelial mechano-activated pathways, and have demonstrated how we could use systems biology approach to unravel complex biological problems.

Thesis Supervisors: C. Forbes Dewey, Jr. & Guillermo García-Cardeña

Acknowledgments

My sincere appreciation to Prof. C. Forbes Dewey, Jr., who brought me to the lab and introduced me to the field of biomechanics and systems biology. He is the kindest and the gentlest person I have known in my life. His continuous encouragement is one of the main forces that propel me through graduate school. This thesis cannot be completed without his guidance, support, and enthusiasm.

I wish to thank Prof. Guillermo García-Cardeña for teaching me all aspects of biomedical research from how to do a western blot, how to think about research, how to make a good presentation, to how to write a decent paper. Most importantly, he taught me the attitude to work everything until perfection.

Tremendous thanks for people who advised me and helped me on this project: my thesis committee chair Prof. Alan Grodzinsky; members from the two labs, Luigi Adamo, Louie Villarreal, Will Adams, Yuzhi Zhang, Hiroshi Kohara, Alexis Turjman, Renato Umeton, Beracah Yankama, David Nordsletten, and Lujie Chen.

I would like to thank the great teachers I had in my childhood and teenage years: Mr. Liu (劉兆文), who encouraged me to think big and do great things; Mrs. Lin (林怡菁), who taught me to always maintain a positive attitude; and Ms. Liu (劉翠華), who inspired my interest in biology.

I am very grateful to the teaching of Prof. Daniel Kohl and Dr. Georgia Shearer, my undergraduate research mentors who introduced me to biological research. They made me see the fun of working in a bio lab!

Special thanks to my friends: Hung-An Chang, Hank Chu, Jen Lee, Ming Yang, and Jiening Zhan. Thank you for helping me enduring through all the ups and downs of graduate school!

Bringing up three boys is not easy. I realized in graduate school that doing this while being a university faculty is even harder. No words can express my gratitude toward my parents. Though they are always busy with work, they still spent much effort leading my brothers and I to the right path. They also encouraged me to study abroad in the United States to pursue a brighter future. This thesis is dedicated to my parents: Dr. Ming-Ru Liu and Dr. Chun-Hao Koo.

Content

Chapter 1: Introduction

1.1 Background and Scope

The vascular endothelium is a thin layer of cells that line the interior surface of blood vessels. The endothelium serves as an interface between bloods and surrounding tissues and plays multiple roles in inflammation, angiogenesis, blood coagulation, and control of vascular tone. Though the endothelium has long been discovered in the 19th century, its function has not been understood until the recent decades. In 1973, scientists were able to culture endothelial cells *in vitro* and begin to study its various properties (34). One of the most interesting observations was its ability to respond to flow: the cultured endothelial cells are able to align to the direction of the flow, suggesting that there are mechanisms for the cells to sense the local hemodynamic environment (13). In the 1990s and 2000s, with the advancement of molecular biology techniques, many of the mechano-sensors and mechanotransduction signaling pathways have been identified (34). Scientists have found mechano-sensors, including trans-membrane proteins and ion channels, on both the apical surface and basolateral surface of the endothelial cells. Upon exposure to specific shear stress waveforms, some transmembrane proteins can transmit the force to other intracellular proteins through the mutually connected cytoskeleton, and others can directly convert the mechanical force to biochemical signals, activating multiple cell-signaling pathways (10). As a result, the endothelial cells increase surface expression of thrombomodulin and decrease surface expression of cell adhesion molecules, leading to the antithrombotic phenotype and anti-inflammatory phenotype. The flow also triggers the endothelial cells to produce nitric oxide (NO), a molecule that can diffuse to smooth muscle cells and lead to vasodilation.

Shear-stress-induced NO production is complexly regulated by multiple pathways. These pathways were studied one at a time and few researchers have analyzed how pathways interact with each other. This is partially due to the fact that in biomedical research, the classical hypothesis driven approach looks into just one factor at a time, making it rigorous but inefficient in dissecting a multi-factor system. To resolve this inefficiency, researchers have developed the systems biology approach. In the systems biology approach (see Fig. 1-1), quantitative mathematical models are constructed based on existing experimental data. The system model reflects the current understanding of the biological system interested and provides a platform for

integrating new information. From analyzing the model structure and simulation data, researchers gain additional biological insight to the system and identify deficiencies that require more understanding. They can then propose new hypothesis and design new experiments, where its data can be used to further improve the model.

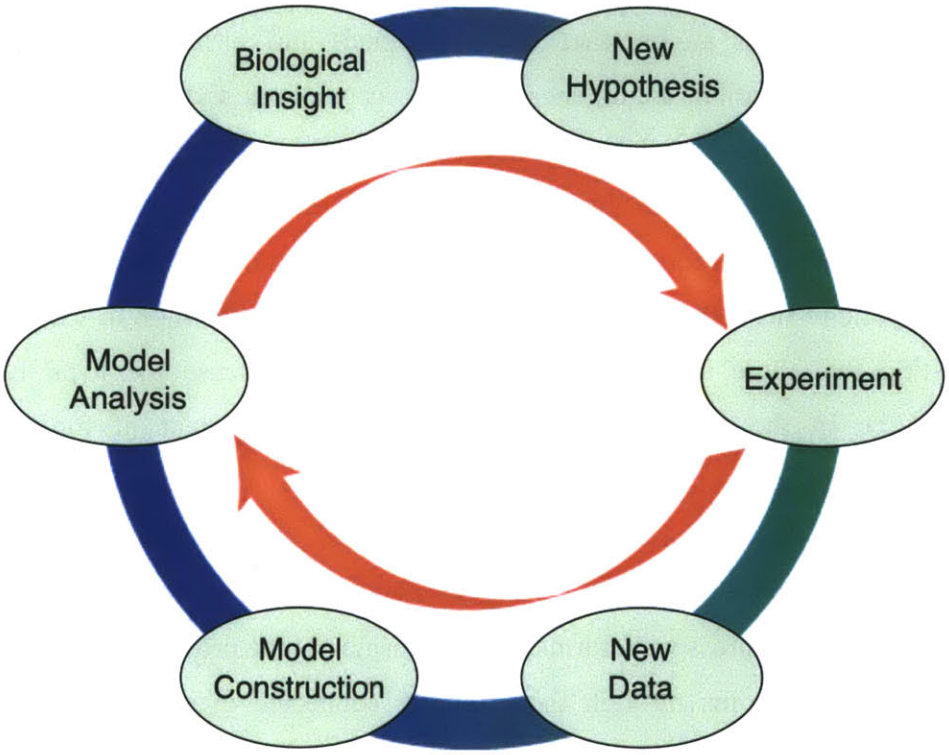

Fig. 1-1. The systems biology approach (figure adapted from http://www.doc.ic.ac.uk/bioinformatics/CISB).

In this thesis, we employ this systems biology approach to study the shear-stress-induced NO production in endothelial cells. We incorporate all previously known pathways to construct the NO model **(Chapter 2)**. We also describe experiments on the endothelial glycocalyx, a glycosaminoglycan layer that has been shown to be a mechanosensor for NO production, seeking to understand how distinct shear stress waveform regulate its expression **(Chapter 3)** and how the glycocalyx might lead to atheroprotection and NO production **(Chapter 4)**. Finally, we conclude on our studies and discuss the future directions **(Chapter 5)**.

The following sections of this chapter provide reviews of the history and findings of the endothelium and the endothelial glycocalyx layer.

1.2 The Endothelium

1.2.1 A Brief History of the Endothelium

Discovery of the Endothelium

In 1852, Dr. Henry Hyde Salter just completed his medical training at King's College and decided to join Charing Cross Hospital, working as a lecturer in the department of physiology and pathology under Prof. Robert Bently Todd. Todd, partnered with Sir William Bowman, who Bowman's capsule is name after, was working on his two finest work: *The Cyclopaedia of Anatomy and Physiology*, and *Physiological Anatomy and Physiology of Man.* Salter joined their endeavor and assisted the two in completing their projects, which includes isolation of the epithelial particles, later known as the endothelium, from the aorta of an ox and a horse (Fig. 1-2). The work is later published in the second volume of the *Physiological Anatomy and Physiology of Man* in 1856. In the book, the epithelial particles were described: "[t]he long axis of each of these particles is parallel to that of the vessel. They are pointed, or, as it were, drawn out at their extremities…they are sometimes elongated into fusiform fibres. They are remarkable for the large size and the distinctness of their nuclei which are often visible when the cell wall cannot be detected. (41)" Salter later became an expert of asthma, a disease he had suffered since childhood, and is the author of the 19th century's best asthma textbook, "*On Asthman: Its Pathology and Treatment. (38)*" Through the effort of Salter, Todd, and Bowman, histologists began to study the mysterious "epithelial particles."

A

Dr. Henry Hyde Salter
(1823 - 71)

Sir Robert Bentley Todd
(1809 - 60)

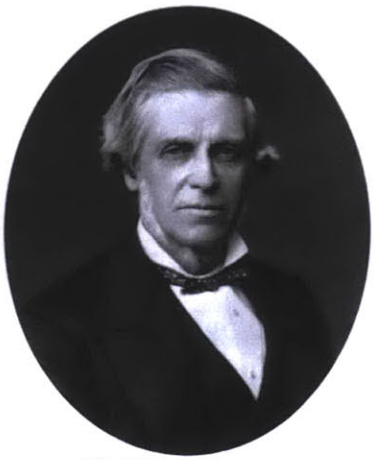

Sir William Bowman
(1816 - 92)

B

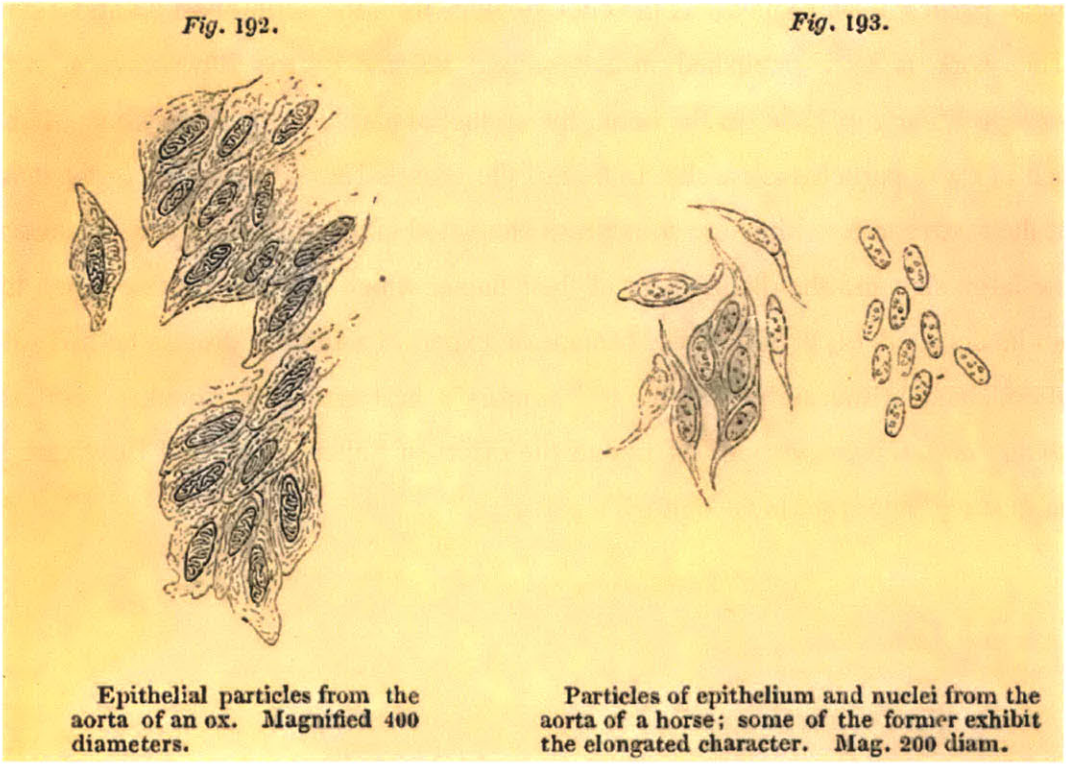

Fig. 1-2. A) The three pioneers who defined the "epithelial particles." (Photo of HHS is from (38); photos of RBT and WB are expired copyright images downloaded from wikipedia) B) The very first documentation of the endothelium (figure adapted from (41)).

Naming of the Endothelium

The term "endothelium" was first introduced by Wilhelm His, Sr. in 1865 (27). He reasoned that even though endothelium and epithelium are both a layer of cells lining a tissue, the developmental origin of the two are quite different. The epithelium arises from all three germ layers: ectoderm, endoderm, and mesoderm; whereas the endothelium is only derived from the mesoderm. Usage of the word "endothelium" leads to some controversy in the 1870s due to etymological and physiological reasons. Dr. Michael Foster argued that since epithelium means "that which covers or is upon a papilla," consequently the endothelium means "that which is inside a papilla," making little sense (18). Dr. Foster also further questioned His' view that the epithelium and endothelium come from distinct origins. Dr. Cavafy, a supporter of the term endothelium, made a counter argument stating that the prefix, "endo-", means *internal* rather than *inside* (6). Therefore, the term endothelium suggests "an internal skin formation of an animal". Dr. Cavafy also emphasized the characteristic difference between the endothelium and the epithelium: the endothelium has a close relationship to the connective tissue, and never form glands nor secrete; whereas the epithelium has no relationship with the connective tissue, and is almost always observed with gland formation and secretion. Nevertheless, to Dr. Foster's dismay, the term "endothelium" is still used until now to define the thin layer of cells that lines the interior surface of blood vessels.

Though the endothelium were discovered in the middle of the 19^{th} century, relatively little was known about the important functions of this monolayer until almost a century later, when the human vascular endothelial cells were successfully cultured in the early 1970s, and thus commence the field of vascular biology.

The Era of Vascular Biology

Dr. Michael A. Gimbrone, Jr., then a Post-doc under Dr. Judah Folkman in 1973, was among the first group of scientists who successfully cultured human endothelial cells from umbilical cord veins (22, 23). Since then, the number of publications studying vascular biology using *in vitro* cultured endothelial cells has experienced great growth. Two years after reporting the successful culture of endothelial cells, Gimbrone and Alexander, who met each other in a poker game at NIH (personal communication with Dr. Gimbrone), demonstrated endothelial cells as a primary

source for production of prostaglandin (21), a family of lipid compounds particularly important in regulation of vascular permeability, vasodilation, and platelet aggregation. One year later in 1976, a research group led by Sir Salvador Moncada and Nobel Laureate Sir John Vane isolated the most potent form of prostaglandin, prostacyclin (PGI_2) (33). In 1980, Furchgott *et al.* further demonstrated the importance of the endothelium by showing that its presence is necessary for acetylcholine-induced relaxation of smooth muscle cells (19). Later effort by Furchgott and Moncada *et al.* identified nitric oxide to be the key vasodilator released by endothelial cells to account for the previous observation (35, 37).

The Endothelial Cells and the Flow

While these progress in endothelial biology was being made, Dr. C. Forbes Dewey, Jr. revolutionize this field in 1981 by combining biology with mechanics, constructing the first cone-plate shear stress apparatus to expose the endothelial cells to flow (13). It was found that the cells are able to respond to flow and align to the direction of the flow. In 1986, Peter Davies *et al.* further applied the cells to various laminar or turbulent shear stress waveforms, and demonstrated turbulent flow characteristic of the atheroprone region of the vasculature may induce cell turnover (11). Since the invention of the *in vitro* flow system, thousands of studies have been made researching on how endothelial cells respond to flow and what is the underlying mechanotransduction mechanisms behind this process.

Endothelial Dysfunction and Atherosclerosis

By the late 1980s, researchers started to realize the importance of a healthy endothelium toward protection against vascular diseases. Endothelial dysfunction, the state in which the endothelial cells can no longer respond to external stimuli to preserve homeostasis, is frequently followed by deterioration of vascular health and development of several pathologies including atherosclerosis (20). One of the early sign of atherogenesis is leukocyte adhesion to the endothelium. In 1897 and 1991, E-selectin and VCAM-1 were identified by Bevilacqua et al. and Cybulsky et al., respectively, to be some of the most important cell adhesion molecules on top of the endothelial apical surface (4, 8). The functions and mechanisms of how these cell adhesion molecules respond to inflammatory stimuli, such as oxidized-LDL or IL-1β, was extensively studied (31,

49). Due to these research efforts, novel therapies were discovered to decrease the risk of atherogenesis. One of these drugs is statin, an HMG Co-A reductase inhibitor which leads to a lower LDL level. Statins were tested among patients with coronary-artery disease in the early 1990s (42) and became the billion-dollar blockbuster Lipitor. Now in the 21st century, continuous effort is being made to understand the various aspect of the endothelium in hope to find innovative therapies for cardiovascular diseases.

1.2.2 Structure and Properties of the Endothelium

The endothelium consists of endothelial cells that are around 30 micron long, 10 micron wide, and 0.2 – 3 micron thick. The endothelium in adult human is only about 0.2% of total body mass but its total area is approximately three quarter of a basketball court. This thin but important layer is responsible for many vascular functions, including:

- **Barrier function**: The endothelium selectively filters or facilitates the transport of ions and macromolecules from the vascular lumen to surrounding tissues (30).
- **Anti-thrombotic**: The endothelium produces factors that inhibit the coagulation cascade. It also releases prostacyclin and nitric oxide to prevent platelet activation (9).
- **Inflammation**: The endothelium binds to the inflammatory cytokines and increases expression of the cell adhesion molecules, which leads to leukocyte adhesion and transmigration (29).
- **Angiogenesis**: The endothelium responds to angiogenic growth factors and releases proteases, degrading the basement membrane to initiate sprouting (5).
- **Vasodilation**: The endothelium produces nitric oxide in response to shear stress stimuli. Nitric oxide diffuses to the smooth muscle cells and leads to vasodilation (28).

Recent studies have demonstrated that the integrity of a glycosaminoglycan layer, or the glycocalyx, on the apical surface of the endothelium is critical for many of the above-mentioned endothelial functions (39). In chapter 3, we will discuss on several key topics of the glycocalyx, including how distinct shear stress waveform leads to the expression of components of the endothelial glycocalxy layer, and how this layer might lead to protection against atherosclerosis.

1.3 The Glycocalyx

1.3.1 A Brief History of the Glycocalyx

In 1957, Dyrbye and Kirk isolated mucopolysaccharide from human aortic tissue at Washington University (14), my alma mater. Through paper electrophoresis and enzymatic method, they have identified three major components constituting the polysaccharide. The first component was chondroitin sulfate; the second one was a substrate of hyaluronidase - the hyaluronic acid; and the third one is a sulfated component containing both galactosamine and glucosamine - the heparan sulfate. Few years later in 1963, the extracellular polysaccharide coating existed in many cell types are name the glycocalyx by H. Stanley Bennett from the University of Chicago (2). Due to the fixation method used at that time, the endothelial glycocalyx was destroyed and thus not observed, and the glycocalyx isolated from aortic tissue was thought mainly located at the intercellular space between the endothelial cells and the smooth muscle cells.

1.3.2 Observation and Measurement of the Glycocalyx

In the 1990s, Vink and Duling used intravital microscopy to observe red blood cells (RBC) going through the hamster cremaster muscle capillaries. Interestingly, the width of the capillary occupied by the RBC and FITC-dextran were significantly smaller than the anatomic capillary diameter, and treatment of the capillary with oxygen radicals increased the RBC and FITC-dextran column (46). These data suggest there is a thin surface coating on top of the endothelium (Fig. 1-3). Due to the fragile nature of the glycocalyx, scientists were not able to have a good view of this thin layer until 2006, when van den Berg *et al.* perfected the sample preparation protocol for electron microscopy and visualized the 0.4 – 0.5 μm bush-like glycocalyx structure (Fig. 1-4) (24, 43). Besides intravital microscopy and electron microscopy, researchers have also attempted to use other techniques to measure the thickness of the glycocalyx. These techniques include microparticle image velocimetry, two-photon laser scanning microscopy, and confocal laser scanning microscopy. These data suggest the glycocalyx thickness *in vivo* or *ex vitro* are in the range of 0.02 – 4.5 μm, depending on the measurement method and vessel origin (15).

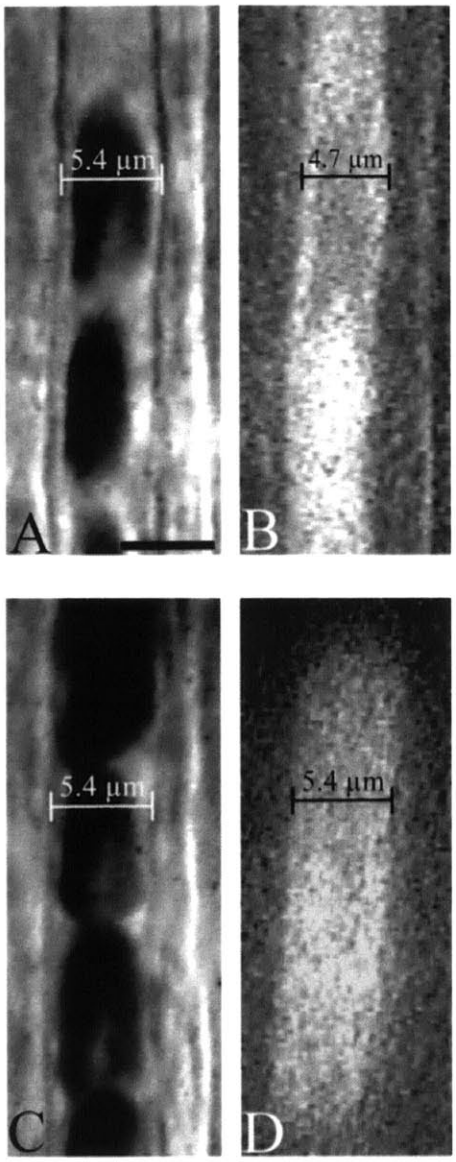

"Light-dye treatment increased capillary tube hematocrit by 60% in 40-µm-long capillary segments compared with untreated sites in the same capillaries. It is concluded that the wall of skeletal muscle capillaries is decorated with a 0.4- to 0.5-µm-thick endothelial surface coat, which may represent the true active interface between blood and the capillary wall."

- Vink & Duling

Fig. 1-3. The width of A) RBC and B) FITC-dextran were significantly smaller than tha antomic capillary diameter. Width of C) RBC and D) FITC-dextran after light-dye (oxygen radical) treatment (46).

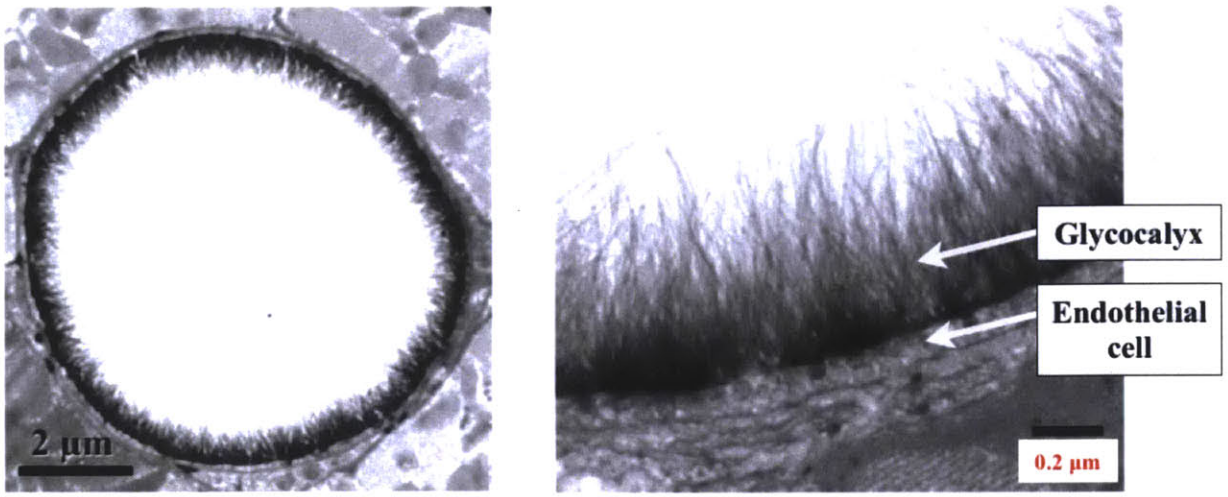

Fig. 1-4. Electron microscopy images of goat capillary glycocalyx (figures adapted from (24)).

1.3.3 Structure of the Endothelial Glycoclayx

In the past decade, components of the endothelial glycocalyx have been identified (Fig. 1-5). The glycocalyx is mainly composed of several transmembrae proteins and three glycosaminoglycans (GAGs): heparan sulfate, chondroitin sulfate, and hyaluronic acid. Heparan-sulfate is attached to proteoglycans such as syndecans and glypicans; chondroitin sulfate is present on top of syndecans; and hyaluronic acid binds to protein receptor CD44 (39). The heparan sulfate and chondroitin sulfate are added to their anchored proteins in the Golgi. Heparan sulfate chain biosynthesis is a process involving multiple steps: First, a series of saccharides (N-acetylglucosaimne – glucuronic acid – galactose – galactose – xylose) are added onto the serine residue of the extracellular domain of syndecan or glypicans. Next, the elongation process starts with the heparin polymerization reaction conducted by glycosyltransferase I, a protein dimer of exostosin-1 (EXT1) and exostosin-2 (EXT2). Finally the elongated chain is deacetylated and sulfated by N-deacetylase/N-sulfotransferase (NDST). Chondroitin sulfate biosynthesis occurs in a highly similar manner, except that the chondroitin polymerization step is catalyzed by chondrotinsulfate synthase 1/3 (CHSY1/3) and the sulfation process is carried out by chondroitin sulfotransferase (CHST) family proteins. In contrast, hyaluronic acid is synthesized at the plasma membrane by three hyaluronan synthase isoforms (HAS1, HAS2, and HAS3). The long

hyaluronic acid chain produced at the membrane is released to the extracellular space and bound to hyaluronic acid binding protein - CD44.

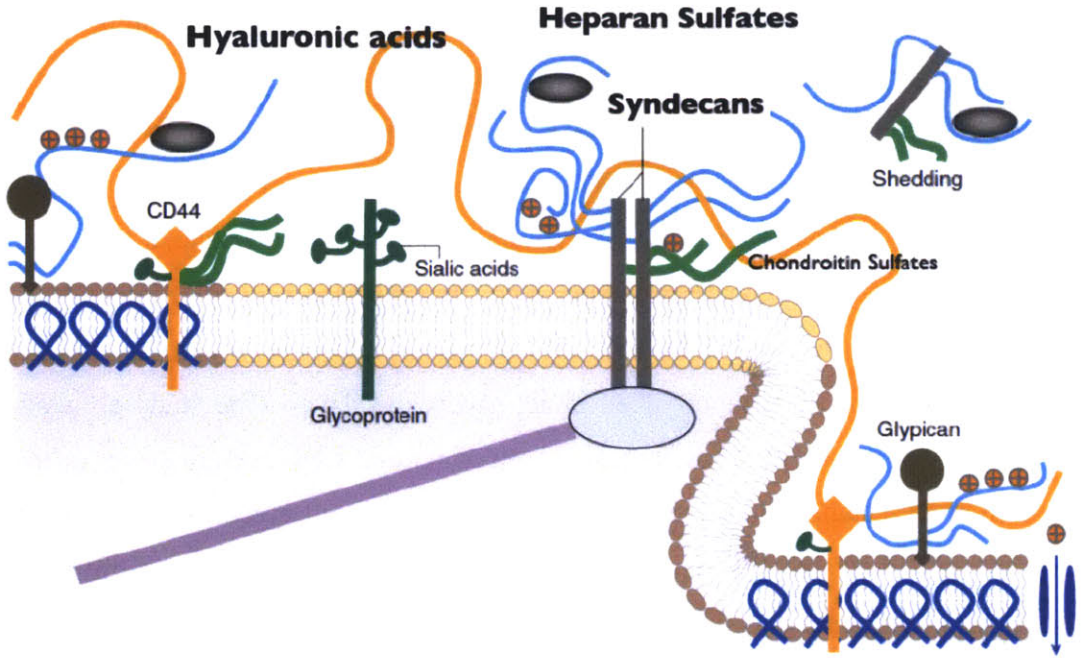

Fig. 1-5. Structure of the endothelial glycocalyx layer (figure adapted from (39)).

1.3.4 Functions of the Endothelial Glycocalyx

Scientists have identified many functions of the glycocalyx. Several key functions are listed below:

- Increase resistance to blood flow and decrease capillary hematocrits: the glycocalyx acts as an interactive surface between blood and the vessel wall (12, 36)
- Associate or permeate ions, amino acids, macromolecules selectively based on size and charge: the glycocalyx can directly bind to some biomolecules and increase their local concentration, and can also selectively block some other biomolecules and prevent them from reaching the endothelial surface (3, 26).
- Remove oxygen-derived free radicals from the blood: the negatively charged heparan sulfate binds tightly with a positively charged domain of the extracellular superoxide dismutase, a radical scavenger, thus reducing the oxidative stress to the endothelium (1).

- Act as a protection layer against leukocyte adhesion: enzymatic removal of heparan sulfate in mouse cremaster venules induces leukocyte adhesion (7).
- Conduct mechanotransduction: flow-mediated responses such as cell alignment, cytoskeleton reorganization, proliferation regulation, and NO production are impaired when component of the glycocalyx is degraded (17, 25, 32, 40, 48).

Studies from syndecan-1 and syndecan-4 knocked-out mice showed that these mice are healthy and fertile under normal condition. However, syndecan-4 K.O. mice were observed with delayed wound healing and impaired angiogenesis after injury (16), and syndecan-1 K.O. mice were observed with enhanced leukocyte adhesion and transmigration after induced myocardial infarction by permanent ligation of the left coronary artery (45). Several researches have also demonstrated the clinical importance of an intact glycocalyx layer. One study showed that an impaired glycocalyx layer is associated with enhanced intimal LDL accumulation in mice (44). Another recent study established a correlation between a damaged glycocalyx and renal disease patients undergoing dialysis (47). The importance of an abundantly and uniformly expressed glycocalyx layer is further discussed in Chapter 3. In the next chapter, we will continue with the original motivation to study the glycocalxy pathway – understanding the shear-stress-induced NO production system.

1.4 References

1. **Abrahamsson T, Brandt U, Marklund SL, and Sjoqvist PO.** Vascular bound recombinant extracellular superoxide dismutase type C protects against the detrimental effects of superoxide radicals on endothelium-dependent arterial relaxation. *Circ Res* 70: 264-271, 1992.
2. **Bennett HS.** Morphological aspects of extracellular polysaccharides. *Journal of Histochemistry & Cytochemistry* 11: 10, 1963.
3. **Bernfield M, Götte M, Park PW, Reizes O, Fitzgerald ML, Lincecum J, and Zako M.** Functions of cell surface heparan sulfate proteoglycans. *Annu Rev Biochem* 68: 729-777, 1999.
4. **Bevilacqua MP, Pober JS, Mendrick DL, Cotran RS, and Gimbrone MA, Jr.** Identification of an inducible endothelial-leukocyte adhesion molecule. *Proc Natl Acad Sci U S A* 84: 9238-9242, 1987.
5. **Carmeliet P.** Mechanisms of angiogenesis and arteriogenesis. *Nat Med* 6: 389-395, 2000.
6. **Cavafy J.** A note on endothelium. *Quarterly Journal of Microscopical Science* s2: 4, 1874.
7. **Constantinescu AA, Vink H, and Spaan JA.** Endothelial cell glycocalyx modulates immobilization of leukocytes at the endothelial surface. *Arterioscler Thromb Vasc Biol* 23: 1541-1547, 2003.
8. **Cybulsky MI, and Gimbrone MA, Jr.** Endothelial expression of a mononuclear leukocyte adhesion molecule during atherogenesis. *Science* 251: 788-791, 1991.
9. **Dahlbäck B.** Blood coagulation. *Lancet* 355: 1627-1632, 2000.
10. **Davies PF.** Flow-mediated endothelial mechanotransduction. *Physiol Rev* 75: 519-560, 1995.
11. **Davies PF, Remuzzi A, Gordon EJ, Dewey CF, Jr., and Gimbrone MA, Jr.** Turbulent fluid shear stress induces vascular endothelial cell turnover in vitro. *Proc Natl Acad Sci U S A* 83: 2114-2117, 1986.
12. **Desjardins C, and Duling BR.** Heparinase treatment suggests a role for the endothelial cell glycocalyx in regulation of capillary hematocrit. *Am J Physiol* 258: H647-654, 1990.
13. **Dewey CF, Bussolari SR, Gimbrone MA, and Davies PF.** The dynamic response of vascular endothelial cells to fluid shear stress. *J Biomech Eng* 103: 177-185, 1981.
14. **Dyrbye M, and Kirk JE.** Mucopolysaccharides of human arterial tissue. I. Isolation of mucopolysaccharide material. *J Gerontol* 12: 20-22, 1957.
15. **Ebong EE, Macaluso FP, Spray DC, and Tarbell JM.** Imaging the endothelial glycocalyx in vitro by rapid freezing/freeze substitution transmission electron microscopy. *Arterioscler Thromb Vasc Biol* 31: 1908-1915, 2011.
16. **Echtermeyer F, Streit M, Wilcox-Adelman S, Saoncella S, Denhez F, Detmar M, and Goetinck P.** Delayed wound repair and impaired angiogenesis in mice lacking syndecan-4. *J Clin Invest* 107: R9-R14, 2001.
17. **Florian JA, Kosky JR, Ainslie K, Pang Z, Dull RO, and Tarbell JM.** Heparan sulfate proteoglycan is a mechanosensor on endothelial cells. *Circ Res* 93: e136-142, 2003.
18. **Foster M.** Memoirs: On the Term Endothelium. *Quarterly Journal of Microscopical Science* s2: 5, 1874.
19. **Furchgott RF, and Zawadzki JV.** The obligatory role of endothelial cells in the relaxation of arterial smooth muscle by acetylcholine. *Nature* 288: 373-376, 1980.
20. **Gimbrone MA, Jr.** Endothelial dysfunction and atherosclerosis. *J Card Surg* 4: 180-183, 1989.
21. **Gimbrone MA, Jr., and Alexander RW.** Angiotensin II stimulation of prostaglandin production in cultured human vascular endothelium. *Science* 189: 219-220, 1975.
22. **Gimbrone MA, Jr., Cotran RS, and Folkman J.** Endothelial regeneration: studies with human endothelial cells in culture. *Ser Haematol* 6: 453-455, 1973.
23. **Gimbrone MA, Jr., Cotran RS, and Folkman J.** Human vascular endothelial cells in culture. Growth and DNA synthesis. *J Cell Biol* 60: 673-684, 1974.
24. **Gouverneur M, Spaan JA, Pannekoek H, Fontijn RD, and Vink H.** Fluid shear stress stimulates incorporation of hyaluronan into endothelial cell glycocalyx. *Am J Physiol Heart Circ Physiol* 290: H458-452, 2006.
25. **Hecker M, Mulsch A, Bassenge E, and Busse R.** Vasoconstriction and increased flow: two principal mechanisms of shear stress-dependent endothelial autacoid release. *Am J Physiol* 265: H828-833, 1993.
26. **Henry CB, and Duling BR.** TNF-alpha increases entry of macromolecules into luminal endothelial cell glycocalyx. *Am J Physiol Heart Circ Physiol* 279: H2815-2823, 2000.
27. **His W.** *Die Häute und Höhlen des Körpers: Academisches Programm.* Schweighauser, 1865.
28. **Luscher TF, Richard V, Tschudi M, Yang ZH, and Boulanger C.** Endothelial control of vascular tone in large and small coronary arteries. *J Am Coll Cardiol* 15: 519-527, 1990.

29. **Luscinskas FW, and Gimbrone MA**. Endothelial-dependent mechanisms in chronic inflammatory leukocyte recruitment. *Annu Rev Med* 47: 413-421, 1996.
30. **Malik AB, Lynch JJ, and Cooper JA**. Endothelial barrier function. *J Invest Dermatol* 93: 62S-67S, 1989.
31. **Marui N, Offermann MK, Swerlick R, Kunsch C, Rosen CA, Ahmad M, Alexander RW, and Medford RM**. Vascular cell adhesion molecule-1 (VCAM-1) gene transcription and expression are regulated through an antioxidant-sensitive mechanism in human vascular endothelial cells. *J Clin Invest* 92: 1866-1874, 1993.
32. **Mochizuki S, Vink H, Hiramatsu O, Kajita T, Shigeto F, Spaan JA, and Kajiya F**. Role of hyaluronic acid glycosaminoglycans in shear-induced endothelium-derived nitric oxide release. *Am J Physiol Heart Circ Physiol* 285: H722-726, 2003.
33. **Moncada S, Gryglewski R, Bunting S, and Vane JR**. An enzyme isolated from arteries transforms prostaglandin endoperoxides to an unstable substance that inhibits platelet aggregation. *Nature* 263: 663-665, 1976.
34. **Nachman RL, and Jaffe EA**. Endothelial cell culture: beginnings of modern vascular biology. *J Clin Invest* 114: 1037-1040, 2004.
35. **Palmer RM, Ferrige AG, and Moncada S**. Nitric oxide release accounts for the biological activity of endothelium-derived relaxing factor. *Nature* 327: 524-526, 1987.
36. **Pries AR, Secomb TW, Gessner T, Sperandio MB, Gross JF, and Gaehtgens P**. Resistance to blood flow in microvessels in vivo. *Circ Res* 75: 904-915, 1994.
37. **Rees DD, Palmer RM, and Moncada S**. Role of endothelium-derived nitric oxide in the regulation of blood pressure. *Proc Natl Acad Sci U S A* 86: 3375-3378, 1989.
38. **Sakula A**. Henry Hyde Salter (1823-71): a biographical sketch. *Thorax* 40: 887-888, 1985.
39. **Tarbell JM, and Pahakis MY**. Mechanotransduction and the glycocalyx. *J Intern Med* 259: 339-350, 2006.
40. **Thi MM, Tarbell JM, Weinbaum S, and Spray DC**. The role of the glycocalyx in reorganization of the actin cytoskeleton under fluid shear stress: a "bumper-car" model. *Proc Natl Acad Sci USA* 101: 16483-16488, 2004.
41. **Todd RB, and Bowman W**. *The physiological anatomy and physiology of man.* London: J.W. Parker, 1845.
42. **Treasure CB, Klein JL, Weintraub WS, Talley JD, Stillabower ME, Kosinski AS, Zhang J, Boccuzzi SJ, Cedarholm JC, and Alexander RW**. Beneficial effects of cholesterol-lowering therapy on the coronary endothelium in patients with coronary artery disease. *N Engl J Med* 332: 481-487, 1995.
43. **van den Berg BM, Spaan JA, Rolf TM, and Vink H**. Atherogenic region and diet diminish glycocalyx dimension and increase intima-to-media ratios at murine carotid artery bifurcation. *Am J Physiol Heart Circ Physiol* 290: H915-920, 2006.
44. **van den Berg BM, Spaan JA, and Vink H**. Impaired glycocalyx barrier properties contribute to enhanced intimal low-density lipoprotein accumulation at the carotid artery bifurcation in mice. *Pflugers Arch* 457: 1199-1206, 2009.
45. **Vanhoutte D, Schellings MW, Gotte M, Swinnen M, Herias V, Wild MK, Vestweber D, Chorianopoulos E, Cortes V, Rigotti A, Stepp MA, Van de Werf F, Carmeliet P, Pinto YM, and Heymans S**. Increased expression of syndecan-1 protects against cardiac dilatation and dysfunction after myocardial infarction. *Circulation* 115: 475-482, 2007.
46. **Vink H, and Duling BR**. Identification of distinct luminal domains for macromolecules, erythrocytes, and leukocytes within mammalian capillaries. *Circ Res* 79: 581-589, 1996.
47. **Vlahu CA, Lemkes BA, Struijk DG, Koopman MG, Krediet RT, and Vink H**. Damage of the endothelial glycocalyx in dialysis patients. *J Am Soc Nephrol* 23: 1900-1908, 2012.
48. **Yao Y, Rabodzey A, and Dewey CF**. Glycocalyx modulates the motility and proliferative response of vascular endothelium to fluid shear stress. *Am J Physiol Heart Circ Physiol* 293: H1023-1030, 2007.
49. **Yoshida M, Westlin WF, Wang N, Ingber DE, Rosenzweig A, Resnick N, and Gimbrone MA, Jr.** Leukocyte adhesion to vascular endothelium induces E-selectin linkage to the actin cytoskeleton. *J Cell Biol* 133: 445-455, 1996.

Chapter 2: *In silico* Modeling of Shear-stress-induced Nitric Oxide Production in Endothelial Cells

2.1 Introduction

One of the most important functions of vascular endothelial cells is to produce nitric oxide (NO). This molecule has a number of different roles in vascular stasis, including acting as a potent vasodilator and a mediator of inflammation (40). Not surprisingly, human vascular endothelial cells have developed multiple pathways by which production of NO is regulated by humoral and biomechnical stimuli via the expression and activation of endothelial nitric oxide synthase (eNOS). Exploring these different pathways one at a time is difficult because the system is not separable - multiple pathways contribute to the production rate under all physiological circumstances. In order to understand and model the rich diversity of responses that have been observed experimentally, it is necessary to account for an ensemble of these pathways acting simultaneously over an extended range of time scales.

The advancements of modern biology and computer science have increasingly enabled researchers to build such multi-pathway models. In the past two decades, experiments have been conducted which provide quantitative information between molecular species in the cell and their evolution under specific stimuli, facilitating construction of quantitative biochemical pathways that may be used as predictors of cellular response under a wider range of physiological or pathophysiological conditions. This sort of quantitative analysis of molecular pathways provides a valuable tool for assessing biological mechanisms and validating hypothetical mechanisms by comparing simulation results with experimental data.

One of the major hurdles in this process has been the development of *in silico* models sufficiently detailed to describe the complex phenomena observed. The current state-of-the-art is to construct quantitative models based on selected sub-paths within a larger molecular pathway. This process is time consuming, requiring in-depth literature searches, experimentation, and parameter estimation. These isolated sub-path models are invaluable and often provide insight into specific biochemical mechanisms. However, these sub-pathway models are often not independent *in vivo* nor *in vitro*, and have cross-sensitivities due to common species and overlapping reactions. As a result, to address more complex questions, such as the evolution of

NO under mechanical shear stress, it is necessary to systematically integrate these sub-paths to provide a more comprehensive and accurate purview of cellular mechanisms.

The current process of integrating multiple molecular pathways involves hand curation of individual models into a single monolithic model (see Fig. 2-1A). Due to the use of different model coding environments, variable names, pathway separation methodologies, and solution strategies, assembly of monolithic models typically requires substantial re-writing of previously published models. In this process, the links to previously published sub-paths become difficult to decipher and the manual work may be prone to errors, especially for large networks. The process of including new data elements to sub-path models that more accurately detail biochemical reaction steps is also non-trivial and often burdensome. Most importantly, scientifically, monolithic model integration loses much of the history and progression of pathway determination and development, particularly the detailed experimental condition where the original models and parameters are based on (36).

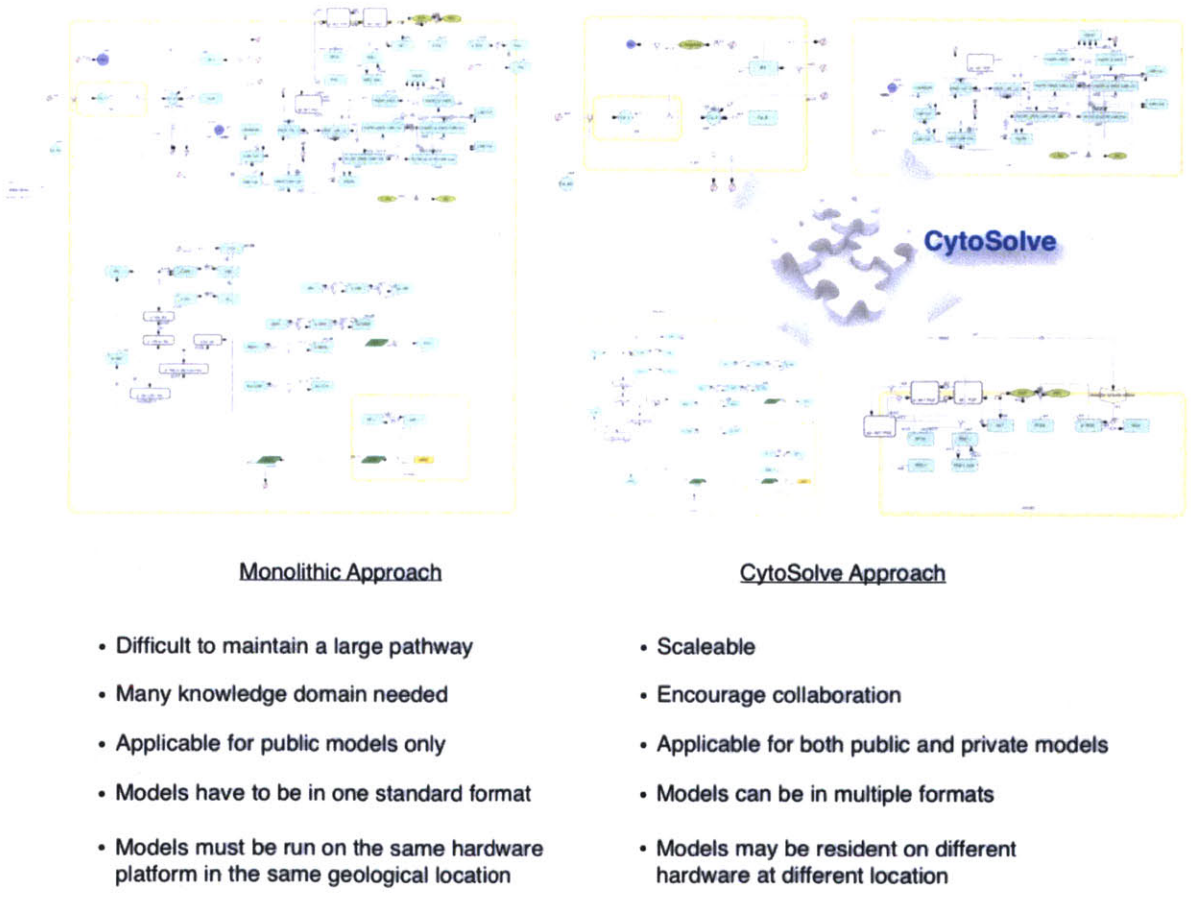

Fig. 2-1. Comparison between the monolithic and the CytoSolve approaches in building an integrated model.

In this paper, an alternative approach, based on the binding-expression concept, is adapted (see Fig. 2-1B) and the integrated model is viewed as an ontology. Any previously published sub-path model is retained in its entirety, allowing it to be updated, extracted, replaced, or removed. Sub-pathway models are then integrated through bindings that identify common species and alterations made to each model due to their integration. In our work, the creation of these bindings has been semi-automated through the use of MIRIAM (31) annotations and XML standard formats – such as SBML (26)– which support computational parsing and reasoning. In this way, common species and reaction pathways can be identified despite variations in nomenclature or the number of reactions, thus lowering the complexity bar for the human curator. These tools are made publicly available through CytoSolve (1), a web-accessible interface (http://cytosolve.mit.edu/) capable of model integration and simulation.

Main Mechanisms of Shear-stress-regulated eNOS Activation

Transcriptional Regulation

Key Proteins	Known Pathway	Note	References	Model Inclusion
AP-1	Shc -> Grb2-Sos -> Ras -> JNK -> AP-1	Transient	Chen (1999), Wedgwood (2003)	eNOS expression
NFκB	Akt -> IκK -> NFκB	Transient (complex)	Wang (2003), Davis (2004), Won (2007)	Not included
KLF2	? -> MEK5 -> ERK5 -> MEF2 -> KLF2	Long term	Parmar (2006)	eNOS expression

Post-translational Regulation

Phosphorylation

Key Kinases	Known Pathway	Phosphorylation Site	References	Model Inclusion
Akt	PI3K -> AKT	Ser1177	Dimmeler (1999)	eNOS phosphorylation
PKA	? -> [cAMP] -> PKA	Ser635 (bovine)	Boo (2001)	Not included
AMPK	? -> [AMP] -> AMPK	Ser1177	Young (2009)	Not included

Protein Partners

Key Partners	Effect on eNOS	References	Model Inclusion
Caveolin-1	Inactivation	García-Cardeña (1996)	NO production
Calmodulin	Activation, facilitate recruitment of Hsp90	Forstermann (1991), Gratton (2000)	Calcium influx, NO production
Hsp90	Activation, facilitate recruitment of Akt	García-Cardeña (1998), Fontana (2002)	NO production

Table 2-1. List of main mechanisms of shear-stress-regulated eNOS activation (5, 8, 11, 15, 19-22, 24, 39, 42, 43, 46, 47).

In the case of endothelia-derived NO, many pathway models governing its production have been previously established (see Table 2-1). In this paper, we integrate four of these molecular pathway models (see Fig. 2-2) that modulate the activation of endothelial nitric oxide synthase (eNOS) by shear stress. Specifically, we focus on the calcium-stimulated binding of calmodulin to eNOS, AKT mediated phosphorylation of eNOS, and up-regulation of eNOS transcription through AP-1 and KLF2. These pathways are linked by an additional model describing eNOS' interaction with its protein partners. By integrating these models in CytoSolve, the dynamic regulation and production of NO by eNOS under both shear stress and static (no shear stress) conditions can be investigated and tested. This use of the NO model illustrates the potential of the partitioned model approach and of the CytoSolve tools, which enable simulation of complex problems involving many parallel pathways that cannot be readily isolated experimentally.

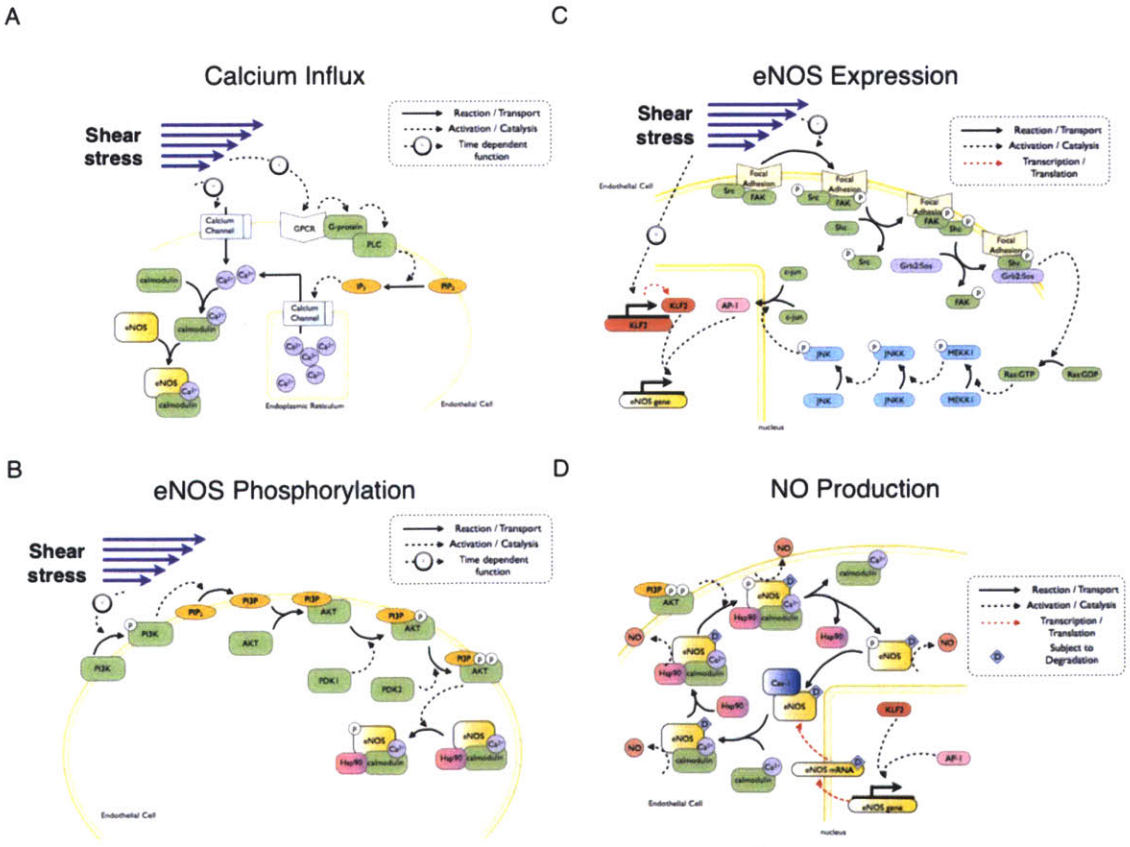

Fig. 2-2. The four models of the shear stress-induced NO production system. A) the calcium influx model, B) the eNOS phosphorylation model, C) the eNOS expression model, and D) the NO production model.

2.2 Methods

In this section we detail the individual well-characterized pathway models which regulate eNOS and, as a result, NO production. These models are linked with a new model describing the interactions of eNOS and its associated binding partners. The section concludes by detailing the tools used to bind the individual models together, creating a partitioned NO pathway model capable of describing the multiple phenomena that regulate NO.

2.2.1 Mechanisms of Shear-Stress-induced NO production

Several key signaling pathways have been identified which modulate the activity of eNOS – the primary source of NO production in vascular endothelial cells. In this section we introduce three pathway models that alter eNOS activation or regulate eNOS protein expression. To link these models, an additional model was constructed that describes the binding of calcium, calmodulin (CaM), Hsp90, eNOS, and phosphorylated eNOS as well as the resulting enzymatic production of NO. The detailed model schemes, inputs, species, reactions, and parameters are described in the Appendix).

Shear-stress-induced calcium influx and eNOS activation

In response to increased fluid shear stress, endothelial cells exhibit transient increase in cytosolic free calcium (see Fig. 2-2A). The influx of calcium is due to mechanisms such as activation of stress-sensitive calcium channel and activation of G-protein pathway (10). A calcium channel is directly activated by the fluid shear stress and this leads to intracellular calcium influx. G-protein coupled receptors can also be activated by shear stress (7). Activated G-protein induces activity of phospholipase C and production of inositol 1,4,5-trisphosphate (IP3). IP3 binds to its receptor on the surface of endoplasmic reticulum and promotes calcium release from this intracellular storage. The increased intracellular Ca^{2+} then rapidly binds to CaM, a calcium-binding protein that significantly up-regulates the activity of eNOS. The elevated intracellular calcium level subsequently leads to increased calcium export via the sodium-calcium exchanger and re-uptake in intracellular stores, making increase in intracellular Ca^{2+} a transient (~5 minutes) event (45).

To describe the calcium dynamics in response to shear stress, a mathematical model published by Wiesner *et al.* was used (44, 45). This model assumes a step change of calcium influx mediated by the stress-sensitive calcium channel at the onset of shear stress (10 dynes/cm^2). The resulting concentration profile of calcium transient is shown in Fig. 2-3A.

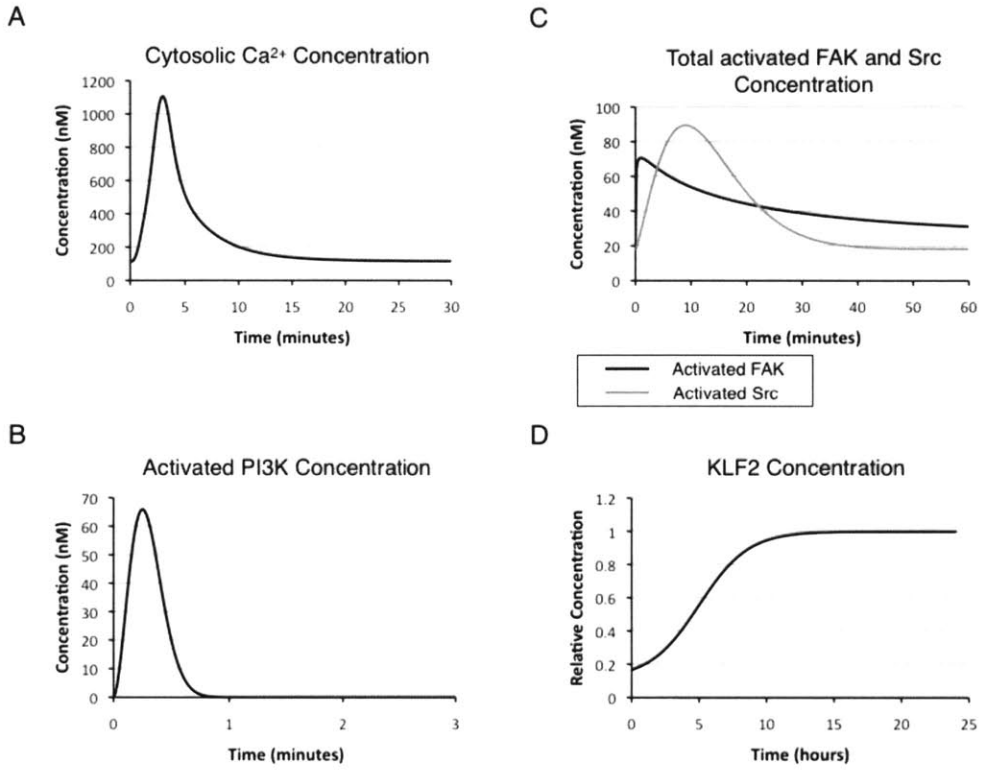

Fig. 2-3. Simulation profiles of shear-induced model inputs: A) cytosolic Ca^{2+}, B) activated PI3K, C) total activated FAK and activated Src, and D) KLF2.

Shear-stress-induced AKT and eNOS phosphorylation

In addition to calcium-dependent calmodulin binding, eNOS activity can also be up-regulated by post-translational modifications, most importantly phosphorylation on serine 1177 of the human eNOS sequence (15). For the model we solely focused on phosphorylation on this site. This reaction is catalyzed by protein kinases including AKT, PKA, and AMPK (40). The mechanism of how shear stress activates AMPK is still unclear, but shear-stress-induced AKT and PKA activation has been shown to be PI3K-dependent (5, 15). Phosphorylation of serine 1177 is significantly decreased when endothelial cells are treated with PI3K inhibitor, Ly294002, or transfected with dominant-negative AKT (15, 17). These data suggest that the PI3K-AKT

pathway plays the most important role in shear-stress-induced eNOS phosphorylation. Based on this experimental observation, it is assumed in our model that PI3K dependent AKT activation is the main pathway responsible for eNOS phosphorylation: PI3K activation leads to production of phosphatidylinositol (3,4,5)- trisphosphate (PIP3). PIP3 subsequently recruits cytosolic free AKT to the membrane; then AKT is phosphorylated by both PDK1 and PDK2 (see Fig. 2-2B). Finally, phopsphorylated AKT phosphorylate eNOS on serine 1177.

The mathematical model used to describe the AKT activation process is taken from Koh *et al.* (29), a model originally established to study the crosstalk between AKT and MAPK pathways upon receptors binding to growth factors. This model provides a detailed illustration of the PI3K-AKT pathway, which we assumed is conserved across different human cell types. In our model, PI3K activation was assigned to be the input signal based on a time-dependent function fit from experimental data by Go *et al.* (23). Time-dependent functions were used as model inputs throughout the NO system as proxies for the mechanotransduction process, due to the fact that how shear stress leads to activation of molecular pathways is still poorly understood. In this paper, laminar shear stress with the magnitude of 5 dynes/cm^2 was used in the experiments. In other papers used to generate model inputs in subsequent models, laminar shear stress or oscillatory shear stress with mean magnitude of 12 dynes/cm^2 were applied. Here we made a general assumption that endothelial cells respond similarly regarding eNOS activation given a shear stress stimuli of 5 to 12 dynes/cm^2.

Shear-stress-induced eNOS expression

A third mechanism leading to an overall increase in NO production is up-regulation of eNOS expression. Key transcription factors governing shear-stress-induced eNOS promoter activity include AP-1, NFκB, and KLF2 (2). The role of NFκB on eNOS expression remains controversial as recent study indicates that expression of NFκB and eNOS is negatively correlated under shear stress (46). Therefore, in our model we focused on simulating the effect of AP-1 and KLF2 on eNOS transcription (Fig. 2-2C). In this model, it is assumed that there is no interaction between these two transcription factors and no synergy on eNOS transcription.

AP-1, a Jun-Jun homodimer or a Jun-Fos heterodimer, is involved in shear-stress-induced eNOS expression. A qualitative pathway model describing how shear stress leads to AP-1 nucleus translocation has been previously established (8). In the proposed model, shear stress

activates the focal adhesion site and leads to phsophorylation of focal adhesion kinase (FAK), Src kinase, and the adaptor protein Shc. Activation of these kinases leads to formation of the first complex, "FAK-Shc", then a second complex between "FAK-Shc" and "Grb2-Sos". The second complex activates Ras protein, and initiates the MAP kinase cascade through MEKK1, JNKK, and JNK. JNK phosphorylates Jun and eventually leads to Jun dimer association to form AP-1, which translocates to nucleus and facilitates eNOS expression.

To quantitatively model the contribution of AP-1 in regulating eNOS expression, two existing mathematical models were used as the bases. The first model, excerpted from Hatakeyama et al. (25), describes the activation pathway from Src, FAK to Ras. However, since the upstream mechanical activation of Src and FAK molecules is not well understood, the kinetics of these two molecules (Fig. 2-3C) were based on time dependent experimental measures observed by (32) and (27). Both shear stress experiments in the two papers used a laminar shear stress of 12 dynes/cm^2. The second model, modified from the Kholodenko study (28), illustrates the kinetics of how Ras initiates the MAP kinase cascade. These two models were combined and integrated with reactions including JNK-mediated Jun phosphorylation/dimerization, AP-1 nuclear translocation, AP-1 mediated eNOS transcription, eNOS translation, and eNOS mRNA degradation. The rates of these reactions were estimated based on experimental observation and previously established models. Parameters of this model were optimized to fit the experimental observation. Further details can be found in the Appendix.

KLF2, the third transcription factor responsible for eNOS expression, is characterized to lead to long-term up-regulated eNOS transcription. Compared to fast and transient nuclear translocation of AP-1 in response to shear stress, the increase in KLF2 concentration inside the nucleus is relatively slow but sustained (47). The upstream mechanosensors for KLF2 expression are still poorly understood, but its expression is known to be MEK5, ERK5, and MEF2 dependent (39). Due to limited experimental data to construct a complete model, KLF2 activation is simulated based upon a time-course shear stress experiment (1 Hz oscillatory shear stress of 12±4 dynes/cm^2) data measured by Young et al. (47) (Fig. 2-3D).

Shear-stress-induced NO production

The previously described models establish the concentration profile of cytosolic free calcium, phosphorylated eNOS, and total eNOS expression in response to shear stress. However, to

integrate these pathways and understand NO production, one additional model was necessary to characterize the interactions of eNOS and its binding partners (Fig. 2-2D).

The biphasic binding of Ca^{2+} to CaM is well-documented in the literature by Bayley (3) and others (34). This has been shown to occur due to the very rapid dissociation of Ca^{2+} from the N-ter EF hand pair compared to the C-ter EF hand pair, although some evidence suggests cooperative binding of Ca^{2+} to CaM (34). Black *et al.* have shown that a number of sequential kinetic models can predict binding response (4). Following their result, Ca^{2+} binding to CaM was modeled using a four-step process, with two fast and two slow steps. In our model, we assumed the fast steps are much faster than the slow steps and therefore $CaM(Ca^{2+})_2$ and $CaM(Ca^{2+})_4$ are the only stable CaM- Ca^{2+} forms. Both species were assumed to bind to eNOS.

Besides CaM, another key regulator for eNOS activation under shear stress is protein Hsp90. Hsp90 does not bind to eNOS under static condition, but significant binding was detected just 15 minutes after initiation of shear stress (21). CaM bound eNOS has been shown to significantly increase the efficiency for Hsp90 recruitment (24). Studies have also shown that the complex formation of eNOS-CaM-Hsp90 is required for Akt mediated eNOS phosphorylation on serine 1177 (16). Once phosphorylated, eNOS is stable in the active state with enhanced NO production efficiency until the phosphate group is removed. A quantitative model is created based on this scheme. All rate constants were either derived from existing models or optimized based on experimental data (see Appendix).

2.2.2 Model Integration

All individual models were built using CellDesigner 4.1 (CellDesigner.org), a visual design tool for cell models and molecular pathways. Each model was coded in SBML, an XML-based format that is widely used to encode biomolecular pathways. SBML (26) was selected due to its wide usage in the molecular modeling community and model repositories (such as Biomodels.net (30) open standard, developers' forum and available API, LibSBML (6)). All models were encoded using MIRIAM (Minimum Information Requested In Annotation of biochemical Models) specifications (31) that provide a rigorous set of information that mathematical models should include in order to be re-used.

An attractive feature of the SBML standard, combined with MARIAM, is the ability to include RDF (Resource Description Framework) statements. These enable the unique

identification of biomolecular components across multiple models irrespectively of an individual model's notation. This is achieved by labeling elements (i.e. species, reactions, etc.) in external resources (ontologies or databases), which provide a mechanism for identifying common species and reactions across models. For a generic SBML and MIRIAM-compliant model, it is possible to associate RDF statements to species, to reactions, and to the model itself, providing a mean to perform more advanced processing and model merging. For example, a DOI number or PubMed paper ID provides a unique link to a published article with the model details, while the URI links to elements in the Systems Biology Ontology (SBO (9)) or the ChEBI (Chemical Entities of Biological Interest) ontology (12) provide extensive information on individual biochemical species used within the model.

Writing each SBML model to be MIRIAM compliant requires additional effort, but the RDF annotations enable models to be parsed and merged by a suitable logical reasoner. For this work, we used the OREMP (Ontology Reasoning Engine for Molecular Pathways) computational code (41) which can automatically identify duplicate species across models. Moreover, OREMP can detect potential redundant reactions or reaction series which are shared across models. Identification of overlapping reactions is critical as the hidden synergistic action of two or more separate mathematical statements of the same reaction leads to erroneous simulation results. The use of both species and reaction annotations becomes very useful in this process as they enable the automatic match of cross-model components, minimizing user input. Using an ontological approach, the properties of each model discovered by the OREMP software can be appended to the description of the sub-models thus archiving these steps for future use.

The duplicate species and reactions between sub-models provide the relevant information for model integration. They act as "bindings" which provide the map between individual model species and reactions within a single model and their interaction in the entire merged model. As newer models become available, they can also be integrated, either augmenting the current model or replacing redundant paths. This process differs significantly from the monolithic process, where each individual model is incorporated into a single model, requiring significant more user effort.

2.2.3 Solving the Model Pathway

The partitioned models and their bindings provide the necessary information to simulate the global behavior of all interacting models. Models are aligned using CytoSolve and OREMP in combination as outlined above, providing the detected duplicates as an editable list to the user. Once the bindings between models have been constructed, the user may then set up the necessary initial conditions, measured experimentally or estimated from computer optimization, for simulating the molecular pathway. Simulation is handled using libSBML to parse the original SBML models and SOSLib with SUNDIALS (35) to compute the sub-models' evolution through time. CytoSolve solves the "joint model" not as a monolithic model, but as a separated system of models. The merging of individual model species' concentrations is handled via a mass-balance controller, which ensures both that aligned "bound" species maintain the same concentration throughout the simulation and that the time steps taken are small enough to guarantee convergence of the separable solution to the true (monolithic) solution (see (1, 37) for further detail).

2.3 Results

2.3.1 A simulation of the integrated shear-stress-induced NO production model

When endothelial cells are exposed to shear stress, one of the first events is influx of calcium from extracellular space and intracellular storage. Fig. 2-3A illustrates the concentration profile of intracellular calcium governed by the calcium influx model. The calcium level increases within the first three minutes after onset of shear stress; this transient response lasts for ten minutes and quickly goes back to the resting state level.

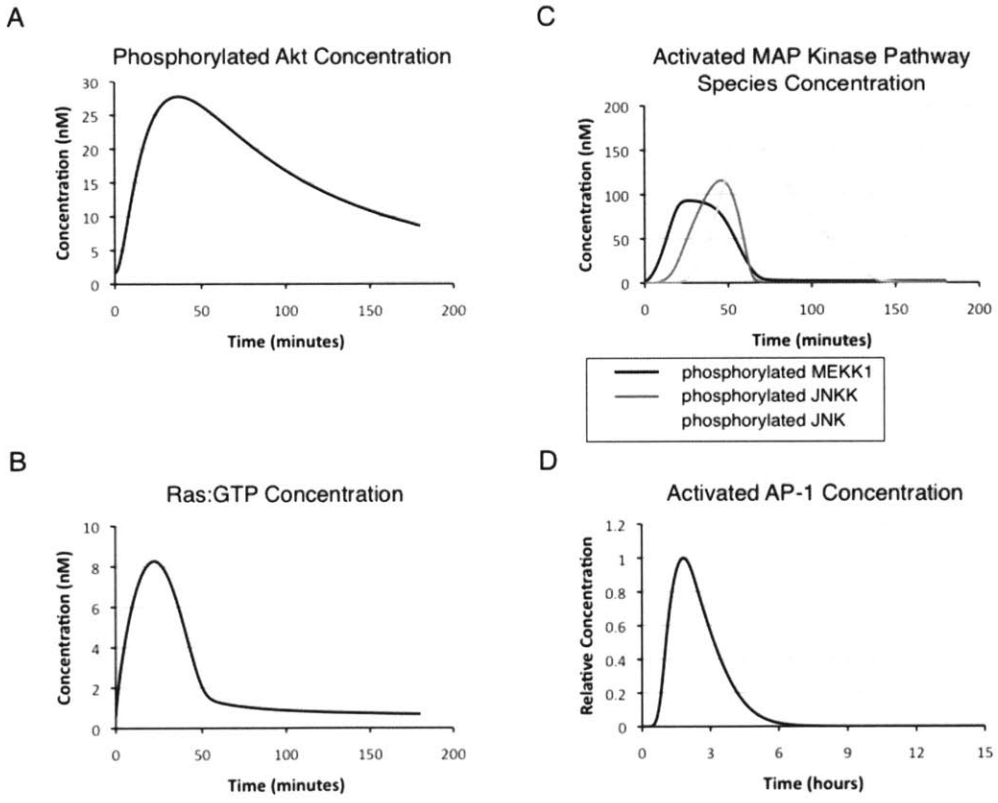

Fig. 2-4. Simulation profiles of intermediate species: A) phophorylated Akt (pp-Akt), B) Ras:GTP, C) Activated MAP kinase pathway species (p-MEKK1, pp-JNKK, pp-JNK), and D) activated AP-1.

Another early event observed after onset of shear stress is activation of phosphoinositide 3-kinase (PI3K). The concentration profile (Fig. 2-3B) of PI3K is simulated based on a time-dependent function generated from experimental data. Activation of PI3K is short and transient but accumulation of PIP3 results to down-stream Akt phosphorylation (Fig. 2-4A). This result is

consistent with experimental observation, where fully active AKT reaches the peak level within 30 minutes after onset of shear stress, and gradually decays back to the initial state in hours (5, 14).

A third early event after initiation of shear stress is activation of focal adhesion complex, including phosphorylation of both focal adhesion kinase (FAK) and Src kinase (Fig. 2-3C). Phosphorylation of the two proteins leads to down-stream activation of Ras (Fig. 2-4B) and the MAP kinase pathway proteins (Fig. 2-4C), and subsequent AP-1 formation and nuclear translocation (Fig. 2-4D). This process is transient with a time span of few hours and is responsible for the fast-responding up-regulation of eNOS mRNA and proteins after the cells experience a change in hemodynamic environment. Besides AP-1, the concentration profile for KLF2, another important transcription factor for eNOS, is shown in Fig. 2-3D. KLF2 is responsible for long-term up-regulation of eNOS mRNA and protein.

The above data describe the simulation results of individual pathways. These pathways interact with each other to control the dynamics of various eNOS species. Under static (no shear stress) condition, eNOS primarily binds to Cav-1. After the onset of shear stress, calcium is transported to the cell and bound to calmodulin. Four calcium ions bind to each calmodulin to make the active form of calmodulin, who associates with eNOS to enhance its catalytic activity to produce NO (Fig. 2-5A). In the meantime, the calmodulin-eNOS complex recruits Hsp90, which stabilize the complex and facilitates Akt mediated eNOS phosphorylation. The simulated concentration profile of phosphorylated eNOS on Ser 1177 (Fig. 2-5B) is consistent with existing experimental observations (5) and depicts a biphasic pattern. In the first ten minutes, when the phosphorylated Akt (enzyme) concentration is low but the CaM-eNOS-Hsp90 (substrate) concentration is high, there is rapid eNOS phosphorylation due to high substrate concentration. From ten to forty minutes, even though the substrate availability becomes low due to lower calcium concentration, phosphorylated eNOS level stays high as a result of increasing phosphorylated Akt.

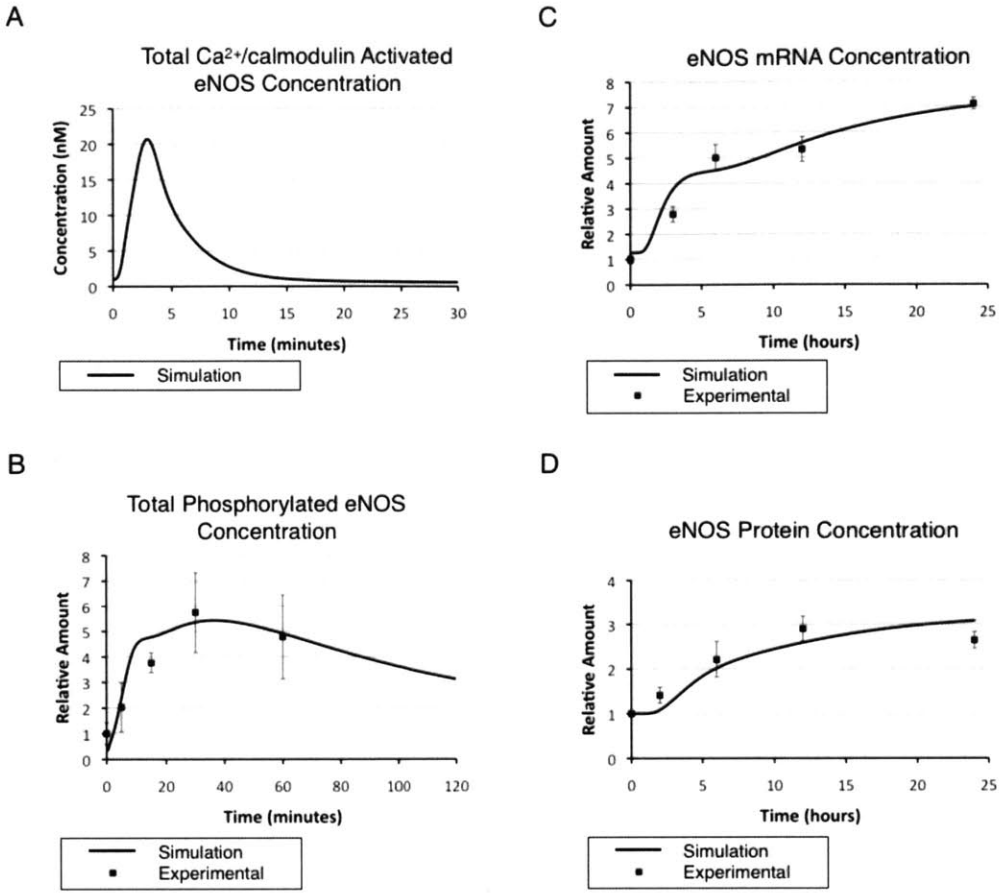

Fig. 2-5. Simulation profiles of eNOS species: A) Total Ca^{2+}/calmodulin activated eNOS; B) total phosphorylated eNOS (Ser 1177), the simulated data is compared with the experimental observation from (5); C) eNOS mRNA, the simulated data is compared with our experimental observation; D) total eNOS protein, the simulated data is compared with the experimental observation from (33).

To maintain long-term NO production, a third mechanism cells employ is increasing eNOS protein expression. Fig. 2-5C and 2-5D demonstrate the increase in eNOS mRNA and protein as catalyzed by the two transcription factor AP-1 and KLF2. The simulated eNOS mRNA and protein expression under shear stress are compared with the experimental data from our lab and Li et al. (33) respectively. The concentration profile of eNOS mRNA also shows a biphasic pattern as a result of early transcription by AP-1 and later transcription by KLF2. This biphasic effect is smoothed out after the eNOS translation process (Fig. 2-5D).

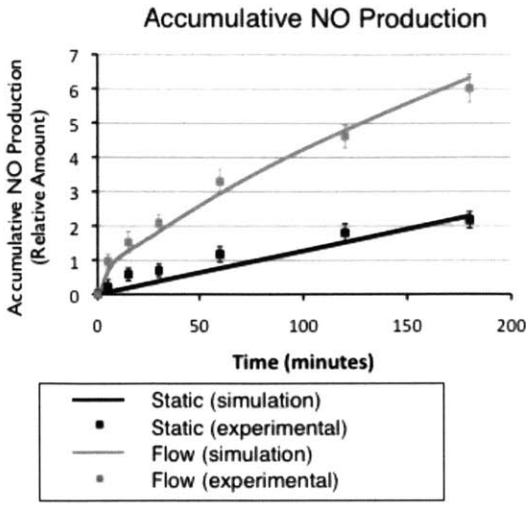

Fig. 2-6. Comparison of the simulation results of cumulative NO production against experimental data (18) under static (no shear stress) and shear stress conditions.

Finally, the total NO production from eNOS is simulated under both static and shear stress condition. Fig. 2-6 shows the accumulated NO production over time from the integrated model. We used relative unit for NO since its experimentally observed concentration varies depending on the cell confluency and media volume of individual experimental setup. The simulated NO production profile was compared to the experimental data measured by Florian et al. (18). Under static condition, there is low NO production from background level of calmodulin-activated eNOS and phosphorylated eNOS. Under shear stress condition, calcium influx in the first few minutes leads to a quick burst of NO production from calmodulin-activated eNOS. As calcium goes back to the basal level, phosphorylated eNOS kicks in to support NO production in the first few hours. The effect of eNOS expression does not come in until few hours later (described in more detail in the section below).

2.3.2 The model integration approach provides insights into the system that could not be easily gathered experimentally

Having established a system model that allows us to simulate the shear-stress-induced NO production that is comparable to the experimental data, we next explored several aspects of the system that can be simulated easily but difficultly tested experimentally. First, we analyzed the contribution of individual pathways to the overall NO production. The integrated modeling

approach allows investigating the relative importance of individual pathways instantaneously. Fig. 2-7A demonstrates the cumulative NO production contributed by different eNOS species. The data show that NO produced in the first 10 minutes almost all come from Ca^{2+}/calmodulin activated eNOS, with later NO produced mostly contributed by phosphorylated eNOS. In contrast, the NO produced by the intermediate species, Ca^{2+}/calmodulin activated phosphorylated eNOS, is not significant.

Secondly, we simulate the siRNA gene silencing approaches by selectively silencing shear-stress-induced activation of individual pathways. This process can be easily done by removing or modifying species in the system, giving reasonable predictions while saving tremendous resources. In the NO system, we assess the effect of modifying individual pathways to the overall NO production. To research on how individual transcription factor affects overall eNOS protein expression, AP-1 and KLF2 activation was respectively blocked (Fig. 2-7B). Blocking AP-1 activation yields a delayed response in eNOS expression under shear stress, whereas blocking KLF2 activation leads to no shear-stress-induced eNOS expression after 24 hours.

Finally we attempt to "predict" the effect of transfecting endothelial cells with Akt siRNA or dominant-negative Akt on eNOS phosphorylation (Fig. 2-7C) under 1 hour of shear stress. Our simulation data suggests that the relationship between silencing efficiency and the resulting decrease in eNOS phosphorylation is not linear. An Akt knock-down efficiency of 25% has little effect on eNOS phosphoryation, a 50% efficiency still retains greater than 60% of phosphorylated eNOS; it is not until a 75% silencing efficiency is achieved where we observe a less than 40% eNOS phosphorylation. A similar effect of decreasing eNOS phosphorylation can be achieved with an alternative approach. Fisslthaler *et al.* has demonstrated that transfecting the cells with dominant-negative Akt (DN-Akt) decreases shear-stress-induced eNOS phosphorylation (17). Here we simulate the condition where there is various amount of DN-Akt (1X, 2X, 5X, 10X relative to wild-type) in the system in addition to wild-type eNOS. DN-Akt competes with the wild-type Akt for binding site on the plasma membrane and significantly reduces shear-stress-activated eNOS phosphorylation.

When a known pathway is knocked down, which, for a given pathway, would yield no shear-stress-induced NO production; the integrated model shows robustness to the knockdown due to parallel pathways. This result emphasizes the importance of systems biology to

quantitatively understand macroscopic cellular response processes as well as the power of such analyses for more comprehensive pathway assessment.

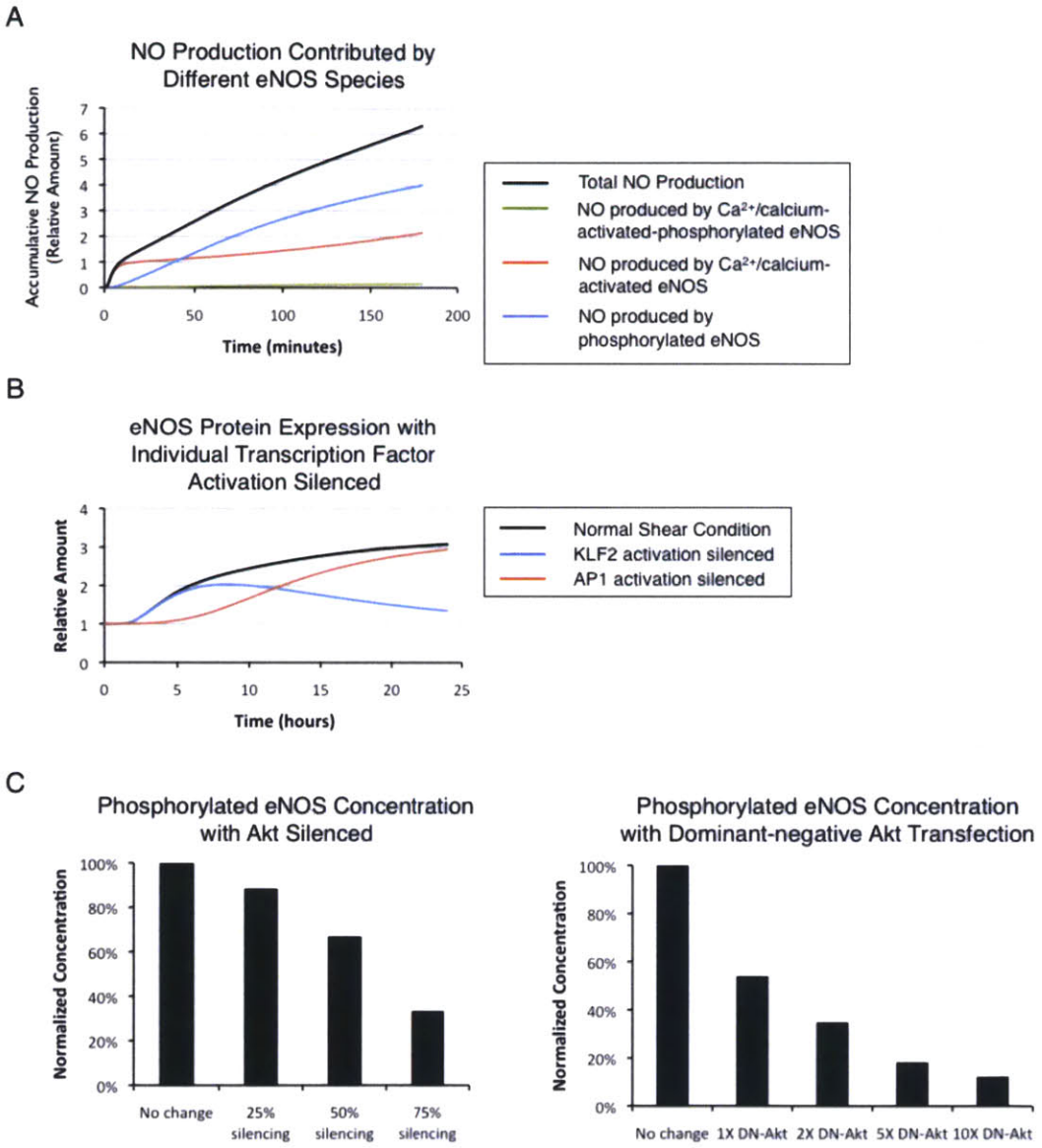

Fig. 2-7. The integrated model allows us to easily assess the contribution of individual eNOS species or simulate the condition where one pathway is modified. A) Contribution of NO production by different eNOS species, B) eNOS protein expression with individual transcription factor activation silenced, concentrations of the specific transcription factor is fixed at the static level. C) Normalized concentration of total phosphorylated eNOS with addition of (*left*) Akt siRNA or (*right*) dominant-negative Akt 1 hour after onset of shear stress. In the Akt siRNA simulation, total Akt concentration was reduced based on the specific silencing efficiency. In the dominant-negative Akt (DN-Akt) simulation, DN-Akt follows the exact kinetics of wild-type Akt except losing its catalytic ability in phosphosrylating eNOS. The amount of wild-type Akt is set constant, where the amount of DN-Akt is 1X, 2X, 5X, and 10X the amount of wild-type Akt.

2.4 Discussion

2.4.1 The Power of Automatic Model Integration

Quantitative modeling of molecular pathways provides a powerful tool for simulating and predicting function. With more and more comprehensive experimental data, it is rapidly becoming possible to construct more complete models of molecular pathways. A major bottleneck in this process, however, is the current model paradigm where models are manually integrated into a single complex model, obscuring the link to previously published pathways. In this paper we introduced an alternative model / binding approach where individual models are written and retained as is in standard MIRIAM compliant SBML format. The alterations, duplicate species and duplicate reactions are then detailed within the model bindings, providing clarity on how past models are incorporated into the current model. The tools for this merger process as well as the simulation of merged models have, as part of our continued work, been made available by CytoSolve.

In this paper, we considered four primary pathways that govern the activation and transcription/translation of eNOS, the NO catalyst. All these paths have been shown to work in tandem to govern the cells transient NO response to shear stress. Indeed, we show that the NO response consists of three primary phases that act on varying time-scales. The transient response is thus governed by the ensemble of molecular pathways, and cannot be accurately modeled considering any component individually. In addition to illustrating the need for model integration, the introduced pathways demonstrate the power of the model / binding approach. As the system is composed of individual models, additional pathways models based on new experimental data can be quickly incorporated into the system without rewriting the existing model. It also allows us to easily investigate the relative contribution from each pathway and conduct *in silico* experiments as demonstrated in Fig. 2-7.

Utilizing MIRIAM standards and references to web-accessible ontologies, this paper also introduces an approach for automating model integration. This strategy is the opposite of the monolithic approach where many models are manually assembled to compose a single new model that is more challenging to further edits, which generally results in valued work with limited re-usability. In contrast to this approach, the partitioned approach introduced in this

paper provides an additive model creation paradigm, where previous knowledge, data and effort can easily be managed, curated, and used by the wider scientific community. This is accomplished by the model / binding approach, where individual models retain their original identity. The bindings between individual models provide the necessary interface for both defining how an original model is used and altered, preserving the original model, its lineage and making the modeling process more straightforward. In addition, the integration of models via the partitioned approach makes updating the model much more straightforward while preserving the remaining bindings and models.

2.4.2 Limitations in Shear-stress-induced NO Pathway Modeling

In this paper, we collect the relevant pathways, species, and reactions to reflect the state of the art understanding of NO production. Though the NO system provides a quantitative link between shear stress and NO through activation and transcription pathways that match well with published experimental data, further work is required to improve and enhance the model. Due to limitations in available data, some model components were based on experiments using different endothelial cell types as well as different experimental conditions (varied cultured condition and mechanisms for applying shear). While these issues are not unique to this model but common to a number of cellular models, they warrant further experimental investigation and validation. These weaknesses can be annotated in the model and be transparent for future improvement. Despite these limitations, the model does demonstrate the general dynamics of multiple pathways acting in concert to up-regulate NO production.

To further improve the integrated NO model, incorporation of other mechanotransduction pathways is necessary. For example, the endothelial glycocalyx has been shown to be an important mechanosensor for shear-stress-induced NO production. Treating the endothelial surface with heparanase to remove heparan sulfate, one major glycosaminoglycan of the glycocalyx layer, significantly reduces the NO production resulting from shear stress (18, 38). The specific signaling pathways that trigger the models used here are still not known. Moreover, we have used a simple heuristic model based on experimental data to represent the up-regulation of KLF2 by shear stress. KLF2, a key regulator for eNOS expression, is also a shear-responding transcription factors leading to anti-inflammatory and anti-thrombotic phenotypes (13). KLF2 expression is known to follow the MEK5-ERK5-MEF2 pathway, but the mechanosensors that

lead to the activation of this pathway are still unclear (39). These additions are currently limited by incomplete knowledge of pathway mechanisms and lack of critical kinetic data. However, the current integrated model creates a platform to identify deficiencies in our current understanding, to provide more suitable parameters, and to embed additional pathways or information in an additive way. This process acts as a communal way of documenting what is understood about cellular mechanisms of NO production in endothelial cells.

2.4.3 Future Model Integration Tools and Development

To facilitate model integration, this paper outlines the use of CytoSolve. While this tool automates the model integration process with minimal input from the user, further development could dramatically improve the effectiveness of the integration process, store relevant changes at various stages in development and provide tools for incorporating input from the wider scientific community.

One of the major aims of this work was to demonstrate that the combination of separate biological models to generate a new larger predictive model is difficult, but becomes tractable with the right tools. Because a model that exists completely independently of other models is of limited use to the research community, it behooves the community to define processes by which existing and new models can be augmented, combined, and increased in depth of complexity so that existing work is properly assimilated.

It is also important to recognize that different models have different aims and often they operate at different time scales, spatial scales, and different initial conditions; most of the models have species exchanges on the order of micro- or nano- molars per minute, but this is not universally suitable for every objective. Because SBML makes it possible to define arbitrary units by composing IS-ones, it is among CytoSolve's goals to resolve and normalize differing units in a transparent manner. A new algorithm will extend the current mass-balance introducing a unit-conversion routine that will be called at run-time, keeping the merged solution independent of any individual model's representation.

Another future addition will be the extension of the actual cross-model information sharing process in order to show users other reactions of interest to them. This will provide an auto-completion for models to include reactions seen in other models. The goal of this functionality is to accelerate the information sharing and model composition process even more:

building models on top of others, reducing unnecessary duplicates, and informing researchers of known existing pathways that may be relevant to their study.

2.5 Conclusions

In this study, we simulated the process of shear-stress-induced NO production in endothelial cells by combining a number of existing published pathway models to describe and predict the complex interactions that occur between them at multiple timescales. The program we used, CytoSolve, is specifically designed to facilitate the federation of individual biological pathways in a manner that allows them to run as a combined monolithic model without losing their individuality and the metadata attached to them. The integrated model reflects the state-of-the-art understanding of the NO system, and the simulation data are able to describe experimental observations resulting from complex interactions between multiple pathways. The system level simulation approach can also provide researchers useful insights into the system that can traditionally only be achieved with challenging and time consuming experiments. Importantly, this approach to biological pathway integration is not only helpful for our understanding of biological system, but also provides a platform to aggregate information in an additive way, which eventually could allow us to predict biology.

2.6 References

1. **Ayyadurai VA, and Dewey CF**. CytoSolve: A Scalable Computational Method for Dynamic Integration of Multiple Molecular Pathway Models. *Cell Mol Bioeng* 4: 28-45, 2011.
2. **Balligand J-L, Feron O, and Dessy C**. eNOS Activation by Physical Forces: From Short-Term Regulation of Contraction to Chronic Remodeling of Cardiovascular Tissues. *Physiol Rev* 89: 481-534, 2009.
3. **Bayley P, Ahlstrom P, Martin SR, and Forsen S**. The kinetics of calcium binding to calmodulin: Quin 2 and ANS stopped-flow fluorescence studies. *Biochemical and biophysical research communications* 120: 185-191, 1984.
4. **Black DJ, Selfridge JE, and Persechini A**. The kinetics of Ca(2+)-dependent switching in a calmodulin-IQ domain complex. *Biochemistry* 46: 13415-13424, 2007.
5. **Boo YC, Sorescu G, Boyd N, Shiojima I, Walsh K, Du J, and Jo H**. Shear stress stimulates phosphorylation of endothelial nitric-oxide synthase at Ser1179 by Akt-independent mechanisms: role of protein kinase A. *J Biol Chem* 277: 3388-3396, 2002.
6. **Bornstein BJ, Keating SM, Jouraku A, and Hucka M**. LibSBML: an API library for SBML. *Bioinformatics* 24: 880-881, 2008.
7. **Chachisvilis M, Zhang YL, and Frangos JA**. G protein-coupled receptors sense fluid shear stress in endothelial cells. *Proc Natl Acad Sci U S A* 103: 15463-15468, 2006.
8. **Chen KD, Li YS, Kim M, Li S, Yuan S, Chien S, and Shyy JY**. Mechanotransduction in response to shear stress. Roles of receptor tyrosine kinases, integrins, and Shc. *J Biol Chem* 274: 18393-18400, 1999.
9. **Courtot M, Juty N, Knupfer C, Waltemath D, Zhukova A, Drager A, Dumontier M, Finney A, Golebiewski M, Hastings J, Hoops S, Keating S, Kell DB, Kerrien S, Lawson J, Lister A, Lu J, Machne R, Mendes P, Pocock M, Rodriguez N, Villeger A, Wilkinson DJ, Wimalaratne S, Laibe C, Hucka M, and Le Novere N**. Controlled vocabularies and semantics in systems biology. *Mol Syst Biol* 7: 543, 2011.
10. **Davies PF**. Flow-mediated endothelial mechanotransduction. *Physiol Rev* 75: 519-560, 1995.
11. **Davis ME, Grumbach IM, Fukai T, Cutchins A, and Harrison DG**. Shear stress regulates endothelial nitric-oxide synthase promoter activity through nuclear factor kappaB binding. *J Biol Chem* 279: 163-168, 2004.
12. **Degtyarenko K, de Matos P, Ennis M, Hastings J, Zbinden M, McNaught A, Alcantara R, Darsow M, Guedj M, and Ashburner M**. ChEBI: a database and ontology for chemical entities of biological interest. *Nucleic Acids Res* 36: D344-350, 2008.
13. **Dekker RJ, van Soest S, Fontijn RD, Salamanca S, de Groot PG, VanBavel E, Pannekoek H, and Horrevoets AJ**. Prolonged fluid shear stress induces a distinct set of endothelial cell genes, most specifically lung Kruppel-like factor (KLF2). *Blood* 100: 1689-1698, 2002.
14. **Dimmeler S, Assmus B, Hermann C, Haendeler J, and Zeiher AM**. Fluid shear stress stimulates phosphorylation of Akt in human endothelial cells: involvement in suppression of apoptosis. *Circ Res* 83: 334-341, 1998.
15. **Dimmeler S, Fleming I, Fisslthaler B, Hermann C, Busse R, and Zeiher AM**. Activation of nitric oxide synthase in endothelial cells by Akt-dependent phosphorylation. *Nature* 399: 601-605, 1999.
16. **Dudzinski DM, and Michel T**. Life history of eNOS: partners and pathways. *Cardiovasc Res* 75: 247-260, 2007.
17. **Fisslthaler B, Dimmeler S, Hermann C, Busse R, and Fleming I**. Phosphorylation and activation of the endothelial nitric oxide synthase by fluid shear stress. *Acta Physiol Scand* 168: 81-88, 2000.
18. **Florian JA, Kosky JR, Ainslie K, Pang Z, Dull RO, and Tarbell JM**. Heparan sulfate proteoglycan is a mechanosensor on endothelial cells. *Circ Res* 93: e136-142, 2003.
19. **Fontana J, Fulton D, Chen Y, Fairchild TA, McCabe TJ, Fujita N, Tsuruo T, and Sessa WC**. Domain mapping studies reveal that the M domain of hsp90 serves as a molecular scaffold to regulate Akt-dependent phosphorylation of endothelial nitric oxide synthase and NO release. *Circ Res* 90: 866-873, 2002.
20. **Forstermann U, Pollock JS, Schmidt HH, Heller M, and Murad F**. Calmodulin-dependent endothelium-derived relaxing factor/nitric oxide synthase activity is present in the particulate and cytosolic fractions of bovine aortic endothelial cells. *Proc Natl Acad Sci U S A* 88: 1788-1792, 1991.

21. **Garcia-Cardena G, Fan R, Shah V, Sorrentino R, Cirino G, Papapetropoulos A, and Sessa WC**. Dynamic activation of endothelial nitric oxide synthase by Hsp90. *Nature* 392: 821-824, 1998.
22. **Garcia-Cardena G, Fan R, Stern DF, Liu J, and Sessa WC**. Endothelial nitric oxide synthase is regulated by tyrosine phosphorylation and interacts with caveolin-1. *J Biol Chem* 271: 27237-27240, 1996.
23. **Go YM, Park H, Maland MC, Darley-Usmar VM, Stoyanov B, Wetzker R, and Jo H**. Phosphatidylinositol 3-kinase gamma mediates shear stress-dependent activation of JNK in endothelial cells. *Am J Physiol* 275: H1898-1904, 1998.
24. **Gratton JP, Fontana J, O'Connor DS, Garcia-Cardena G, McCabe TJ, and Sessa WC**. Reconstitution of an endothelial nitric-oxide synthase (eNOS), hsp90, and caveolin-1 complex in vitro. Evidence that hsp90 facilitates calmodulin stimulated displacement of eNOS from caveolin-1. *J Biol Chem* 275: 22268-22272, 2000.
25. **Hatakeyama M, Kimura S, Naka T, Kawasaki T, Yumoto N, Ichikawa M, Kim JH, Saito K, Saeki M, Shirouzu M, Yokoyama S, and Konagaya A**. A computational model on the modulation of mitogen-activated protein kinase (MAPK) and Akt pathways in heregulin-induced ErbB signalling. *Biochem J* 373: 451-463, 2003.
26. **Hucka M, Finney A, Sauro HM, Bolouri H, Doyle JC, Kitano H, Arkin AP, Bornstein BJ, Bray D, Cornish-Bowden A, Cuellar AA, Dronov S, Gilles ED, Ginkel M, Gor V, Goryanin, II, Hedley WJ, Hodgman TC, Hofmeyr JH, Hunter PJ, Juty NS, Kasberger JL, Kremling A, Kummer U, Le Novere N, Loew LM, Lucio D, Mendes P, Minch E, Mjolsness ED, Nakayama Y, Nelson MR, Nielsen PF, Sakurada T, Schaff JC, Shapiro BE, Shimizu TS, Spence HD, Stelling J, Takahashi K, Tomita M, Wagner J, and Wang J**. The systems biology markup language (SBML): a medium for representation and exchange of biochemical network models. *Bioinformatics* 19: 524-531, 2003.
27. **Jalali S, Li YS, Sotoudeh M, Yuan S, Li S, Chien S, and Shyy JY**. Shear stress activates p60src-Ras-MAPK signaling pathways in vascular endothelial cells. *Arterioscler Thromb Vasc Biol* 18: 227-234, 1998.
28. **Kholodenko BN**. Negative feedback and ultrasensitivity can bring about oscillations in the mitogen-activated protein kinase cascades. *Eur J Biochem* 267: 1583-1588, 2000.
29. **Koh G, Teong HFC, Clément M-V, Hsu D, and Thiagarajan PS**. A decompositional approach to parameter estimation in pathway modeling: a case study of the Akt and MAPK pathways and their crosstalk. *Bioinformatics* 22: e271-280, 2006.
30. **Le Novere N, Bornstein B, Broicher A, Courtot M, Donizelli M, Dharuri H, Li L, Sauro H, Schilstra M, Shapiro B, Snoep JL, and Hucka M**. BioModels Database: a free, centralized database of curated, published, quantitative kinetic models of biochemical and cellular systems. *Nucleic Acids Res* 34: D689-691, 2006.
31. **Le Novere N, Finney A, Hucka M, Bhalla US, Campagne F, Collado-Vides J, Crampin EJ, Halstead M, Klipp E, Mendes P, Nielsen P, Sauro H, Shapiro B, Snoep JL, Spence HD, and Wanner BL**. Minimum information requested in the annotation of biochemical models (MIRIAM). *Nat Biotechnol* 23: 1509-1515, 2005.
32. **Li S, Kim M, Hu YL, Jalali S, Schlaepfer DD, Hunter T, Chien S, and Shyy JY**. Fluid shear stress activation of focal adhesion kinase. Linking to mitogen-activated protein kinases. *J Biol Chem* 272: 30455-30462, 1997.
33. **Li Y, Zheng J, Bird IM, and Magness RR**. Effects of pulsatile shear stress on signaling mechanisms controlling nitric oxide production, endothelial nitric oxide synthase phosphorylation, and expression in ovine fetoplacental artery endothelial cells. *Endothelium* 12: 21-39, 2005.
34. **Linse S, Helmersson A, and Forsen S**. Calcium binding to calmodulin and its globular domains. *J Biol Chem* 266: 8050-8054, 1991.
35. **Machne R, Finney A, Muller S, Lu J, Widder S, and Flamm C**. The SBML ODE Solver Library: a native API for symbolic and fast numerical analysis of reaction networks. *Bioinformatics* 22: 1406-1407, 2006.
36. **Niederer SA, Fink M, Noble D, and Smith NP**. A meta-analysis of cardiac electrophysiology computational models. *Exp Physiol* 94: 486-495, 2009.
37. **Nordsletten DA, Yankama B, Umeton R, Ayyadurai VA, and Dewey CF, Jr.** Multiscale mathematical modeling to support drug development. *IEEE Trans Biomed Eng* 58: 3508-3512, 2011.
38. **Pahakis MY, Kosky JR, Dull RO, and Tarbell JM**. The role of endothelial glycocalyx components in mechanotransduction of fluid shear stress. *Biochem Biophys Res Commun* 355: 228-233, 2007.

39. **Parmar KM, Larman HB, Dai G, Zhang Y, Wang ET, Moorthy SN, Kratz JR, Lin Z, Jain MK, Gimbrone MA, and García-Cardeña G**. Integration of flow-dependent endothelial phenotypes by Kruppel-like factor 2. *J Clin Invest* 116: 49-58, 2006.
40. **Sessa WC**. eNOS at a glance. *Journal of cell science* 117: 2427-2429, 2004.
41. **Umeton R, Nicosia G, and Dewey CF, Jr.** OREMPdb: a semantic dictionary of computational pathway models. *BMC bioinformatics* 13 Suppl 4: S6, 2012.
42. **Wang Y, Chang J, Li YC, Li YS, Shyy JY, and Chien S**. Shear stress and VEGF activate IKK via the Flk-1/Cbl/Akt signaling pathway. *Am J Physiol Heart Circ Physiol* 286: H685-692, 2004.
43. **Wedgwood S, Mitchell CJ, Fineman JR, and Black SM**. Developmental differences in the shear stress-induced expression of endothelial NO synthase: changing role of AP-1. *Am J Physiol Lung Cell Mol Physiol* 284: L650-662, 2003.
44. **Wiesner TF, Berk BC, and Nerem RM**. A mathematical model of cytosolic calcium dynamics in human umbilical vein endothelial cells. *Am J Physiol* 270: C1556-1569, 1996.
45. **Wiesner TF, Berk BC, and Nerem RM**. A mathematical model of the cytosolic-free calcium response in endothelial cells to fluid shear stress. *Proc Natl Acad Sci USA* 94: 3726-3731, 1997.
46. **Won D, Zhu SN, Chen M, Teichert AM, Fish JE, Matouk CC, Bonert M, Ojha M, Marsden PA, and Cybulsky MI**. Relative reduction of endothelial nitric-oxide synthase expression and transcription in atherosclerosis-prone regions of the mouse aorta and in an in vitro model of disturbed flow. *Am J Pathol* 171: 1691-1704, 2007.
47. **Young A, Wu W, Sun W, Benjamin Larman H, Wang N, Li YS, Shyy JY, Chien S, and Garcia-Cardena G**. Flow activation of AMP-activated protein kinase in vascular endothelium leads to Kruppel-like factor 2 expression. *Arterioscler Thromb Vasc Biol* 29: 1902-1908, 2009.

2.7 Appendix - Model Reactions and Parameters

Model 1: Shear stress-induced calcium influx

Model Diagram (Figure legends at the end of appendix):

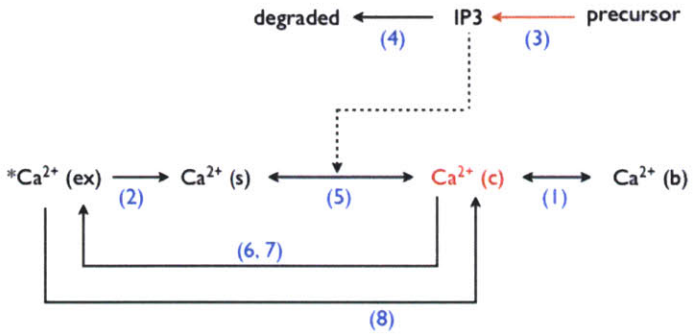

List of species:

Species	Name	Initial Amount	Ref.
Ca^{2+} (b)	Calcium complexed to intracellular binding proteins	3870 nM	(1)
Ca^{2+} (ex)	Extracellular calcium	$1.5 * 10^6$ nM	(1)
Ca^{2+} (s)	Calcium in intracellular storage	$2.83 * 10^6$ nM	(1)
Ca^{2+} (c)	Cytosolic calcium	117.2 nM	Steady state value for the integrated model under "no flow" condition
IP3	Inositol 1,4,5-triphosphate	0 nM	(1)

List of reactions:

#	Description	Rate equation	Ref.
1	$[Ca^{2+}$ (b)$] \leftrightarrow [Ca^{2+}$ (c)$]$	$k_7[Ca^{2+}(b)] - k_6[Ca^{2+}(c)] \cdot (B_T - [Ca^{2+}(b)])$	(1)
2	$[Ca^{2+}$ (ex)$] \rightarrow [Ca^{2+}$ (s)$]$	$k_{CCE} \cdot \left(\frac{fracK \cdot Ca_0^{2+}}{K3 + Ca_0^{2+}} - [Ca^{2+}(s)]\right) \cdot ([Ca^{2+}(ex)] - [Ca^{2+}(s)])$	(1)
3	$\phi \rightarrow [IP3]$	$k_1 \cdot \left(R_T - \frac{R_T}{2} \cdot (e^{-t/\tau_I} + e^{-t/\tau_{II}}) + \left(\frac{\tau_I + \tau_{II}}{\tau_I - \tau_{II}}\right) \cdot (e^{-t/\tau_I} - e^{-t/\tau_{II}})\right) \cdot \left(\frac{[Ca^{2+}(c)]}{K_1 + [Ca^{2+}(c)]}\right)$	(1)
4	$[IP3] \rightarrow \phi$	$k_2[IP3]$	(1)
5	$[Ca^{2+}$ (s)$] \leftrightarrow [Ca^{2+}$ (c)$]$	$k_3 \frac{k_{CICR}[Ca^{2+}(c)]}{K_{CICR} + [Ca^{2+}(c)]} \cdot \left(\frac{[IP3]}{K_2 + [IP3]}\right)^3 \cdot [Ca^{2+}(s)] - k_4\left(\frac{[Ca^{2+}(c)]}{K_3 + [Ca^{2+}(c)]}\right)^2 + k_5\left([Ca^{2+}(s)]\right)^2$	(1)
6	$[Ca^{2+}$ (c)$] \rightarrow [Ca^{2+}$ (ex)$]$	$\dot{V}_{ex} \frac{[Ca^{2+}(c)]}{K_5 + [Ca^{2+}(c)]}$	(1)

7	$[Ca^{2+}(c)] \rightarrow [Ca^{2+}(ex)]$	$\dot{V}_p \frac{\left([Ca^{2+}(c)]\right)^2}{K_4^2 + \left([Ca^{2+}(c)]\right)^2} + \dot{V}_{hi} \frac{\left([Ca^{2+}(c)]\right)^4}{K_{hi}^4 + \left([Ca^{2+}(c)]\right)^4}$	(1)
8	$[Ca^{2+}(ex)] \rightarrow [Ca^{2+}(c)]$	$\dot{Q}_{shear}$	(2)

List of parameters:

	Units	Ref.	Ref. value	Model value
R_T	# / cell	(1)	$4.4 * 10^4$	$4.4 * 10^4$
k_1	$nM \bullet s^{-1}$	(1)	$1.2 * 10^{-3}$	$6.0 * 10^{-4}$
k_2	s^{-1}	(1)	2	1
k_3	s^{-1}	(1)	6.64	3.32
k_4	$nM \bullet s^{-1}$	(1)	5000	2500
k_5	$nM^{-1} \bullet s^{-1}$	(1)	$1.0 * 10^{-10}$	$5.0 * 10^{-11}$
k_6	$nM^{-1} \bullet s^{-1}$	(1)	0.1	0.05
k_7	s^{-1}	(1)	300	150
K_1	nM	(1)	0	0
K_2	nM	(1)	200	200
K_3	nM	(1)	150	150
K_4	nM	(1)	80	80
K_5	nM	(1)	321	321
K_{hi}	nM	(1)	380	380
k_{CICR}	dimensionless	(1)	1	1
K_{CICR}	nM	(1)	0	0
k_{CCE}	$nM^{-1} \bullet s^{-1}$	(1)	0	0
B_T	nM	(1)	$1.2 * 10^5$	$1.2 * 10^5$
Ca_0^{2+}	nM	(1)	100	100
$\dot{Q}_{shear}$	$nM^{-1} \bullet s^{-1}$	(2), based on 10 dynes/cm^2	6000	3000
$\dot{V}_p$	$nM^{-1} \bullet s^{-1}$	(1)	1630	815
$\dot{V}_{ex}$	$nM^{-1} \bullet s^{-1}$	(1)	18330	9165
$\dot{V}_{hi}$	$nM^{-1} \bullet s^{-1}$	(1)	4760	2380
τ_I	s	(1)	33	33
τ_{II}	s	(1)	0.005	0.005
fracK	dimensionless	(1)	$7.1 * 10^6$	$7.1 * 10^6$

References for model 1:
(1, 2)

Model 2: Shear stress-induced AKT phosphorylation

Model Diagram:

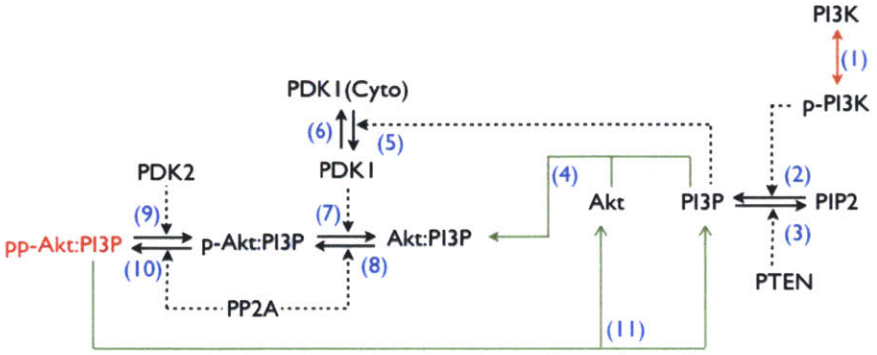

List of species:

Species	Name	*Initial Amount	Ref.
PI3K	PI 3-kinases	99.97 nM	Total PI3K concentration 100 nM (3)
p-PI3K	Phosphorylated PI 3-kinases	0.03 nM	---
PIP2	Phosphatidylinositol-4,5-biphosphate	6967.27 nM	Total PIP2 concentration 7000 nM (3)
PI3P	Phosphatidylinositol-3,4,5-triphosphate	0.35 nM	---
PTEN	Phosphatase and tensin homolog	0.1 nM	Constant (3)
Akt	Akt, or Protein Kinase B	167.62 nM	Total Akt concentration 200 nM (3)
Akt: PI3P	Membrane bound Akt	29.2 nM	---
p-Akt:PI3P	Monophosphorylated Akt	1.46 nM	---
pp-Akt:PI3P	Biphosphorylated Akt	1.72 nM	---
PDK1 (cyto)	Cytosolic phosphoinositide-dependent kinase-1	999.75 nM	Total PDK1 concentration 1000 nM (3)
PDK1	Phosphoinositide-dependent kinase-1	0.25 nM	---
PDK2	Phosphoinositide-dependent kinase-2	3 nM	Constant (3)
PP2A	Protein phosphatase 2	150 nM	Constant (3)

*** Initial amounts were obtained by simulating the model under "no flow" condition, with the reference value as initial concentrations, for a sufficient amount of time to reach steady state.**

List of reactions:

#	Description	Rate equation	Ref.
*1	[PI3K] ↔ [p-PI3K]	$\exp(1-\left(\frac{t}{15}\right)^{1.8})\cdot 0.907\cdot t^{0.8}\cdot(1-\left(\frac{t}{15}\right)^{1.8})$	(4)
2	[PIP2] → [PI3P]	$k_2\frac{[p-PI3K][PIP2]}{K_{m2}+[PIP2]}$	(3)
3	[PI3P] → [PIP2]	$k_3\frac{[PTEN][PI3P]}{K_{m3}+[PI3P]}$	(3)

4	[Akt] + [PI3P] ↔ [Akt:PI3P]	$k_4[PI3P][Akt] - k_{r4}[Akt:PI3P]$	(3)
5	[PDK1 (cyto)] → [PDK1]	$k_5[PI3P][PDK1]$	(3)
6	[PDK1] → [PDK1 (cyto)]	$k_6[PDK1]$	(3)
7	[p-Akt:PI3P] → [Akt:PI3P]	$k_7 \frac{[PP2A][p-Akt:PI3P]}{K_{m7}+[p-Akt:PI3P]}$	(3)
8	[Akt:PI3P] → [p-Akt:PI3P]	$k_8 \frac{[PDK1][Akt:PI3P]}{K_{m8}+[Akt:PI3P]}$	(3)
9	[pp-Akt:PI3P] → [p-Akt:PI3P]	$k_9 \frac{[PP2A][pp-Akt:PI3P]}{K_{m9}+[pp-Akt:PI3P]}$	(3)
10	[p-Akt:PI3P] → [pp-Akt:PI3P]	$k_{10} \frac{[PDK2][Akt:PI3P]}{K_{m10}+[Akt:PI3P]}$	(3)
11	[pp-Akt:PI3P] → [Akt] + [PI3P]	$k_{11} \frac{[PP2A][pp-Akt:PI3P]}{K_{m11}+[pp-Akt:PI3P]}$	(3)

*** Time-dependent function describing PI3K activation was generated from the experimental data in [4]. The shear stress waveform used in this paper is a laminar flow of 5 dynes/cm^2.**

List of parameters:

	Units	Ref.	Ref. value	Model value
k_2	s^{-1}	(3)	0.05	0.2
K_{m2}	nM	(3)	6170	6170
k_3	s^{-1}	(3)	5.5	7.5
K_{m3}	nM	(3)	80.9	80.9
k_4	$nM^{-1} \cdot s^{-1}$	(3)	0.045	0.045
k_{r4}	s^{-1}	(3)	0.089	0.089
k_5	$nM^{-1} \cdot s^{-1}$	(3)	0.0007	0.0007
k_6	s^{-1}	(3)	0.98	0.98
k_7	s^{-1}	(3)	0.037	0.037
K_{m7}	nM	(3)	8800	8800
k_8	s^{-1}	(3)	20	20
K_{m8}	nM	(3)	80000	80000
k_9	s^{-1}	(3)	0.04	0.04
K_{m9}	nM	(3)	48000	48000
k_{10}	s^{-1}	(3)	20	20
K_{m10}	nM	(3)	80000	80000
k_{11}	s^{-1}	(3)	0.163	0.163
K_{m11}	nM	(3)	48000	48000

References for model 2:

(3, 4)

Model 3: Shear stress-induced eNOS expression

Model Diagram:

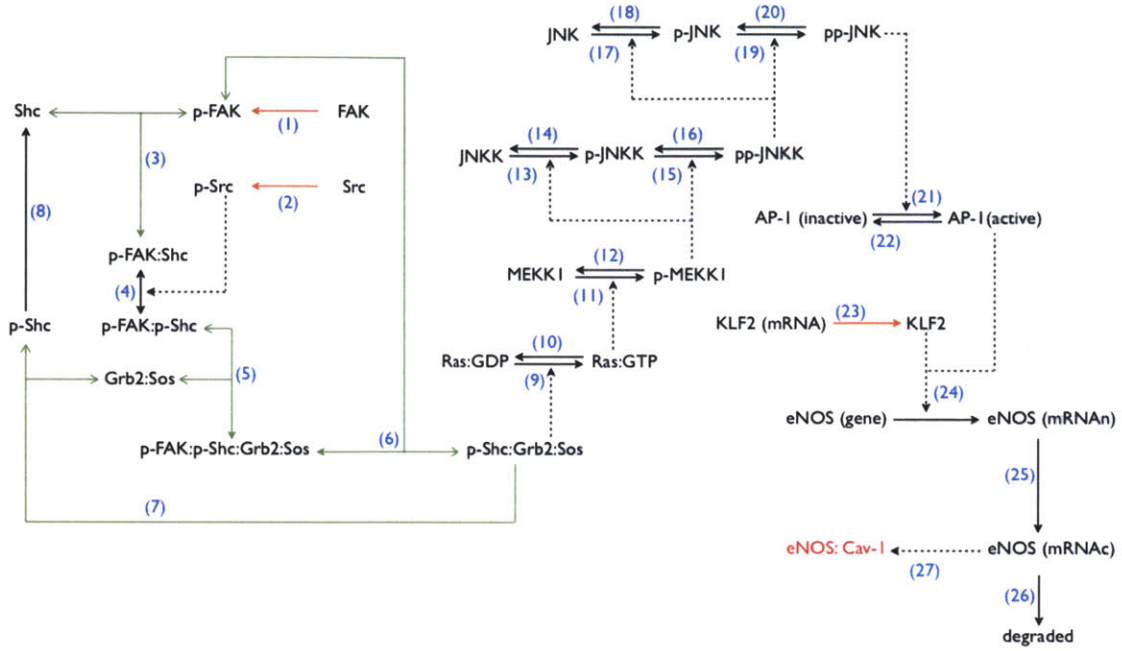

List of species:

Species	Name	*Initial Amount	Ref.
FAK	Focal adhesion kinase	57 nM	Total FAK concentration 80 nM (7)
p-FAK	Phosphorylated FAK	0.605 nM	---
Src	Src kinase	72 nM	Total Src concentration 90 nM (7)
p-Src	Phosphorylated Src	18 nM	---
Shc	Shc adaptor protein	819.25 nM	Total Shc concentration 1000 nM (8)
p-FAK:Shc	Protein complex	0.857 nM	---
p-FAK:p-Shc	Protein complex	15.962 nM	---
Grb2:Sos	Grb2:Sos adaptor protein	3.23 nM	Total Grb2:Sos concentration 10 nM (8)
p-FAK:p-Shc:Grb2:Sos	Protein complex	5.577 nM	---
p-Shc:Grb2:Sos	Protein complex	1.193 nM	---
p-Shc	Phosphorylated Shc	157.162 nM	---
Ras:GDP	Ras protein (GDP state)	119.384 nM	Total Ras concentration 120 nM (8)
Ras:GTP	Ras protein (GTP state)	0.616 nM	---
MEKK1	MEKK1 kinase	98.514 nM	Total MEKK1 concentration 100 nM (10)
p-MEKK1	Phosphorylated MEKK1	1.486 nM	---
JNKK	JNK-activated kinase	299.706 nM	Total JNKK concentration 300 nM (10)
p-JNKK	Monophosphorylated JNKK	0.288 nM	---
pp-JNKK	Biphosphorylated JNKK	0.006 nM	---
JNK	c-Jun N-terminal kinases	299.997 nM	Total JNK concentration 300 nM (10)
p-JNK	Monophosphorylated JNK	0.003 nM	---
pp-JNK	Biphosphorylated JNK	0 nM	---
eNOS (mRNAn)	Nuclear eNOS mRNA	0.09 nM	Estimate

eNOS (mRNAc)	Cytosolic eNOS mRNA	3.214 nM	Estimate
eNOS: Cav-1	eNOS (inactive due to Cav-1 binding)	34.98 nM	See model 4
AP-1 (inactive)	Activator Protein-1 (inactive)	50 nM	Total AP-1 concentration 50 nM (estimate)
AP-1 (active)	Activator Protein-1 (active)	0 nM	---
KLF2 (protein)	Krueppel-like factor 2	10 nM	Estimate

*** Initial amounts were obtained by simulating the model under "no flow" condition, with the reference value as initial concentrations, for a sufficient amount of time to reach steady state.**

List of reactions:

#	Description	Rate equation	Ref.
*1	[FAK] ↔ [p-PI3K]	$\exp(1-\left(\frac{t}{60}\right)^{0.35})\cdot 4\cdot t^{-0.65}\cdot(1-\left(\frac{t}{60}\right)^{0.35})$	(5)
*2	[Src] ↔ [p-Src]	$\exp(1-\left(\frac{t}{540}\right)^{1.3})\cdot 0.026\cdot t^{0.3}\cdot(1-\left(\frac{t}{540}\right)^{1.3})$	(6)
3	[p-FAK] + [Shc] ↔ [p-FAK:Shc]	$k_3[p-FAK][Shc]-k_{r3}[p-FAK:Shc]$	(8)
4	[p-FAK:Shc] ↔ [p-FAK:p-Shc]	$k_4[p-Src][p-FAK:Shc]-k_{r4}[p-FAK:p-Shc]$	(7, 8)
5	[p-FAK:Shc] + [Grb2:Sos] ↔ [p-FAK:Shc:Grb2:Sos]	$k_5[p-FAK:Shc][Grb2:Sos]-$ $k_{r5}[p-FAK:p-Shc:Grb2:Sos]$	(8)
6	[p-FAK:p-Shc:Grb2:Sos] ↔ [p-FAK] + [p-Shc:Grb2:Sos]	$k_6[p-FAK:p-Shc:Grb2:Sos]-$ $k_{r6}[p-FAK][p-Shc:Grb2:Sos]$	(8)
7	[p-Shc:Grb2:Sos] → [p-Shc] + [Grb2:Sos]	$k_7[p-Shc:Grb2:Sos]$	(8)
8	[p-Shc] → [Shc]	$\frac{V_8[p-Shc]}{K_{m8}+[p-Shc]}$	(8)
9	[Ras:GDP] → [Ras:GTP]	$k_9\frac{[p-Shc:Grb2:Sos][Ras:GTP]}{K_{m9}+[Ras:GTP]}$	(8)
10	[Ras:GTP] → [Ras:GDP]	$\frac{V_{10}[Ras:GTP]}{K_{m10}+[Ras:GTP]}$	(8)
11	[MEKK1] → [p-MEKK1]	$k_{11}\frac{[Ras:GTP][MEKK1]}{K_{m11}+[MEKK1]}$	(10)
12	[p-MEKK1] → [MEKK1]	$\frac{V_{12}[p-MEKK1]}{K_{m12}+[p-MEKK1]}$	(10)
13	[JNKK] → [p-JNKK]	$k_{13}\frac{[p-MEKK1][JNKK]}{K_{m13}+[JNKK]}$	(10)
14	[p-JNKK] → [JNKK]	$\frac{V_{14}[p-JNKK]}{K_{m14}+[p-JNKK]}$	(10)
15	[p-JNKK] → [pp-JNKK]	$k_{15}\frac{[p-MEKK1][p-JNKK]}{K_{m15}+[p-JNKK]}$	(10)
16	[pp-JNKK] → [p-JNKK]	$\frac{V_{16}[pp-JNKK]}{K_{m16}+[pp-JNKK]}$	(10)
17	[JNK] → [p-JNK]	$k_{17}\frac{[pp-JNKK][JNK]}{K_{m17}+[JNK]}$	(10)
18	[p-JNK] → [JNK]	$\frac{V_{18}[p-JNK]}{K_{m18}+[p-JNK]}$	(10)

19	[p-JNK] → [pp-JNK]	$k_{19}\frac{[pp-JNKK][p-JNK]}{K_{m19}+[p-JNK]}$	(10)
20	[pp-JNK] → [p-JNK]	$\frac{V_{20}[pp-JNK]}{K_{m20}+[pp-JNK]}$	(10)
21	[AP-1 (inactive)] → [AP-1 (active)]	$k_{21}\frac{[pp-JNK][AP-1_{(inactive)}]}{K_{m21}+[AP-1_{(inactive)}]}$	Assum.
22	[AP-1 (active)] → [AP-1 (inactive)]	$\frac{V_{22}[AP-1_{(active)}]}{K_{m22}+[AP-1_{(active)}]}$	Assum.
*23	ϕ → [KLF2]	$\frac{\exp(0.55(5-t/3600))/(3600\cdot 29.256)}{(1+2\cdot\exp(0.55(5-t/3600))+\exp(1.1(5-t/3600)))}$	(12)
24	ϕ → [eNOS (mRNAn)]	$k_{24t1}[AP-1_{(active)}]+k_{24t2}[KLF2]$	Assum.
25	[eNOS (mRNAn)] → [eNOS (mRNAc)]	$k_{25}[eNOS_{mRNAn}]$	(9)
26	[eNOS (mRNAc)] → ϕ	$k_{26}[eNOS_{mRNAc}]$	(11)
27	ϕ → [eNOS:Cav-1]	$\frac{V_{27}[eNOS_{mRNAc}]}{K_{m27}+[eNOS_{mRNAc}]}$	Assum.

*** Time-dependent functions describing FAK, Src activation, and KLF2 expression were generated from the experimental data in (5, 6, 12). The shear stress waveform used in (5, 6) is a laminar flow of 12 dynes/cm^2, the shear stress waveform used in (12) is an oscillatory (1 Hz) flow of 12±4 dynes/cm^2.**

List of parameters:

	Units	Ref.	Ref. value	Model value
k_3	$nM^{-1} \cdot s^{-1}$	(8)	0.1	0.1
k_{r3}	s^{-1}	(8)	1.0	1.0
k_4	$nM^{-1} \cdot s^{-1}$	(7)	8.33	8.33
k_{r4}	s^{-1}	(8)	5.0	5.0
k_5	$nM^{-1} \cdot s^{-1}$	(8)	60	60
k_{r5}	s^{-1}	(8)	546	546
k_6	s^{-1}	(8)	2040	2040
k_{r6}	$nM^{-1} \cdot s^{-1}$	(8)	15700	15700
k_7	s^{-1}	(8)	40.8	40.8
V_8	$nM \cdot s^{-1}$	(8)	0.0154	154
K_{m8}	nM	(8)	340	340
k_9	s^{-1}	(8)	0.222	0.222
K_{m9}	nM	(8)	0.181	0.181
V_{10}	$nM \cdot s^{-1}$	(8)	0.289	0.289
K_{m10}	nM	(8)	0.0571	0.0571
k_{11}	s^{-1}	Estimated from (10)	---	0.035
K_{m11}	nM	(10)	10	10
V_{12}	$nM \cdot s^{-1}$	(10)	0.25	0.125
K_{m12}	nM	(10)	8.0	8.0
k_{13}	s^{-1}	(10)	0.025	0.005
K_{m13}	nM	(10)	15.0	15.0
V_{14}	$nM \cdot s^{-1}$	(10)	0.75	0.375
K_{m14}	nM	(10)	15.0	15.0
k_{15}	s^{-1}	(10)	0.025	0.005
K_{m15}	nM	(10)	15.0	15.0
V_{16}	$nM \cdot s^{-1}$	(10)	0.75	0.375
K_{m16}	nM	(10)	15.0	15.0

k_{17}	s^{-1}	(10)	0.025	0.002
K_{m17}	nM	(10)	15.0	30.0
V_{18}	nM• s^{-1}	(10)	0.5	0.05
K_{m18}	nM	(10)	15.0	15.0
k_{19}	s^{-1}	(10)	0.025	0.002
K_{m19}	nM	(10)	15.0	30.0
V_{20}	nM• s^{-1}	(10)	0.5	0.05
K_{m20}	nM	(10)	15.0	15.0
k_{21}	s^{-1}	Estimated from fitting exp. data	---	$5.0 * 10^{-5}$
K_{m21}	nM	Estimated from fitting exp. data	---	25.0
V_{22}	nM• s^{-1}	Estimated from fitting exp. data	---	0.002
K_{m22}	nM	Estimated from fitting exp. data	---	5
k_{24t1}	s^{-1}	Estimated from fitting exp. data	---	$1.2 * 10^{-4}$
k_{24t2}	s^{-1}	Estimated from fitting exp. data	---	$9.0 * 10^{-6}$
k_{25}	s^{-1}	(9)	0.001	0.001
k_{26}	s^{-1}	Estimated from (11)	$1.1 * 10^{-5}$	$2.8 * 10^{-5}$
V_{27}	nM• s^{-1}	Estimated from fitting exp. data	---	0.02824
K_{m27}	nM	Estimated from fitting exp. data	---	16

References for model 3:
(5-12)

Model 4: Shear stress-induced NO production

Model Diagram:

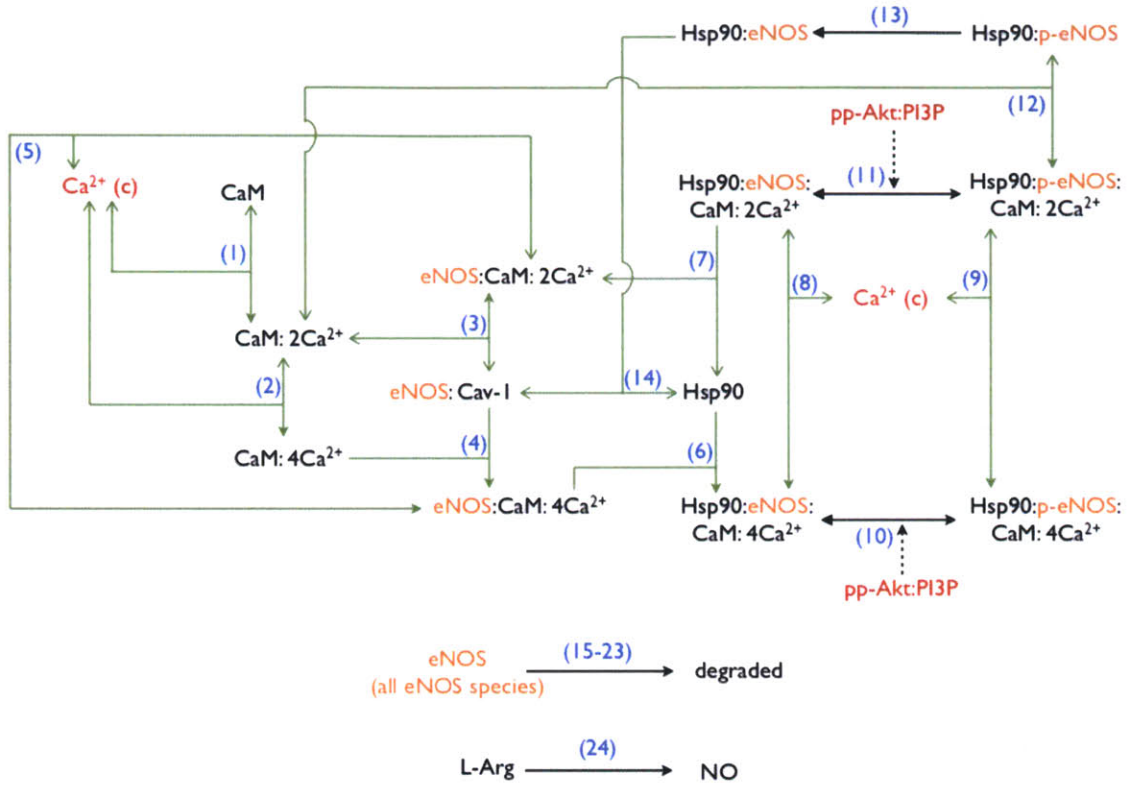

List of species:

Species	Name	*Initial Amount	Ref.
Ca^{2+} (c)	Cytosolic calcium	117.2 nM	See Model 1
pp-Akt:PI3P	Biphosphorylated Akt	1.72 nM	See Model 2
CaM	Calmodulin	7635.36 nM	Total CaM concentration 8000 nM (estimate)
CaM:2Ca^{2+}	2 calcium bound calmodulin	347.52 nM	---
CaM:4Ca^{2+}	4 calcium bound calmodulin	2.83 nM	---
eNOS: Cav-1	eNOS (inactive due to Cav-1 binding)	34.98 nM	Total eNOS concentration 50 nM (estimate)
eNOS:CaM:2Ca^{2+}	eNOS protein complex	2.12 nM	---
eNOS:CaM:4Ca^{2+}	eNOS protein complex with calcium/calmodulin-induced activation	0.04 nM	---
Hsp90	Heat shock protein 90	199987 nM	Total Hsp90 concentration 200000 nM (estimate)
Hsp90:eNOS: CaM:2Ca^{2+}	eNOS protein complex	10.98 nM	---
Hsp90:p-eNOS: CaM:2Ca^{2+}	Phosphorylated eNOS protein complex	0.11 nM	---
Hsp90:eNOS: CaM:4Ca^{2+}	eNOS protein complex with calcium/calmodulin-induced activation	1.04 nM	---

Hsp90:p-eNOS: CaM:4Ca^{2+}	Phosphorylated eNOS protein complex with calcium/calmodulin-induced activation	0.01 nM	---
Hsp90:eNOS	eNOS protein complex	0.08 nM	---
Hsp90:p-eNOS	Phosphorylated eNOS protein complex	0.64 nM	---
NO	Nitric Oxide	0 (relative scale)	---

*** Initial amounts were obtained by simulating the model under "no flow" condition, with the reference value as initial concentrations, for a sufficient amount of time to reach steady state.**

List of reactions:

#	Description	Rate equation	*Ref.
1	[CaM] ↔ [CaM:2Ca^{2+}]	$k_1 \cdot [CaM][Ca^{2+}] - k_{1r} \cdot [CaM:2Ca^{2+}]$	Assum.
2	[CaM:2Ca^{2+}] ↔ [CaM:4Ca^{2+}]	$k_2 \cdot [CaM:2Ca^{2+}][Ca^{2+}] - k_{2r} \cdot [CaM:4Ca^{2+}]$	Assum.
3	[CaM:2Ca^{2+}] + [eNOS:Cav-1] ↔ [eNOS:CaM:2Ca^{2+}]	$k_3 \cdot [CaM:2Ca^{2+}][eNOS:Cav-1] - k_{3r} \cdot [eNOS:CaM:2Ca^{2+}]$	Assum.
4	[CaM:4Ca^{2+}] + [eNOS:Cav-1] → [eNOS:CaM:4Ca^{2+}]	$k_4 \cdot [CaM:4Ca^{2+}][eNOS:Cav-1]$	Assum.
5	[eNOS:CaM:4Ca^{2+}] ↔ [eNOS:CaM:2Ca^{2+}]	$k_5 \cdot [eNOS:CaM:4Ca^{2+}] - k_{5r} \cdot [eNOS:CaM:2Ca^{2+}][Ca^{2+}]$	Assum.
6	[eNOS:CaM:4Ca^{2+}] + [Hsp90] → [Hsp90:eNOS:CaM:4Ca^{2+}]	$k_6 \cdot [eNOS:CaM:4Ca^{2+}][Hsp90]$	Assum.
7	[Hsp90:eNOS:CaM:2Ca^{2+}] → [eNOS:CaM:2Ca^{2+}] + [Hsp90]	$k_7 \cdot [Hsp90:eNOS:CaM:2Ca^{2+}]$	Assum.
8	[Hsp90:eNOS:CaM:4Ca^{2+}] ↔ [Hsp90:eNOS:CaM:2Ca^{2+}]	$k_8 \cdot [Hsp90:eNOS:CaM:4Ca^{2+}] - k_{8r} \cdot [Hsp90:eNOS:CaM:2Ca^{2+}][Ca^{2+}]$	Assum.
9	[Hsp90:p-eNOS:CaM:4Ca^{2+}] ↔ [Hsp90:p-eNOS:CaM:2Ca^{2+}]	$k_9 \cdot [Hsp90:p-eNOS:CaM:4Ca^{2+}] - k_{9r} \cdot [Hsp90:p-eNOS:CaM:2Ca^{2+}][Ca^{2+}]$	Assum.
10	[Hsp90:eNOS:CaM:4Ca^{2+}] ↔ [Hsp90:p-eNOS:CaM:4Ca^{2+}]	$\frac{k_{10}[pp-AKT:PI3P][Hsp90:eNOS:CaM:4Ca^{2+}]}{K_{m10}+[Hsp90:eNOS:CaM:4Ca^{2+}]} - \frac{V_{10r}[Hsp90:p-eNOS:CaM:4Ca^{2+}]}{K_{m10r}+[Hsp90:p-eNOS:CaM:4Ca^{2+}]}$	Assum.
11	[Hsp90:eNOS:CaM:2Ca^{2+}] ↔ [Hsp90:p-eNOS:CaM:2Ca^{2+}]	$\frac{k_{11}[pp-AKT:PI3P][Hsp90:eNOS:CaM:2Ca^{2+}]}{K_{m11}+[Hsp90:eNOS:CaM:2Ca^{2+}]} - \frac{V_{11r}[Hsp90:p-eNOS:CaM:2Ca^{2+}]}{K_{m11r}+[Hsp90:p-eNOS:CaM:2Ca^{2+}]}$	Assum.
12	[Hsp90:p-eNOS:CaM:2Ca^{2+}] ↔ [Hsp90:p-eNOS] +	$k_{12} \cdot [Hsp90:p-eNOS:CaM:2Ca^{2+}] - k_{12r} \cdot [Hsp90:p-eNOS][CaM:2Ca^{2+}]$	Assum.

12	[Hsp90:p-eNOS:CaM:2Ca^{2+}] ↔ [Hsp90:p-eNOS] + [CaM:2Ca^{2+}]	$k_{12} \cdot [Hsp90 : p-eNOS : CaM : 2Ca^{2+}] - k_{12r} \cdot [Hsp90 : p-eNOS][CaM : 2Ca^{2+}]$	Assum.
13	[Hsp90:p-eNOS] → [Hsp90: eNOS]	$\frac{V_{13}[Hsp90 : p-eNOS]}{K_{m13} + [Hsp90 : p-eNOS]}$	Assum.
14	[Hsp90:eNOS] → [Hsp90] + [eNOS:Cav-1]	$k_{14} \cdot [Hsp90 : eNOS]$	Assum.
15	[eNOS:Cav-1] → ϕ	$k_D \cdot [eNOS : Cav-1]$	Assum.
16	[eNOS:CaM:2Ca^{2+}] → ϕ + [CaM:2Ca^{2+}]	$k_D \cdot [eNOS : CaM : 2Ca^{2+}]$	Assum.
17	[eNOS:CaM:4Ca^{2+}] → ϕ + [CaM:4Ca^{2+}]	$k_D \cdot [eNOS : CaM : 4Ca^{2+}]$	Assum.
18	[Hsp90:eNOS:CaM:2Ca^{2+}] → ϕ + [CaM:2Ca^{2+}] + [Hsp90]	$k_D \cdot [Hsp90 : eNOS : CaM : 2Ca^{2+}]$	Assum.
19	[Hsp90:eNOS:CaM:4Ca^{2+}] → ϕ + [CaM:4Ca^{2+}] + [Hsp90]	$k_D \cdot [Hsp90 : eNOS : CaM : 4Ca^{2+}]$	Assum.
20	[Hsp90:p-eNOS:CaM:2Ca^{2+}] → ϕ + [CaM:2Ca^{2+}] + [Hsp90]	$k_D \cdot [Hsp90 : p-eNOS : CaM : 2Ca^{2+}]$	Assum.
21	[Hsp90:p-eNOS:CaM:4Ca^{2+}] → ϕ + [CaM:4Ca^{2+}] + [Hsp90]	$k_D \cdot [Hsp90 : p-eNOS : CaM : 4Ca^{2+}]$	Assum.
22	[Hsp90:p-eNOS] → ϕ + [Hsp90]	$k_D \cdot [Hsp90 : p-eNOS]$	Assum.
23	[Hsp90:eNOS] → ϕ + [Hsp90]	$k_D \cdot [Hsp90 : eNOS]$	Assum.
24	ϕ → [NO]	$k_{CaM} \cdot [Hsp90 : eNOS : CaM : 4Ca^{2+}] + k_{CaM} \cdot [Hsp90 : p-eNOS : CaM : 4Ca^{2+}] + k_{CaM} \cdot [eNOS : CaM : 4Ca^{2+}] + k_p \cdot [Hsp90 : p-eNOS : CaM : 2Ca^{2+}] + k_p \cdot [Hsp90 : p-eNOS]$	Assum.

*** All reactions from this model were generated based on our assumptions.**

List of parameters:

	Units	Ref.	Ref. value	Model value
k_1	$nM^{-1} \cdot s^{-1}$	Estimated from (13)	---	0.004
k_{1r}	s^{-1}	Estimated from (13)	---	10.3
k_2	$nM^{-1} \cdot s^{-1}$	Estimated from (13)	---	0.08
k_{2r}	s^{-1}	Estimated from (13)	---	1152
k_3	$nM^{-1} \cdot s^{-1}$	Initial estimate	---	$1.5 * 10^{-4}$
k_{3r}	s^{-1}	Initial estimate	---	1.5
k_4	$nM^{-1} \cdot s^{-1}$	Initial estimate	---	0.015
k_5	s^{-1}	Estimated from (13)	---	115.2
k_{5r}	$nM^{-1} \cdot s^{-1}$	Estimated from (13)	---	0.08
k_6	$nM^{-1} \cdot s^{-1}$	Estimated from (15)	---	0.002
k_7	s^{-1}	Estimated from (15)	---	1.5
k_8	s^{-1}	Estimated from (13)	---	115.2
k_{8r}	$nM^{-1} \cdot s^{-1}$	Estimated from (13)	---	0.08

k_9	s^{-1}	Estimated from (13)	---	115.2
k_{9r}	$nM^{-1} \bullet s^{-1}$	Estimated from (13)	---	0.08
k_{10}	s^{-1}	Estimated from fitting exp. data	---	0.1
K_{m10}	nM	Estimated from fitting exp. data	---	5
V_{10r}	$nM \bullet s^{-1}$	Estimated from fitting exp. data	---	4
K_{m10r}	nM	Estimated from fitting exp. data	---	20
k_{11}	s^{-1}	Estimated from fitting exp. data	---	0.1
K_{m11}	nM	Estimated from fitting exp. data	---	5
V_{11r}	$nM \bullet s^{-1}$	Estimated from fitting exp. data	---	4
K_{m11r}	nM	Estimated from fitting exp. data	---	20
k_{12}	s^{-1}	Initial estimate	---	1.5
k_{12r}	$nM^{-1} \bullet s^{-1}$	Initial estimate	---	$1.5 * 10^{-4}$
V_{13}	$nM \bullet s^{-1}$	Estimated from fitting exp. data	---	4
K_{m13}	nM	Estimated from fitting exp. data	---	20
k_{14}	s^{-1}	Estimated from (15)	---	1.5
k_D	s^{-1}	Estimated from half life (16)	$1.13 * 10^{-5}$	$9.45 * 10^{-5}$
k_{CaM}	s^{-1}	Estimated from (14)	---	17
k_p	s^{-1}	Estimated from (14)	---	5

References for model 4:
(13-16)

Model diagram legends:

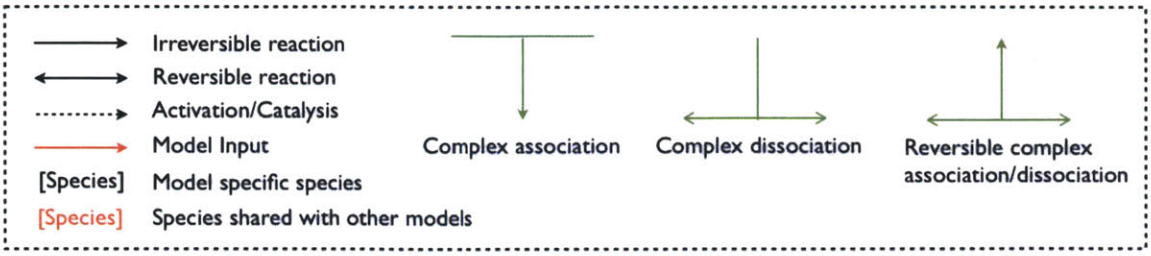

APPENDIX REFERENCES

1. Wiesner, T. F., B. C. Berk, and R. M. Nerem. 1996. A mathematical model of cytosolic calcium dynamics in human umbilical vein endothelial cells. Am J Physiol 270:C1556-1569.
2. Wiesner, T. F., B. C. Berk, and R. M. Nerem. 1997. A mathematical model of the cytosolic-free calcium response in endothelial cells to fluid shear stress. Proc Natl Acad Sci USA 94:3726-3731.
3. Koh, G., H. F. C. Teong, M.-V. Clément, D. Hsu, and P. S. Thiagarajan. 2006. A decompositional approach to parameter estimation in pathway modeling: a case study of the Akt and MAPK pathways and their crosstalk. Bioinformatics 22:e271-280.
4. Go, Y. M., H. Park, M. C. Maland, V. M. Darley-Usmar, B. Stoyanov, R. Wetzker, and H. Jo. 1998. Phosphatidylinositol 3-kinase gamma mediates shear stress-dependent activation of JNK in endothelial cells. Am J Physiol 275:H1898-1904.
5. Li, S., M. Kim, Y. L. Hu, S. Jalali, D. D. Schlaepfer, T. Hunter, S. Chien, and J. Y. Shyy. 1997. Fluid shear stress activation of focal adhesion kinase. Linking to mitogen-activated protein kinases. J Biol Chem 272:30455-30462.
6. Jalali, S., Y. S. Li, M. Sotoudeh, S. Yuan, S. Li, S. Chien, and J. Y. Shyy. 1998. Shear stress activates p60src-Ras-MAPK signaling pathways in vascular endothelial cells. Arterioscler Thromb Vasc Biol 18:227-234.
7. Yee, K. L., V. M. Weaver, and D. A. Hammer. 2008. Integrin-mediated signalling through the MAP-kinase pathway. IET Syst Biol 2:8-15.
8. Hatakeyama, M., S. Kimura, T. Naka, T. Kawasaki, N. Yumoto, M. Ichikawa, J. H. Kim, K. Saito, M. Saeki, M. Shirouzu, S. Yokoyama, and A. Konagaya. 2003. A computational model on the modulation of mitogen-activated protein kinase (MAPK) and Akt pathways in heregulin-induced ErbB signalling. Biochem J 373:451-463.
9. Yamada, S., S. Shiono, A. Joo, and A. Yoshimura. 2003. Control mechanism of JAK/STAT signal transduction pathway. FEBS Lett 534:190-196.
10. Kholodenko, B. N. 2000. Negative feedback and ultrasensitivity can bring about oscillations in the mitogen-activated protein kinase cascades. Eur J Biochem 267:1583-1588.
11. Weber, M., C. H. Hagedorn, D. G. Harrison, and C. D. Searles. 2005. Laminar shear stress and 3' polyadenylation of eNOS mRNA. Circ Res 96:1161-1168.
12. Young, A., W. Wu, W. Sun, H. Benjamin Larman, N. Wang, Y. S. Li, J. Y. Shyy, S. Chien, and G. Garcia-Cardena. 2009. Flow activation of AMP-activated protein kinase in vascular endothelium leads to Kruppel-like factor 2 expression. Arterioscler Thromb Vasc Biol 29:1902-1908.
13. Black, D. J., J. Leonard, and A. Persechini. 2006. Biphasic Ca2+-dependent switching in a calmodulin-IQ domain complex. Biochemistry 45:6987-6995.
14. Kuchan, M. J., and J. A. Frangos. 1994. Role of calcium and calmodulin in flow-induced nitric oxide production in endothelial cells. Am J Physiol 266:C628-636.
15. Garcia-Cardena, G., R. Fan, V. Shah, R. Sorrentino, G. Cirino, A. Papapetropoulos, and W. C. Sessa. 1998. Dynamic activation of endothelial nitric oxide synthase by Hsp90. Nature 392:821-824.
16. Liu, J., G. Garcia-Cardena, and W. C. Sessa. 1995. Biosynthesis and palmitoylation of endothelial nitric oxide synthase: mutagenesis of palmitoylation sites, cysteines-15 and/or -26, argues against depalmitoylation-induced translocation of the enzyme. Biochemistry 34:12333-12340.

Chapter 3: Hemodynamic Shear Stress Characteristic of Atherosclerosis–Resistant Regions Promotes Glycocalyx Formation in Cultured Endothelial Cells

3.1 Introduction

The vascular endothelium is a single layer of cells lining the inner surface of blood vessels. This cellular layer not only serves as an interface between blood and surrounding tissues, but also plays important roles in inflammation (28), angiogenesis (5), blood coagulation (9), and control of vascular tone (27). Endothelial dysfunction, the state in which the endothelial cells can no longer respond to external stimuli to preserve homeostasis, is frequently followed by deterioration of vascular function and development of several vascular pathologies including atherosclerosis (17). Interestingly, multiple studies have shown in both experimental animals and human subjects that the location where early lesions of atherosclerosis develop is highly focal in nature. For example, in the carotid artery, early atherosclerotic lesions are more frequently observed at the carotid sinus bifurcation, where the endothelium is exposed to disturbed flow and displays several distinct cell biological features, including scarce expression of the endothelial glycocalyx layer (EGL) (10, 18, 22, 55, 56). In contrast, the common carotid region is resistant to the development of early lesions of atherosclerosis where the endothelium is exposed to laminar flow and displays abundant expression of the EGL (10, 18, 22, 55, 56). Collectively, these observations have defined a correlation between atheroprotection, shear stress, and EGL expression.

The EGL is a gel like structure present on the apical surface of the endothelial cells (13, 46, 59). It is mainly composed of three glycosaminoglycans (GAGs), heparan sulfate, chondroitin sulfate, and hyaluronic acid. Heparan sulfate is bound to proteoglycans including syndecan-1, syndecan-2, syndecan-4, and glypican-1; chondroitin sulfate is bound to biglycan and the above mentioned syndecans; and hyaluronic acid is electrostatically attached to CD44 (50). All three negatively charged GAGs tangle together and form the characteristic glycocalyx structure observed by electron microscopy (48, 55, 59).

One of the main functions of the glycocalyx is to regulate vascular permeability and modulate binding of molecules that interact with the endothelial receptors. This process is

achieved through two main mechanisms. The EGL can directly bind to some biomolecules and increase their local concentration, and it can also selectively block some other biomolecules and prevent them from reaching the endothelial surface (1, 3, 33). There is also evidence that the endothelial glycocalyx may act as a mechanosensor. When endothelial cells are subjected to flow, the cells adapt to the mechanical stimuli by reorganizing the cytoskeleton (24, 34, 53), aligning to the direction of the flow (42), releasing the vasodilator nitric oxide (NO)(43), suppressing the proliferation rate (34), and decreasing the migration speed (25). Interestingly, these flow-mediated responses are impaired when the EGL is compromised: For example, studies by the laboratory of J. Tarbell have demonstrated that when cultured endothelial cells are pretreated with heparinase or hyaluronidase to remove heparan sulfate or hyaluronic acid from the EGL, these cells no longer reorganize the cytoskeleton or produce NO in response to flow (14, 35, 53). Previous work by our laboratory and others have also shown that after heparanase-based removal of heparan sulfate proteoglycans, the endothelial cells lose the ability to sense flow and to modulate its migration speed and proliferation rate (32, 60). Finally, recent studies by Constantinescu *et al.* and Mulivor and Lipowsky (8, 33) established a correlation between damaged EGL and leukocyte adhesion, linking the presence of EGL to endothelial activation. Collectively, these studies document that expression of the EGL is critical for the endothelium to properly respond to the hemodynamic environment and to function as a protective barrier in the context of inflammation.

The abundance of EGL is dynamically controlled by both production and degradation - transport of newly produced proteoglycans from the ER/Golgi to the cellular membrane, and endocytic degradation or shedding of the proteoglycans from the cell surface by matrix metalloprotease family proteins and other enzymes such as heparanase, chondroitinase, and hyaluronidase. Several *in vivo* measurements have been made on EGL thickness. The pioneering intravital microscopy work by Vink and Duling showed the EGL height in hamster muscle capillaries to be 0.4 to 0.5 μm (58). A similar value was found in Potter and Damiano's microparticle image velocimetry measurement on mouse cremaster venules (38) and Chappell's transmission electron microscopy work on human umbilical vein (6). Recent work by van den Berg *et al.* using confocal laser scanning microscopy demonstrated the EGL thickness in mouse aorta can go as high as 2 to 4 μm (54). The conclusion from these *in vivo* measurements is that the EGL is 0.4 – 4 μm thick. However, whether the glycocalyx layer is also present in cultured

endothelial cells remains a major question in the field. Several studies have demonstrated that the EGL is almost absent in various cultured endothelial cell types, including human umbilical vein endothelial cells (HUVEC) and bovine aortic endothelial cells (BAEC) (6, 20, 38). In contrast, data from other studies support the presence of similar EGL abundance *in vitro* as *in vivo* (11, 49, 53). A recent work by Ebong *et al.* using rapid freezing/freeze substitution transmission electron microscopy has even shown an EGL thickness of 11 μm in cultured BAEC (13). These contradictory data suggest that the integrity of EGL *in vitro* may be highly sensitive to factors such as cell type, cultured condition, and preservation/processing techniques. However, to date little is known regarding specific biomechanical or biochemical inputs capable of inducing or suppressing the expression of components of the EGL.

In this study, we hypothesized that the expression of critical components of the EGL is regulated by specific shear stress waveforms present in atherosclerosis-resistant or atherosclerosis-susceptible regions of the human vasculature.

3.2 Material and Methods

Endothelial Cell Culture

Primary human umbilical endothelial cells (HUVEC) were isolated in the Department of Pathology, Center for Excellence in Vascular Biology, Brigham and Women's Hospital, as previously described (16). HUVEC were cultured in M199 medium containing 20% calf serum, 1% L-glutamine, 1% penicillin/ streptomycin, 50 μg/ml endothelial cell growth supplement (Biomedical Technologies, Stoughton, MA), and 100 μg/ml heparin. Cells were incubated in a humidified incubator at 37° C and 5% CO_2. After reaching confluence, cells were detached with 1% trypsin and plated onto a 0.1% gelatin coated 10.8 cm polystyrene plate surface (Plaskolite, Inc., Columbus, OH) for shear stress experiments.

Hemodynamic Shear Stress *in vitro* System

The shear experiments implementing the atheroprotective and atheroprone shear stress waveforms were conducted in a modified dynamic flow system as previously described (10). For these experiments, the culture medium was supplemented with 1.7 % dextran (MW 1.5-2.8 million, Sigma-Aldrich, St. Louis, MO) to increase media viscosity to 2.1 cP. The flow system was kept at 37° C and 5% CO_2 in humidified air.

Flow Cytometric Analysis

Surface expression of glycosaminoglycans and their protein carriers were measured using flow cytometry. The following primary antibodies were used: anti-syndecan-1 antibody (1:10, Biotin-conjugated mouse IgG_1, clone B-A38, Abcam, Cambridge, MA), anti-syndecan-2 antibody (1:10, APC-conjugated rat IgG_{2B}, R&D Systems, Minneapolis, MN), anti-syndecan-4 antibody (1:5, Biotin-conjugated goat IgG, R&D Systems), anti-glypican-1 antibody (1:5, Biotin-conjugated goat IgG, R&D Systems), anti-CD44 antibody (1:5, Biotin-conjugated mouse IgG_{2B}, BD Biosciences, Bedford, MA), anti-heparan sulfate antibody (1:100, mouse IgM, clone 10E4, US Biological, Swampscott, MA), anti-chondroitin sulfate antibody (1:50, mouse IgG_{2A}, BD Pharmingen, San Diego, CA). The primary antibodies were coupled with the appropriate Alexa Fluor 488 conjugated secondary antibodies below: goat anti-mouse IgM, goat anti-mouse IgG,

streptavidin (1:400, Invitrogen, Carlsbed, CA). Briefly, HUVEC were detached from the surface using enzyme-free PBS-based cell dissociation buffer (Invitrogen). The isolated cells were then resuspended in PBS containing 15% fetal calf serum and 0.2 mM EDTA, and blocked for 30 minutes at 4°C. The appropriate primary antibody was subsequently added to the cell suspensions and incubated at 4°C for 45 minutes. The cells were then centrifuged at 1200 rcf, washed once with PBS, and incubated with both the secondary antibody and 7AAD (1:20, BD Pharmingen) for 30 minutes. Cells were washed an additional two times before the fluorescent signal is measured with FACS (FACSCablibur, BD Biosciences). The data were analyzed and quantified with FlowJo (version 9.1, Ashland, OR).

Immunoflourescence Microscopy

Immediately after flow exposure, cells were fixed in 4% paraformaldehyde for 5 minutes. The cells were subsequently washed three times with PBS at room temperature, then blocked in 1% BSA for 30 minutes. The samples were then incubated with anti-heparan sulfate antibody (1:100, 10E4, US Biological), anti-syndecan-1 antibody (1:50, B-A38, Abcam), or anti-hyaluronic acid antibody (1:100, Abcam) for an hour, washed three times with PBS, and then incubated with the appropriate Alexa Fluor 488 secondary antibody for another hour. For nuclear staining, the cells were either incubated with DAPI (600 nM, Invitrogen) for 5 minutes, or permeabilized with 0.2% Triton X-100 in PBS for 10 minutes and then incubated with TO-PRO-3 dye (1 μM, Invitrogen) for 15 minutes. The coverslips were mounted with Gel/Mount mounting medium (Biomeda, Foster City, CA). Images were taken using a Nikon Eclipse Ti microscope. Quantification of hyaluronic acid signal was conducted using ImageJ. The relative hyaluronic acid signal was calculated by subtracting the mean signal intensity of the background (2^{nd} antibody-only control) from that of the samples. Three fields from a sample were used to derive the average signal intensity. The histogram and statistics were generated from samples collected from three independent experiments.

Confocal Immunofluorescence Microscopy

Z-stacks (0.05 micron apart) of the sample were taken using the PerkinElmer UltraView RS spinning disk confocal imaging system (PerkinElmer, Inc., Waltham, MA). Deconvolution of the

images was performed using AutoQuant Deconvolution software (MediaCybernetics, Bethesda, MD) and the 3D reconstruction was made using ImageJ (Image 3D Viewer Toolbox).

Quantitative Analysis of the Glycocalyx Coverage and the Glycocalyx Thickness

Percent coverage of the glycocalyx was calculated by determining the acquired fluorescent image's percentage of pixels in which heparan sulfate signal intensity is above a specific threshold. This threshold was set at the value where the corresponding 2nd antibody-only control had less than 0.5% "positive" pixels. Three fields (432 μm X 329 μm) from a sample were used to derive the glycocalyx coverage.

shRNA Experiments

HUVEC were transfected at 50% confluency with a lentiviral shRNA targeting human syndecan-1 (MOI: 5, TRCN000072580, Sigma-Aldrich) or a lentiviral non-target shRNA control (MOI: 5, SHC016V, Sigma-Aldrich) in media supplemented with hexadimethrine bromide (8 μg/mL). Lentiviral particles were washed out after 24 hours and the cells were grown to confluence. The cells were then treated with puromycin (5 μg/mL, Sigma-Aldrich) for 72 hours to select for transfected HUVEC followed by incubation in media without puromycin for 48 hours before conducting the flow experiments.

RNA isolation and Quantitative PCR Analysis

Cells were lysed for RNA isolation and real-time TaqMan PCR was performed as previously described (36).

Statistics

A 2-tailed Student's t test was used to determine statistical significance between two groups. Difference at $p < 0.05$ was considered statistically significant.

3.3 Results

3.3.1 Expression of components of the endothelial glycocalyx on the cell surface of static cultured HUVEC

The abundance and composition of the EGL varies across different endothelial cell types. In this study, we focused on HUVEC since these cells have been extensively used by our laboratory and others to assess the role of biomechanical forces on endothelial gene expression (10, 12, 16, 36, 47). Interestingly, out of the three GAGs commonly present on the endothelial surface, heparan sulfate is the only one that has been previously shown to be expressed in HUVEC (Fig. 3-1A)(6, 60). Hyaluronic acid, on the other hand, was reported to be absent in one study (26). The status of chondroitin sulfate is unclear since there is no study directly measuring the abundance of chondroitin sulfate expressed in HUVEC. As for the protein anchors of the glycosaminoglycans, the major carriers of heparan sulfate and chondrotin sulfate are the syndecan and glypican family proteins. Among the syndecan family members, syndecan-3 is only expressed in the neuronal cells, and the other three (syndecan-1, 2, 4) have been shown to be expressed in endothelial cells (3). Among the glypican family, glypican-1 is the only member present in endothelial cells (3, 15). Hyaluronic acid, on the other hand, is non-covalently bound to cell-surface glycoprotein CD44. For sydecan-2, syndecan-4, glycpican-1, and CD44, their expressions in HUVEC have been previously documented (Fig. 3-1A). For syndecan-1, there are studies supporting either its presence or absence in HUVEC (6, 40).

A

Components of the Endothelial Glycocalyx

Glycosaminoglycans

Name	Carrier/Receptor	Key Biosynthesis Enzymes	Expression in HUVEC	Reference
Heparan sulfate	Syndecans, Glypicans	EXT1, EXT2	Yes (IM)	Yao, Chappell
Chondroitin sulfate	Syndecans	CHSY1	Not Determined	
Hyaluronic acid	CD44	HAS1, HAS2, HAS3	No (static culture)	Lokeshwar

Protein Carriers of Glycosaminoglycans

Gene Name	Gene Symbol	Expression in HUVEC	Reference
Syndecan 1	SDC1	Unclear (IM, WB)	Chappell, Qiao
Syndecan 2	SDC2	Yes (WB)	Qiao
Syndecan 4	SDC4	Yes (WB)	Qiao
Glypican 1	GPC1	Yes (WB)	Mertens
CD44	CD44	Yes (FC, IM)	Savani

B **Surface Expression of Components of the Glycocalyx in HUVEC Cultured under Static (No Flow) Conditions**

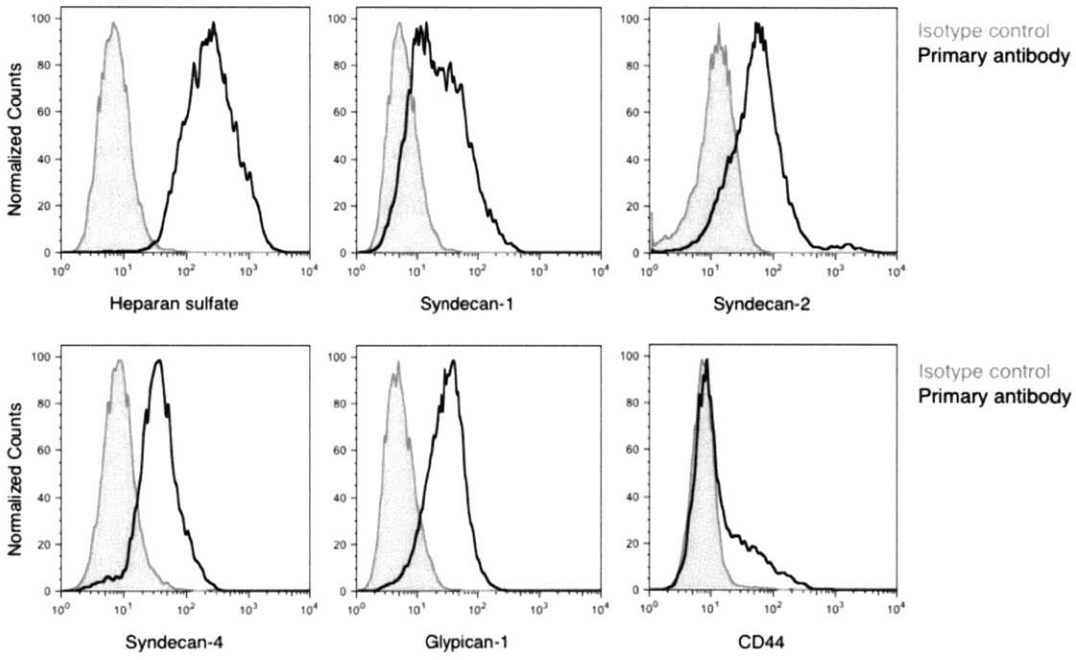

Fig. 3-1. Components of the endothelial glycocalyx in HUVEC. A) List of protein carriers and glycosaminoglycans previously documented to be part of the endothelial glycocalyx, and their expression in HUVEC (6, 26, 31, 40, 45, 60) (IM: immunostaining; WB: western blot; FC: flow cytometry). B) Representative flow cytometry analysis of the endothelial glycocalyx components present in our static cultured HUVEC.

Because the expression and subcellular localization of glycosaminoglycans and glycoproteins may be affected by the specific cultured conditions, we first examined the expression of components of the EGL in our static (no flow) primary cultured HUVEC. We used FACS analysis to directly assess the surface expression of these EGL components in these cells. As seen in Fig. 3-1B, these analyses confirmed the cell surface expression of heparan sulfate, syndecan-1, syndecan-2, syndecan-4, glypican-1, and CD44. However, signals from chondroitin sulfate and hyaluronic acid were very weak. Therefore, we conclude that the EGL in static cultured HUVEC comprises heparan sulfate anchored by syndecan-1, syndecan-2, syndecan-4, and glypican-1.

3.3.2 The expression of heparan sulfate and hyaluronic acid is regulated by specific shear stress waveforms

Given that heparan sulfate is the predominant GAG in HUVEC, we first sought to test the hypothesis that shear stress regulates its expression by quantitatively measuring heparan sulfate expression in endothelial cells exposed to two well-characterized shear stress waveforms, namely the atheroprotective waveform and the atheroprone waveform (10). Previous studies by Potter *et al.* (39) have demonstrated that the time scale for glycocalyx growth is in the order of days. When the glycocalyx was enzymatically degraded, significant recovery was observed as soon as 3 days, and a full recovery was observed after 5 to 7 days. These data suggested that 2-3 days are required for the generation of glycocalyx. Therefore, we maintained endothelial cells under static (no flow) conditions or exposed them to the atheroprotective or atheroprone waveforms for 3 days and 7 days, followed by the quantitative measurement of heparan sulfate surface expression via FACS. After exposure to atheroprotective flow for 3 days and 7 days, heparan sulfate expression was significantly increased by 54.6 ± 6.7 % and 80.6 ± 33.0 %, respectively (Figs. 3-2A and 3-2B). In contrast, atheroprone flow suppressed the heparan sulfate expression and caused a 37.2 ± 5.1 % and 28.5 ± 10.2% decrease after 3 days and 7 days, respectively. These data are consistent with our hypothesis that the expression of this GAG is regulated by the specific shear stress waveform and demonstrates that the differential expression is time dependent.

Knowing that expression of heparan sulfate can be significantly regulated by shear stress after 7 days, we next sought to find whether chondroitin sulfate and hyaluronic acid expression,

though absent in static *in vitro* cultures, can also be induced by flow. HUVEC were similarly exposed to atheroprotective or atheroprone flow for 7 days, then chondrotin sulfate surface expression was measured by FACS and hyaluronic acid expression was evaluated by immunostaining (due to electrostatic binding to its protein carriers). Our data indicated that chondroitin sulfate is still absent after exposure to either flow condition (Fig. 3-2C). Interestingly, expression of hyaluronic acid was strongly up-regulated by the atheroprotective waveform (Fig. 3-2D). Quantification of the immunostaining data (Fig. 3-2E) showed an increase to 464.7 ± 15.6 % relative to the static culture. Finally we assessed if the atheroprotective shear-stress-induced hyaluronic acid up-regulation is correlated with the expression of hyaluronic acid binding protein CD44. As seen in Fig. 3-2F, FACS data indicated that CD44 expression is not shear-stress-dependent, suggesting that the increase in hyaluronic acid under atheroprotective condition may be due to higher rate of hyaluronic acid synthesis. Collectively, our experimental data demonstrated that the two major GAGs of the endothelial glycocalyx, heparan sulfate and hyaluronic acid, are both strongly promoted by the shear stress waveform found at the atherosclerosis-resistant regions of human arteries.

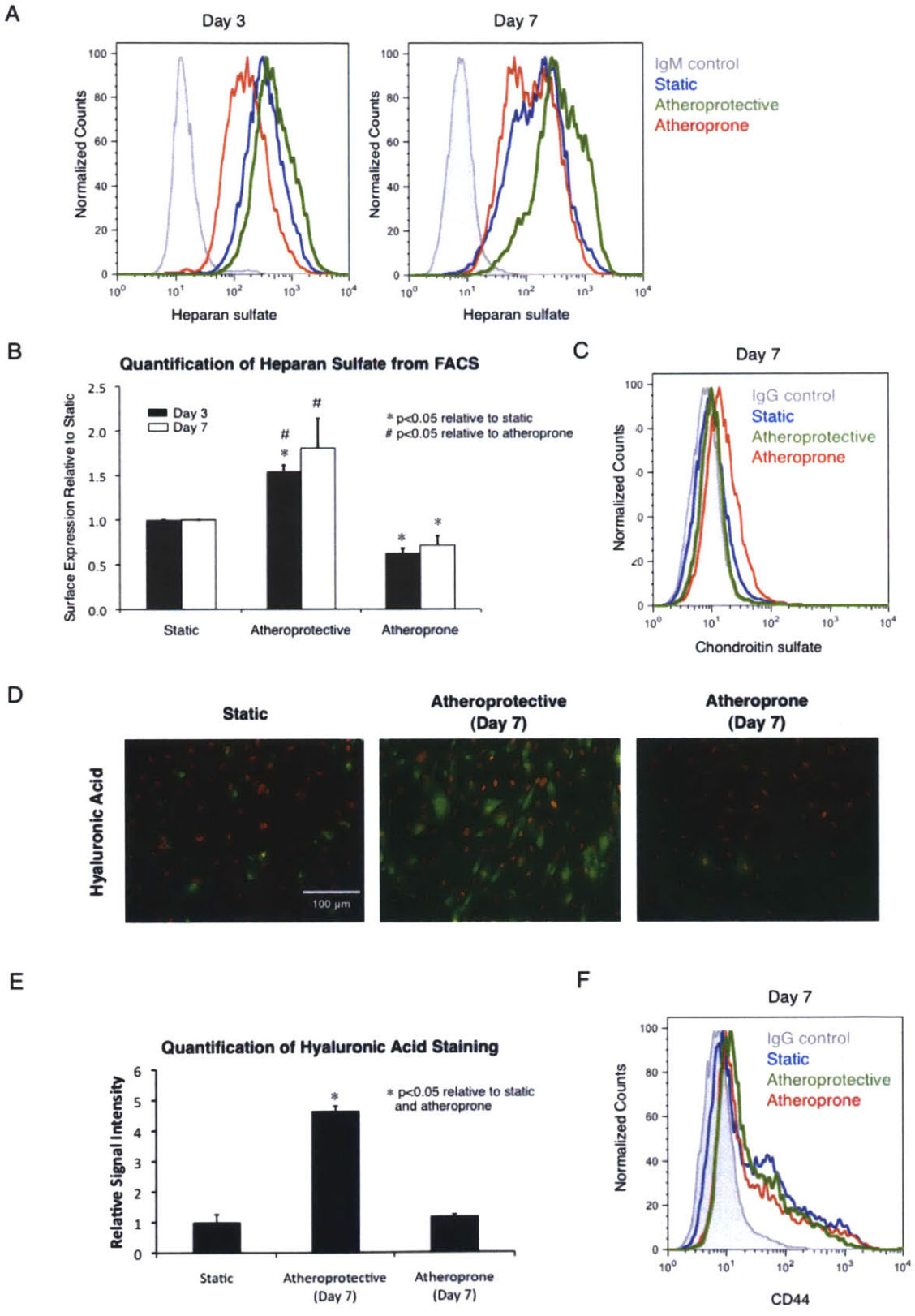

Fig. 3-2. Exposure of atheroprotective waveform leads to induced expression of heparan sulfate and hyaluronic

acid, but not chondroitin sulfate. A) Representative flow cytometry histogram of cell surface heparan sulfate expression after being cultured under static condition or being exposed to the atheroprotective or atheroprone flow for 3 days (*Left*) or 7 days (*Right*). B) Quantitative analysis of the flow cytometry data from three independent experiments (means ± SE; *$p < 0.05$ vs. static; #$p<0.05$ vs. atheroprone; N=3). C) Flow cytometry histogram of chondroitin sulfate surface expression under static condition or after exposure to atheroprone or atheroprotective shear stress waveform for 7 days. D) Representative immunostaining images of hyaluronic acid under static condition or after exposure to atheroprotective or atheroprone flow for 7 days. Hyaluronic acid is shown in green, and nucleus (DAPI) is shown in red. E) Quantitative analysis of the hyaluronic acid staining signal based on the immunostaining images (means ± SE; *$p < 0.05$ vs. static and atheroprone; N=3). F) Flow cytometry histogram of CD44 surface expression under static condition or after exposure to atheroprotective or atheroprone shear stress waveform for 7 days.

3.3.3 The distribution of heparan sulfate at the apical endothelial surface is changed after prolonged exposure to atheroprotective waveform

Since heparan sulfate is the predominant GAG constituent of the glycocalyx, and multiple studies have demonstrated its functional importance, we further investigated the cell surface distribution of this GAG in the context of the two distinct shear stress waveforms. Confocal immunofluorescence microscopy was performed in cells under static condition, and after 3 days or 7 days of exposure to atheroprotective or atheroprone shear stress waveforms. These experiments revealed that heparan sulfate distribution is also shear-stress-dependent (Fig. 3-3A). Under static or atheroprone conditions, heparan sulfate was located mostly in patches and relatively little heparan sulfate was present on the apical surface. However, a different pattern was observed for the atheroprotective condition; there was abundant expression of heparan sulfate uniformly distributed on the apical surface of the monolayer. The 3D reconstruction and the X-Z volume view of the samples in Fig. 3A were also performed to confirm this finding and validate that only the heparan sulfate on the apical surface was being analyzed. Quantification of the immunostaining images (Fig. 3-3B) showed that 42.7% (3 days) - 44.0% (7 days) of the HUVEC monolayer was covered by the EGL under static conditions. After just 3 days of atheroprotective shear stress exposure, there was no significant change in glycocalyx coverage (44.4%). However, we observed a decrease in glycocalyx coverage to 22.9% under the atheroprone waveform. The difference in glycocalyx coverage became more pronounced after 7 days of flow exposure since the coverage increased to 66.7% in the atheroprotective shear stress condition, approximately three times the expression present in the atheroprone condition (22.5%). These data document that the hemodynamic shear stress waveform not only changes the quantitative amount but also the qualitative distribution of the EGL.

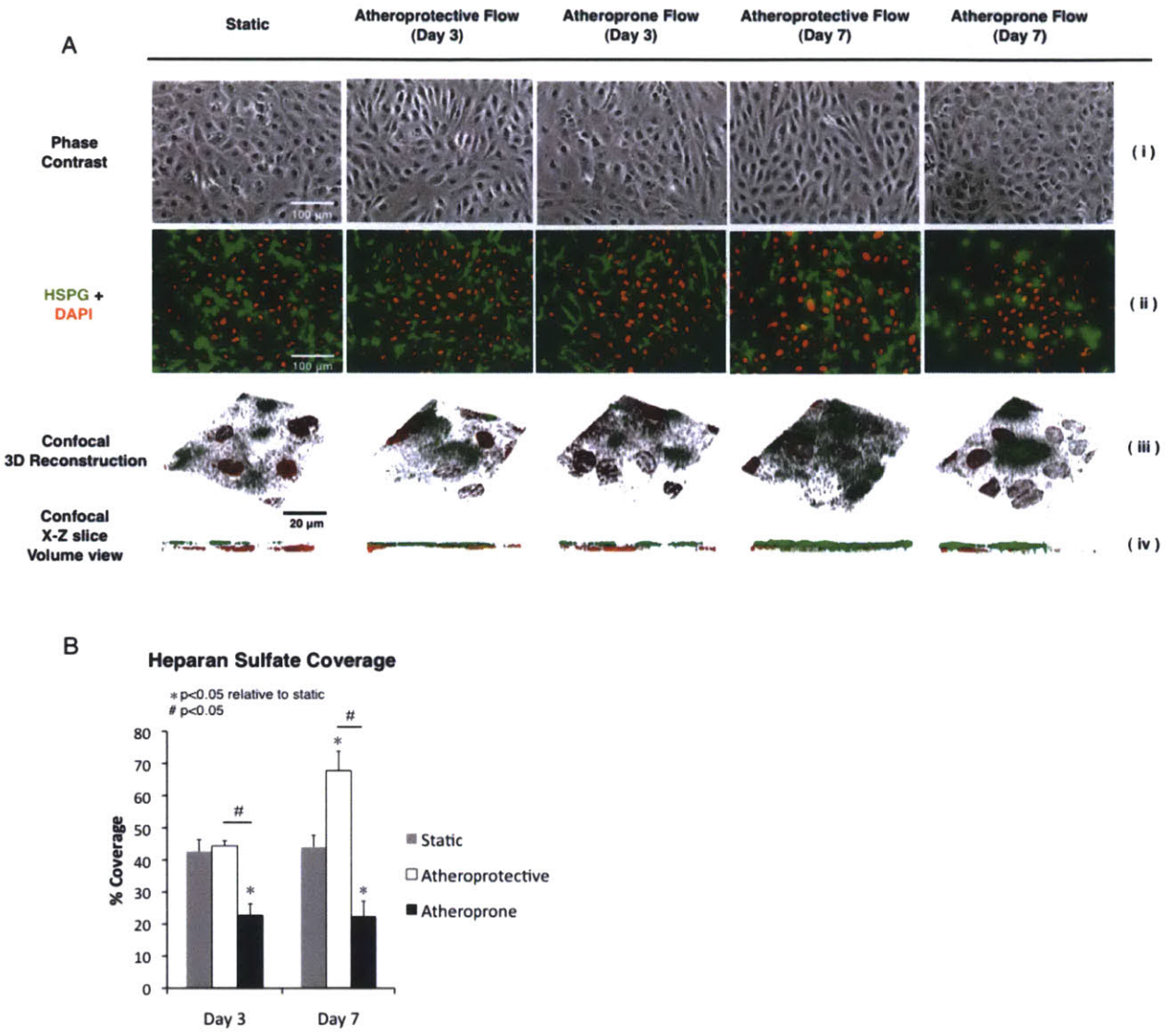

Fig. 3-3. Prolonged exposure to atheroprotective flow induces expression of heparan sulfate on the apical surface of endothelial cells. A) Representative microscopic images of endothelial cells under static condition, after 3 days exposure to atheroprotective or atheroprone flow, or after 7 days exposure to atheroprotective or atheroprone flow. i) Phase contrast; ii) Heparan sulfate is shown in green, and nucleus (DAPI) is shown in red. iii) 3D reconstruction from Z-stacks taken with confocal microscopy. Heparan sulfate is shown in green, and nucleus (TO-PRO-3) is shown in red. iv) X-Z plane side-view of the 3D reconstruction above. B) Quantitative analysis of the percentage area covered by heparan sulfate based on immunostaining images from three independent experiments (means ± SE; *$p < 0.05$ vs. static; #$p<0.05$ between samples; N=3).

3.3.4 The surface expression of Syndecan-1 is regulated by the specific shear stress waveforms

Having established that heparan sulfate expression is regulated by distinct shear stress, we next explored whether its underlying mechanism is through controlling the expression of heparan sulfate proteoglycans or modulating heparan sulfate biosynthesis. To this end we first measured the change in surface expression of heparan sulfate carrier proteins, namely syndecan-1,2,4 and glypican-1 after 7-day exposure to specific shear stress waveforms (Fig. 3-4A). For syndecan-2 and glypican-1, presence of either atheroprotective or atheroprone shear stress decreased their expression. Syndecan-4 seems to be more highly expressed (though not statistically significant) under the atheroprone condition compared to the atheroprotective condition. Syndecan-1 expression, most interestingly, was up-regulated after exposure to the atheroprotective flow but down-regulated after exposure to the atheroprone flow. These flow cytometry data were confirmed by immunostaining (Fig. 3-4B) and measurement of mRNA expression (Fig. 3-4C, *left panel*). Immunostaning of syndecan-1 revealed that the atheroprotective-flow-mediated expression is suppressed under atheroprone condition. Experiments measuring the mRNA expression of the heparan sulfate proteoglycan established a high correlation between mRNA expression and protein expression. For syndecan-1, its mRNA was expressed more than ten times in the cells exposed to the atheroprotective flow versus the atheroprone flow.

We also assessed whether shear stress affects the expression level of EXT1 and EXT2, two enzymes responsible for heparan sulfate biosynthesis. As seen in Fig. 3-4C (*right panel*), there was no significant change in EXT1 and EXT2 expression under the two shear stress conditions. These data suggest that expression of EXT1 and EXT2 is shear stress independent, and may not be critical for the flow-mediated expression of heparan sulfate. Therefore, syndecan-1 transcriptional regulation may play the most important role in shear stress-regulated heparan sulfate expression.

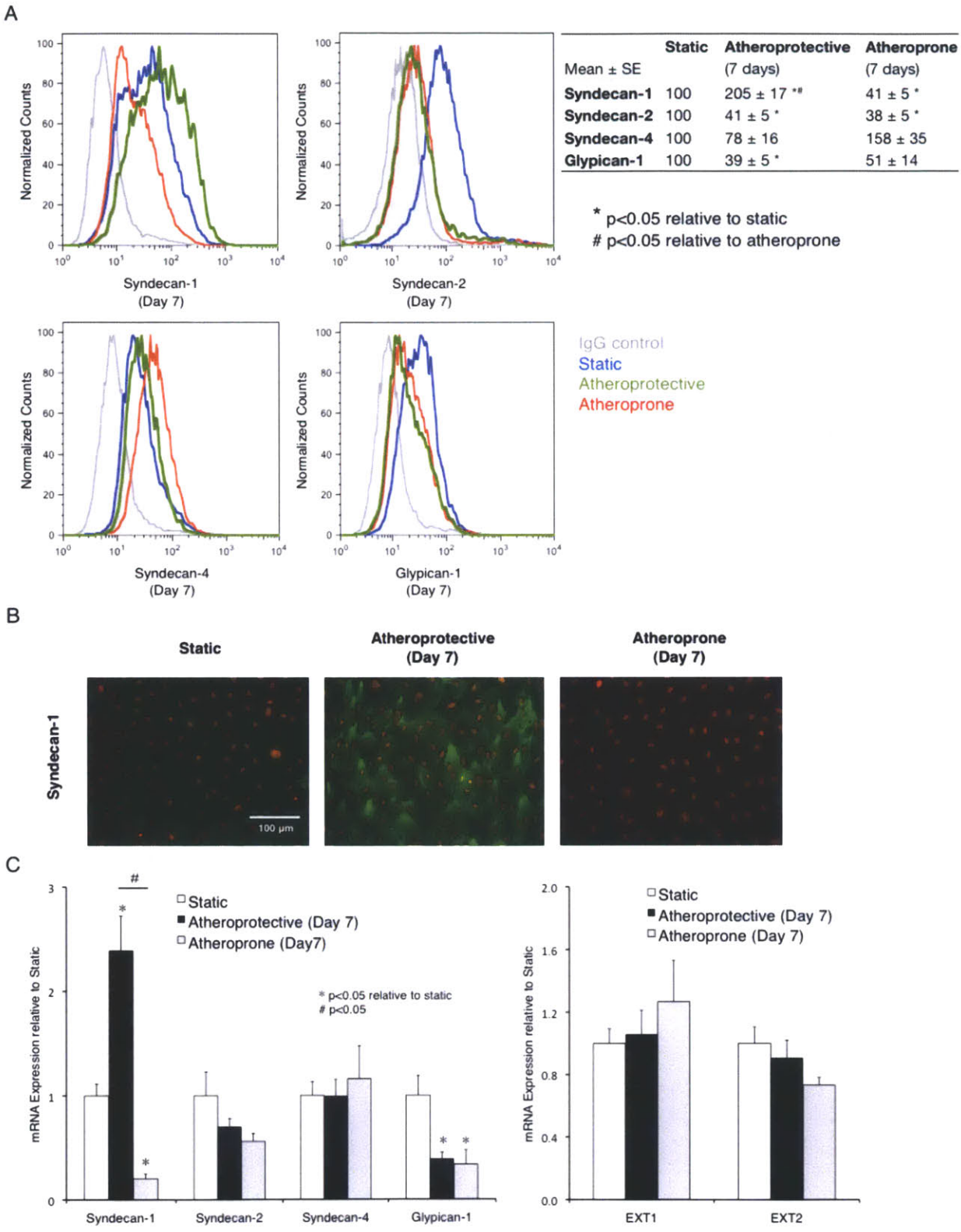

	Static	Atheroprotective (7 days)	Atheroprone (7 days)
Mean ± SE			
Syndecan-1	100	205 ± 17 *#	41 ± 5 *
Syndecan-2	100	41 ± 5 *	38 ± 5 *
Syndecan-4	100	78 ± 16	158 ± 35
Glypican-1	100	39 ± 5 *	51 ± 14

* p<0.05 relative to static
# p<0.05 relative to atheroprone

Fig. 3-4. Prolonged exposure to atheroprotective flow induces expression of syndecan-1 on the apical surface of endothelial cells. A) *Left*, Flow cytometry histogram of syndecan-1, syndecan-2, syndecan-4, and glypican-1 surface expression under static condition or after exposure to atheroprotective or atheroprone shear stress waveform

for 7 days. *Right*, Quantitative analysis of the flow cytometry data from three independent experiments (*$p < 0.05$ vs. static; #$p<0.05$ vs. atheroprone; means ± SE; N=3). B) Representative immunostaining images of syndecan-1 under static condition or after exposure to atheroprotective or atheroprone flow for 7 days. Syndecan-1 is shown in green, and nucleus (DAPI) is shown in red. C) mRNA expression of (*Left*) the heparan sulfate protein carriers and (*Right*) key enzyme specifically responsible for heparan sulfate chain biosynthesis (means ± SE, *$p < 0.05$ vs. static; #$p<0.05$ between samples; N=3).

3.3.5 Syndecan-1 silencing blocks the shear-stress-induced heparan sulfate expression

Having demonstrated that there is a high correlation between the quantitative expression of heparan sulfate and syndecan-1 under distinct hemodynamic environment, we next tested the hypothesis that the atheroprotective shear-tress-induced heparan sulfate expression is mediated through syndecan-1 regulation. To this end, HUVEC were transfected with syndecan-1 shRNA to silence syndecan-1 expression and compared with cells transfected with control (non-target) shRNA under both static (no flow) or exposed to atheroprotective shear stress for 7 days. As seen in Fig. 3-5, the use of Syndecan-1 shRNA led to an averaged 78.6% syndecan-1 silencing under atheroprotective shear stress (Figs. 3-5A and 3-5B). Notably, the atheroprotective shear-stress-mediated increase in expression of cell surface heparan sulfate was completely abolished by suppressing syndecan-1 expression. These data demonstrates that syndecan-1 is the major heparan sulfate carrier regulated by atheroprotective flow and that syndecan-1 up-regulation is a critical mechanism behind the atheroprotective shear-stress-induced heparan sulfate expression.

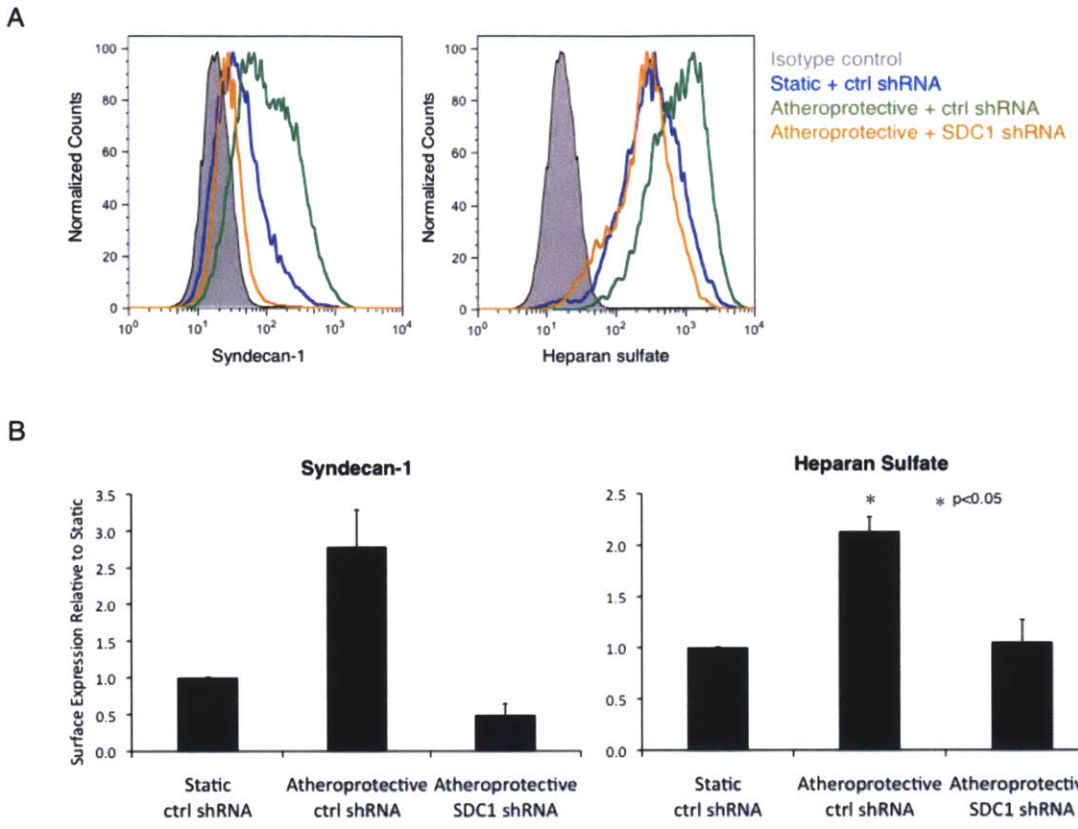

Fig. 3-5. Silencing syndecan-1 expression in endothelial cells blocks atheroprotective flow-induced heparan sulfate expression. A) Representative flow cytometry histogram of syndecan-1 (*Left*) and heparan sulfate (*Right*) surface expression in cells treated with control (non-targeting) or syndecan-1 (SDC1) shRNA and then maintained under static conditions or exposed to atheroprotective flow for 7 days. B) Quantitative analysis of the flow cytometry data from three independent experiments (*$p < 0.05$; means ± SE; N=3).

3.4 Discussion and Conclusions

The abundance of endothelial glycocalyx has been associated with the vasoprotective phenotype of the endothelium (7, 8, 33, 54). Though there are many studies investigating the numerous functions of the EGL, few focuses on how the EGL expression is regulated. The data presented here demonstrate that the expression of some components of the EGL is directly regulated by specific shear stress waveforms. In particular, we found that the expression of heparan sulfate, the major GAG of the EGL, is up-regulated after prolonged atheroprotective shear stress treatment, and down-regulated after exposed to the atheroprone waveform. Moreover, we documented that heparan sulfate is present at the apical surface in cultured endothelial cells exposed to the atheroprotective waveform. Besides heparan sulfate, hyaluronic acid expression is also induced by the atheroprotective waveform, establishing that the hemodynamic shear stress waveform found in atherosclerosis-resistant regions is a direct cause of observed abundant EGL expression.

In the past ten years, several studies have used *in vitro* cultured endothelial cells to gain a better understanding of the EGL. Potter *et al.* (38) and Chappell *et al.* (6) have recently reported that the glycocalyx structure observed *in vivo* is absent *in vitro*, questioning the conclusion derived from experiments using *in vitro* models. Potter *et al.* used microparticle image velocimetry to measure EGL thickness and found that the glycocalyx in mouse cremaster muscle venules (around 520 nm) is much more abundant than either cultured BAEC (20 nm) or cultured HUVEC (30 nm). Their data are further supported by electron microscopy studies by Chappell *et al.*, who measured the thickness of the glycocalyx in *ex vivo* human umbilical vein endothelium to be 878 nm and that of cultured HUVEC to be 29 nm. However, a most recent study by Ebong *et al.* (13) argued that these *in vitro* estimations may be flawed due to artifact from alcohol dehydration, substrates used to coat the surface, or media supplements of high concentration dextran (4%). Importantly, our data indicated the EGL expression for HUVEC under static conditions is irregular and discontinuous, suggesting that the EGL distribution is highly heterogeneous and, depending on the area chosen for measurement, its measured dimensions (e.g., thickness) can be dramatically different.

Several earlier studies have indicated that shear stress may play an important role in regulating EGL expression: in endothelial cells subjected to flow, GAG synthesis was increased,

hyaluronic acid incorporation into EGL was induced, and hyaluronan synthase 2 expression was upregulated (2, 19, 30). Our study has further shown that 7-days exposure to the atheroprotective shear stress waveform is necessary for the high and uniform apical cell surface expression of some components of the glycocalyx, such as heparan sulfate and hyaluronic acid in cultured endothelial cells.

Having demonstrated that the atheroprotective shear stress enhances heparan sulfate expression, an interesting question arises, what is the mechanism behind this process? The abundance of the EGL is controlled by several factors: 1) the abundance of its protein carriers; 2) the expression and activity of enzymes responsible for biosynthesis of GAGs; 3) degradation following endocytosis; and 4) the expression and activity of matrix metalloprotease responsible for shedding of the glycoproteins. Here we report on some of these possible mechanisms that influence the cell surface expression of heparan sulfate. We measured the mRNA and protein expression of all HUVEC heparan sulfate anchors under static and different flow conditions and found syndecan-1 to be uniquely up-regulated by the atheroprotective waveform. Furthermore, silencing of syndecan-1 under flow results in the suppression of shear-stress-induced heparan sulfate expression, suggesting that among all heparan sulfate proteoglycans, syndecan-1 plays a critical role in regulating the cell surface expression of heparan sulfate under atheroprotective shear stress. On the other hand, we did not find the mRNA expression of EXT1 and EXT2, the two key enzymes responsible for heparan sulfate biosynthesis, to be shear-stress-dependent. Currently, we cannot rule out that the enzymatic activities of these two proteins are regulated through post-translational modifications leading to an increase in their specific activities, nor a role for changes in endocytic degradation in controlling the surface expression of heparan sulfate.

Shedding of the proteoglycans is catalyzed by the matrix metalloproteinase (MMP) family proteins. Four members from this family, MMP1, MMP2, MMP3, and MMP9, have been shown to take parts in shedding of the glycocalyx protein carriers (4). Magid *et al.* have demonstrated that the activity of MMP9 promoter and protein level of Tissue Inhibitor of MMP1 (TIMP-1) can be differentially regulated by shear stress (29). However, because of limited understanding of the role of shear stress in post-translational regulation of members of MMPs and TIMPs, we cannon conclude whether MMPs plays an important role behind shear-stress-induced expression or suppression of components of the glycocalyx. Investigating the

relationship between shear stress and glycocalyx shedding may be a critical step for our understanding of the dynamics of glycocaclyx expression.

As we have established the cause-effect relationship between shear stress and the expression of the components of the EGL, the next question to ask is if this change in EGL expression contributes to the atheroprone or atheroprotective behaviors observed *in vivo* in different ways. First, as previously discussed, the EGL may bind and thus increase the local concentration of some macromolecules. One of such molecule is the extracellular superoxide dismutase (EC-SOD), an enzyme responsible for controlling the redox state of the cells. The C class EC-SOD has been shown to bind tightly to the EGL. This class of EC-SOD possesses a protein domain containing many positively charged amino acids facilitating its binding to the negatively charged heparan sulfate (21, 44). By providing more binding sites to the EC-SOD, an increased EGL expression may help reducing the oxidative stress to the endothelium.

The second impact of a more abundant EGL expression is increased sensitivity to shear stress. Previously, theoretical models have established that the fluid shear stress acting on the endothelium by flowing blood is fully dissipated in the glycocalyx layer and the apical membrane essentially is not expose to shear stress forces. To deliver the force into the cell, the stress is transmitted by the glycocalyx to the cell cytoskeleton through proteoglycans such as syndecans or glypicans (51, 59). In this scenario, the heparan sulfate acts as an amplifier that increases the surface area for the core protein carriers exposed to shear stress. These models predict that if heparan sulfate is removed, the ability of the cell to sense the fluid shear stress will be significantly impaired. Indeed, it is evident from previous experimental data that when heparan sulfate is removed through enzymatic treatment, the endothelial cell can no longer respond to the mechanical stimuli by modulating the proliferation and migration rate, reorganizing the cytoskeleton, and aligning to the direction of the flow (32, 53, 60). Some studies also reported that heparan sulfate and hyaluronic acid are also important for flow-induced NO production, and enzymatic removal of these two glycosaminoglycans attenuate this effect (14, 35). However, this view has been challenged by a recent paper showing that suppression of flow-mediate NO production by enzymatic removal of heparan sulfate can be rescued by addition of tempol, a radical scavenger. These data suggest that increased NO production under flow is contributed by heparan sulfate hosting the ecSOD and, thereby, increasing the NO half-life, rather than by heparan sulfate acting as a mechanosensor. This study, on the other hand,

confirmed that hyalurnoic acid is indeed a mechanosensor for NO production (23). These theoretical models and experimental data suggest the presence of EGL is critical to the activation of shear stress-regulated mechanotransduction pathways.

The third impact of a thicker EGL is prevention of leukocyte adhesion, an early step in atherogenesis. Constantinescu *et al.* (7, 8) demonstrated that addition of Ox-LDL or enzymatic removal of heparan sulfate in mouse cremaster venules induces leukocyte adhesion. Perfusing the venules with heparan sulfate or heparin, however, reverses this effect. van den Berg *et al.* further showed the accumulation of Ox-LDL in the intimal layer beneath the EGL is in fact inversely correlated to the EGL abundance (54). Mulivor and Lipowsky *et al.* (33) also found that chemoattractant fMLP leads to glycocalyx shedding and leukocytes attachment in the rat right internal juguar vein due to MMP activation. Adding doxycycline, a MMP inhibitor, attenuates this process. Some investigators have attributed these experimental observations to steric hindrance (41). It is argued that the length of the cell adhesion molecules such as P-selectin (around 38 nm) is significantly small compared to the thickness of the glycocalyx (around 400 to 4000 nm). Therefore, the heparan sulfate and other GAGs shield the cell adhesion molecules from interacting with the nearby leukocytes (41). One study supporting this idea observed that when P-selectin length is shortened by decreasing the number of consensus repeats, it is less likely for culture cells to recruit neutrophils (37). Several other studies can further be used in interpreting our data to suggest that syndecan-1 might be the most prominent heparan sulfate anchor and play the most important role in shear-stress-induced heparan sulfate expression. Previously studies have demonstrated that Syndecan-1 knockout mice are healthy under normal condition, but a more dramatic pathological phenotype is shown after being challenged with pathological stimuli (52). For example, when myocardial infarction was induced in syndecan-1 knockout mice by permanent ligation of the left coronary artery, enhanced leukocyte adhesion and transendothelial migration were observed (57). Since plasma-B-cell is the only type of leukocyte presenting syndecan-1 under normal condition, syndecan-1 expression on endothelial cells may inhibit leukocyte adhesion (52). Collectively, these studies provide evidence that a thicker EGL layer may be a stronger steric protection against leukocyte attachment.

In conclusion, this study establishes a cause-effect relationship between distinct shear stress waveforms and the expression of components of the endothelial glycocalyx, revealing a

specific environmental cue that may be responsible for the previously documented relationship between the glycocalyx and atheroprotection.

3.5 References

1. **Abrahamsson T, Brandt U, Marklund SL, and Sjöqvist PO.** Vascular bound recombinant extracellular superoxide dismutase type C protects against the detrimental effects of superoxide radicals on endothelium-dependent arterial relaxation. *Circ Res* 70: 264-271, 1992.
2. **Arisaka T, Mitsumata M, Kawasumi M, Tohjima T, Hirose S, and Yoshida Y.** Effects of shear stress on glycosaminoglycan synthesis in vascular endothelial cells. *Ann N Y Acad Sci* 748: 543-554, 1995.
3. **Bernfield M, Götte M, Park PW, Reizes O, Fitzgerald ML, Lincecum J, and Zako M.** Functions of cell surface heparan sulfate proteoglycans. *Annu Rev Biochem* 68: 729-777, 1999.
4. **Birkedal-Hansen H, Moore WG, Bodden MK, Windsor LJ, Birkedal-Hansen B, DeCarlo A, and Engler JA.** Matrix metalloproteinases: a review. *Crit Rev Oral Biol Med* 4: 197-250, 1993.
5. **Carmeliet P.** Mechanisms of angiogenesis and arteriogenesis. *Nat Med* 6: 389-395, 2000.
6. **Chappell D, Jacob M, Paul O, Rehm M, Welsch U, Stoeckelhuber M, Conzen P, and Becker BF.** The glycocalyx of the human umbilical vein endothelial cell: an impressive structure ex vivo but not in culture. *Circ Res* 104: 1313-1317, 2009.
7. **Constantinescu AA, Vink H, and Spaan JA.** Elevated capillary tube hematocrit reflects degradation of endothelial cell glycocalyx by oxidized LDL. *Am J Physiol Heart Circ Physiol* 280: H1051-1057, 2001.
8. **Constantinescu AA, Vink H, and Spaan JA.** Endothelial cell glycocalyx modulates immobilization of leukocytes at the endothelial surface. *Arterioscler Thromb Vasc Biol* 23: 1541-1547, 2003.
9. **Dahlbäck B.** Blood coagulation. *Lancet* 355: 1627-1632, 2000.
10. **Dai G, Kaazempur-Mofrad MR, Natarajan S, Zhang Y, Vaughn S, Blackman BR, Kamm RD, García-Cardeña G, and Gimbrone MA.** Distinct endothelial phenotypes evoked by arterial waveforms derived from atherosclerosis-susceptible and -resistant regions of human vasculature. *Proc Natl Acad Sci USA* 101: 14871-14876, 2004.
11. **Devaraj S, Yun JM, Adamson G, Galvez J, and Jialal I.** C-reactive protein impairs the endothelial glycocalyx resulting in endothelial dysfunction. *Cardiovasc Res* 84: 479-484, 2009.
12. **Diamond SL, Eskin SG, and McIntire LV.** Fluid flow stimulates tissue plasminogen activator secretion by cultured human endothelial cells. *Science* 243: 1483-1485, 1989.
13. **Ebong EE, Macaluso FP, Spray DC, and Tarbell JM.** Imaging the endothelial glycocalyx in vitro by rapid freezing/freeze substitution transmission electron microscopy. *Arterioscler Thromb Vasc Biol* 31: 1908-1915, 2011.
14. **Florian JA, Kosky JR, Ainslie K, Pang Z, Dull RO, and Tarbell JM.** Heparan sulfate proteoglycan is a mechanosensor on endothelial cells. *Circ Res* 93: e136-142, 2003.
15. **Fransson LA, Belting M, Cheng F, Jonsson M, Mani K, and Sandgren S.** Novel aspects of glypican glycobiology. *Cell Mol Life Sci* 61: 1016-1024, 2004.
16. **Garcia-Cardena G, Comander J, Anderson KR, Blackman BR, and Gimbrone MA, Jr.** Biomechanical activation of vascular endothelium as a determinant of its functional phenotype. *Proc Natl Acad Sci U S A* 98: 4478-4485, 2001.
17. **Gimbrone MA, Jr.** Endothelial dysfunction and atherosclerosis. *J Card Surg* 4: 180-183, 1989.
18. **Gouverneur M, Berg B, Nieuwdorp M, Stroes E, and Vink H.** Vasculoprotective properties of the endothelial glycocalyx: effects of fluid shear stress. *J Intern Med* 259: 393-400, 2006.
19. **Gouverneur M, Spaan JA, Pannekoek H, Fontijn RD, and Vink H.** Fluid shear stress stimulates incorporation of hyaluronan into endothelial cell glycocalyx. *Am J Physiol Heart Circ Physiol* 290: H458-452, 2006.
20. **Janczyk P, Hansen S, Bahramsoltani M, and Plendl J.** The glycocalyx of human, bovine and murine microvascular endothelial cells cultured in vitro. *J Electron Microsc (Tokyo)* 59: 291-298, 2010.
21. **Karlsson K, and Marklund SL.** Extracellular superoxide dismutase in the vascular system of mammals. *Biochem J* 255: 223-228, 1988.
22. **Ku DN, Giddens DP, Zarins CK, and Glagov S.** Pulsatile flow and atherosclerosis in the human carotid bifurcation. Positive correlation between plaque location and low oscillating shear stress. *Arterioscler Thromb Vasc Biol* 5: 293-302, 1985.
23. **Kumagai R, Lu X, and Kassab GS.** Role of glycocalyx in flow-induced production of nitric oxide and reactive oxygen species. *Free Radic Biol Med* 47: 600-607, 2009.

24. **Langille BL, Graham JJ, Kim D, and Gotlieb AI**. Dynamics of shear-induced redistribution of F-actin in endothelial cells in vivo. *Arterioscler Thromb* 11: 1814-1820, 1991.
25. **Levesque MJ, Nerem RM, and Sprague EA**. Vascular endothelial cell proliferation in culture and the influence of flow. *Biomaterials* 11: 702-707, 1990.
26. **Lokeshwar VB**. Differences in hyaluronic acid-mediated functions and signaling in arterial, microvessel and vein-derived human endothelial cells. *Journal of Biological Chemistry* 1-9, 2000.
27. **Luscher TF, Richard V, Tschudi M, Yang ZH, and Boulanger C**. Endothelial control of vascular tone in large and small coronary arteries. *J Am Coll Cardiol* 15: 519-527, 1990.
28. **Luscinskas FW, and Gimbrone MA**. Endothelial-dependent mechanisms in chronic inflammatory leukocyte recruitment. *Annu Rev Med* 47: 413-421, 1996.
29. **Magid R, Murphy TJ, and Galis ZS**. Expression of matrix metalloproteinase-9 in endothelial cells is differentially regulated by shear stress. Role of c-Myc. *J Biol Chem* 278: 32994-32999, 2003.
30. **Maroski J, Vorderwulbecke BJ, Fiedorowicz K, Da Silva-Azevedo L, Siegel G, Marki A, Pries AR, and Zakrzewicz A**. Shear stress increases endothelial hyaluronan synthase 2 and hyaluronan synthesis especially in regard to an atheroprotective flow profile. *Exp Physiol* 96: 977-986, 2011.
31. **Mertens G, Cassiman JJ, Van den Berghe H, Vermylen J, and David G**. Cell surface heparan sulfate proteoglycans from human vascular endothelial cells. Core protein characterization and antithrombin III binding properties. *J Biol Chem* 267: 20435-20443, 1992.
32. **Moon JJ, Matsumoto M, Patel S, Lee L, Guan JL, and Li S**. Role of cell surface heparan sulfate proteoglycans in endothelial cell migration and mechanotransduction. *J Cell Physiol* 203: 166-176, 2005.
33. **Mulivor A, and Lipowsky H**. Inhibition of Glycan Shedding and Leukocyte-Endothelial Adhesion in Postcapillary Venules by Suppression of Matrixmetalloprotease Activity with Doxycycline. *UMIC* 1-10, 2009.
34. **Osborn EA, Rabodzey A, Dewey CF, Jr., and Hartwig JH**. Endothelial actin cytoskeleton remodeling during mechanostimulation with fluid shear stress. *Am J Physiol Cell Physiol* 290: C444-452, 2006.
35. **Pahakis MY, Kosky JR, Dull RO, and Tarbell JM**. The role of endothelial glycocalyx components in mechanotransduction of fluid shear stress. *Biochem Biophys Res Commun* 355: 228-233, 2007.
36. **Parmar KM, Larman HB, Dai G, Zhang Y, Wang ET, Moorthy SN, Kratz JR, Lin Z, Jain MK, Gimbrone MA, and García-Cardeña G**. Integration of flow-dependent endothelial phenotypes by Kruppel-like factor 2. *J Clin Invest* 116: 49-58, 2006.
37. **Patel KD, Nollert MU, and McEver RP**. P-selectin must extend a sufficient length from the plasma membrane to mediate rolling of neutrophils. *J Cell Biol* 131: 1893-1902, 1995.
38. **Potter DR, and Damiano ER**. The Hydrodynamically Relevant Endothelial Cell Glycocalyx Observed In Vivo Is Absent In Vitro. *Circ Res* 102: 770-776, 2008.
39. **Potter DR, Jiang J, and Damiano ER**. The Recovery Time Course of the Endothelial Cell Glycocalyx In Vivo and Its Implications In Vitro. *Circ Res* 104: 1318-1325, 2009.
40. **Qiao D, Meyer K, Mundhenke C, Drew SA, and Friedl A**. Heparan sulfate proteoglycans as regulators of fibroblast growth factor-2 signaling in brain endothelial cells. Specific role for glypican-1 in glioma angiogenesis. *J Biol Chem* 278: 16045-16053, 2003.
41. **Reitsma S, Slaaf DW, Vink H, van Zandvoort MA, and oude Egbrink MG**. The endothelial glycocalyx: composition, functions, and visualization. *Pflugers Arch* 454: 345-359, 2007.
42. **Remuzzi A, Dewey CF, Jr., Davies PF, and Gimbrone MA, Jr.** Orientation of endothelial cells in shear fields in vitro. *Biorheology* 21: 617-630, 1984.
43. **Rubanyi GM, Romero JC, and Vanhoutte PM**. Flow-induced release of endothelium-derived relaxing factor. *Am J Physiol* 250: H1145-1149, 1986.
44. **Sandstrom J, Carlsson L, Marklund SL, and Edlund T**. The heparin-binding domain of extracellular superoxide dismutase C and formation of variants with reduced heparin affinity. *J Biol Chem* 267: 18205-18209, 1992.
45. **Savani RC, Cao G, Pooler PM, Zaman A, Zhou Z, and DeLisser HM**. Differential involvement of the hyaluronan (HA) receptors CD44 and receptor for HA-mediated motility in endothelial cell function and angiogenesis. *J Biol Chem* 276: 36770-36778, 2001.
46. **Secomb TW, Hsu R, and Pries AR**. Effect of the endothelial surface layer on transmission of fluid shear stress to endothelial cells. *Biorheology* 38: 143-150, 2001.
47. **Shyy YJ, Hsieh HJ, Usami S, and Chien S**. Fluid shear stress induces a biphasic response of human monocyte chemotactic protein 1 gene expression in vascular endothelium. *Proc Natl Acad Sci U S A* 91: 4678-4682, 1994.

48. **Squire JM, Chew M, Nneji G, Neal C, Barry J, and Michel C**. Quasi-periodic substructure in the microvessel endothelial glycocalyx: a possible explanation for molecular filtering? *J Struct Biol* 136: 239-255, 2001.
49. **Stevens AP, Hlady V, and Dull RO**. Fluorescence correlation spectroscopy can probe albumin dynamics inside lung endothelial glycocalyx. *Am J Physiol Lung Cell Mol Physiol* 293: L328-335, 2007.
50. **Tarbell JM, and Pahakis MY**. Mechanotransduction and the glycocalyx. *J Intern Med* 259: 339-350, 2006.
51. **Tarbell JM, Weinbaum S, and Kamm RD**. Cellular fluid mechanics and mechanotransduction. *Ann Biomed Eng* 33: 1719-1723, 2005.
52. **Teng YH, Aquino RS, and Park PW**. Molecular functions of syndecan-1 in disease. *Matrix Biol* 31: 3-16, 2012.
53. **Thi MM, Tarbell JM, Weinbaum S, and Spray DC**. The role of the glycocalyx in reorganization of the actin cytoskeleton under fluid shear stress: a "bumper-car" model. *Proc Natl Acad Sci USA* 101: 16483-16488, 2004.
54. **van den Berg BM, Spaan JA, and Vink H**. Impaired glycocalyx barrier properties contribute to enhanced intimal low-density lipoprotein accumulation at the carotid artery bifurcation in mice. *Pflugers Arch* 457: 1199-1206, 2009.
55. **van den Berg BM, Spaan JAE, Rolf TM, and Vink H**. Atherogenic region and diet diminish glycocalyx dimension and increase intima-to-media ratios at murine carotid artery bifurcation. *Am J Physiol Heart Circ Physiol* 290: H915-920, 2006.
56. **Vanderlaan PA**. Site Specificity of Atherosclerosis: Site-Selective Responses to Atherosclerotic Modulators. *Arterioscler Thromb Vasc Biol* 24: 12-22, 2004.
57. **Vanhoutte D, Schellings MW, Gotte M, Swinnen M, Herias V, Wild MK, Vestweber D, Chorianopoulos E, Cortes V, Rigotti A, Stepp MA, Van de Werf F, Carmeliet P, Pinto YM, and Heymans S**. Increased expression of syndecan-1 protects against cardiac dilatation and dysfunction after myocardial infarction. *Circulation* 115: 475-482, 2007.
58. **Vink H, and Duling BR**. Identification of distinct luminal domains for macromolecules, erythrocytes, and leukocytes within mammalian capillaries. *Circ Res* 79: 581-589, 1996.
59. **Weinbaum S, Zhang X, Han Y, Vink H, and Cowin SC**. Mechanotransduction and flow across the endothelial glycocalyx. *Proc Natl Acad Sci U S A* 100: 7988-7995, 2003.
60. **Yao Y, Rabodzey A, and Dewey CF**. Glycocalyx modulates the motility and proliferative response of vascular endothelium to fluid shear stress. *Am J Physiol Heart Circ Physiol* 293: H1023-1030, 2007.

3.6 Appendix

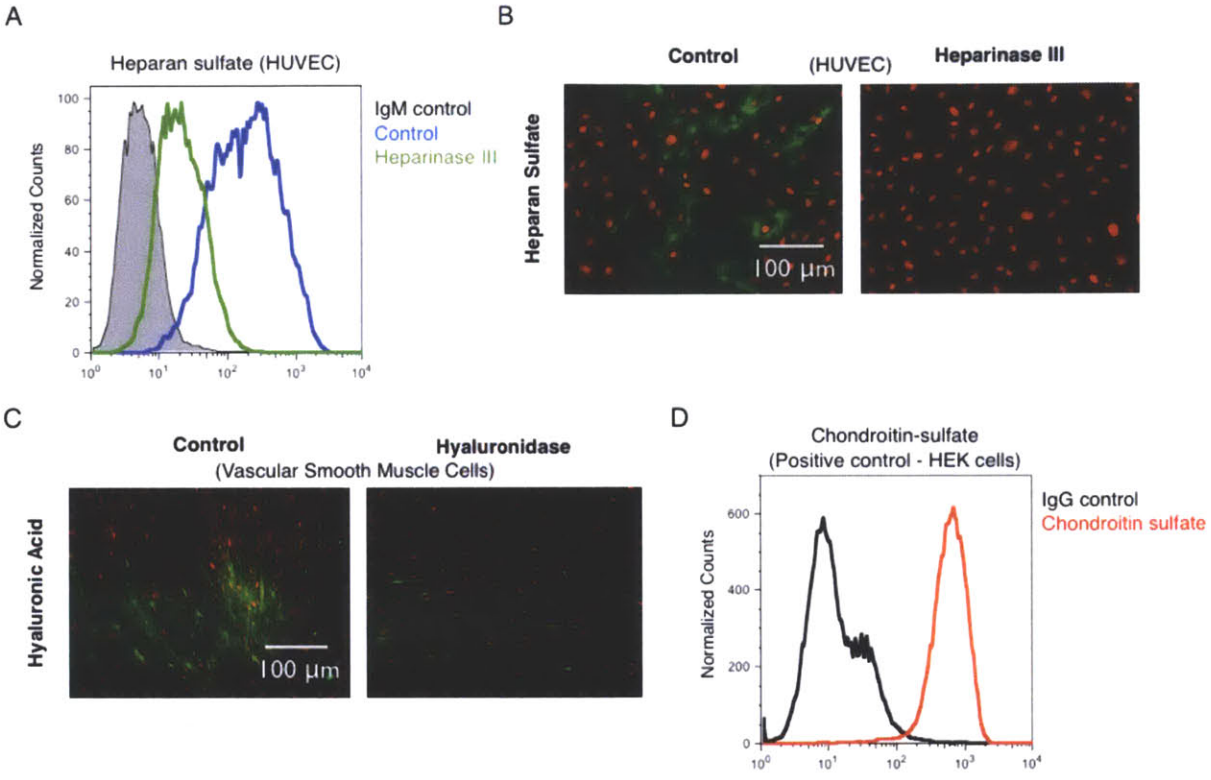

Validation of heparan sulfate, hyaluronic acid, and chondroitin sulfate staining: A) Flow cytometry histogram of heparan sulfate expression on HUVEC treated with vehicle (PBS) or Heparanase III (50 mU/mL, Ibex Technologies) for 10 minutes. B) Immunoflourescence microscopy image of cell surface heparan sulfate in the previous experiment. Heparan sulfate is shown in green, and nucleus (DAPI) is shown in red. C) Representative immunoflourescence microscopy image of cell surface hyaluronic acid on vascular smooth muscle cells treated with vehicle (PBS) or Hyaluronidase (50 U/mL, Sigma-Aldrich) for 1 hour. Hyaluronic acid is shown in green, and nucleus (DAPI) is shown in red. D) Flow cytometry histogram of chondroitin sulfate expression on HEK293 cells as a positive control.

Chapter 4: Bridging the Endothelial Glycocalyx to Atheroprotection and NO Production

4.1 Introduction

In the previous chapter, we have established a cause-effect relationship that distinct hemodynamic shear stress waveforms regulate the expression of components of the endothelial glycocalyx. In this chapter, we wish to further bridge the expression of the endothelial glycocalyx layer (EGL) to protection against atherosclerosis and shear-stress-induced NO production. To connect the EGL to atheroprotection, we suppressed the surface expression of heparan sulfate through a siRNA approach and measured how the absence of heparan sulfate affects leukocyte adhesion. To link the EGL to NO production, we silenced syndecan-1 and observe whether it changes shear-stress-induced expression of eNOS and its two important transcriptions factors – KLF2 and KLF4. We also tested, inversely, whether over-expressing KLF2 affects syndecan-1 and heparan sulfate expression. These experiments provide useful information that allows us to blueprint the next sets of experiments that are required to advance our understanding of the glycocalyx and shear-stress-induced NO production.

4.2 Material and Methods

General

The protocols regarding endothelial cell culture, hemodynamic shear stress *in vitro* system, shRNA experiments, FACS analysis, RNA isolation / quantitative PCR analysis, and statistics, were as described in Chapter 3.

siRNA-mediated Gene Silencing

HUVECs were plated at a density of 30,000 cells/cm^2 and cultured in the HUVEC growth medium 16 hours before transfection to reach 60% confluency. The sequences of human EXT1 siRNA (30 nM) were: 5′-GGAGC UGCUAUUUACCACAAAUAUU-3′ (sense) and 5′-AAUAUUUGUGGUAAAUAGC AGCUCC-3′ (antisense). For transfection, siRNA was firstly diluted with Opti-MEM reduced serum medium (Invitrogen). Concomitantly, oligofectamine (Invitrogen) was diluted with Opti-MEM and incubated for 5 minutes at room temperature. The siRNA and Oligofectamine solutions were then mixed and incubated for another 15 minutes. The HUVEC were washed twice with Opti-MEM and added with Oligofectamine-siRNA complex solution. Cells were incubated at 37°C for 6 hours, and then regular HUVEC growth medium was added (without antibiotics).

Leukocyte Adhesion Assay

Leukocyte attachment was measured using an established leukocyte attachment assay (3, 7). One million HL-60 cells pre-stained with CellTracker Orange (Invitrogen) were added to vehicle (PBS) or IL-1β (0.1 unit/mL, 4 hours) treated HUVEC. The cells were placed onto a horizontal rotator at 60 rpm at room temperature for 10 minutes. The unattached HL-60 cells were removed through gently washing the cells three times with PBS. The attached HL-60 was visualized using a fluorescent microscope. After imaging, the cells were lysed in the lysis buffer (0.1% NaOH, 0.01% sodium dodecyl sulfate) to allow quantification using a spectrophotometer (SpectraMax M3, Molecular Device, Sunnyvale, CA).

Adenoviral-mediated Infection

For KLF2 over-expression experiments, HUVEC at 80 – 90% confluency were infected with either Ad-GFP (Harvard Gene Therapy Initiative Core) or Ad-mKLF2-GFP (made by the García-Cardeña lab) at MOI=10. The adenoviral particles were incubated with the cells for 48 hours or 72 hours before the viral particles were washed away with PBS and HUVEC surface expression of heparan sulfate and syndecan-1 were assessed with FACS.

4.3 Results

4.3.1 Suppression of heparan sulfate expression by EXT1 siRNA

Knowing that the glycocalyx is differentially expressed under static and specific shear stress conditions, we developed an efficient way to silence the individual glycosaminoglycan of the glycoclayx without disturbing the anchored proteins. The genetic target we selected for the siRNA-based approach is EXT1, whose protein product forms a dimer with EXT2 protein and is responsible for heparan sulfate chain elongation, a critical step for heparan sulfate biosynthesis (5). Fig. 4-1A demonstrates the effectiveness of this approach. Heparan sulfate surface expression of cells pretreated with EXT1 siRNA versus control siRNA is almost completely suppressed even 96 hours after adding siRNA, suggesting EXT1 siRNA as a useful tool to study the function of glycocalyx.

4.3.2 Increase in leukocyte adhesion for endothelial cells treated with EXT1 siRNA

Having shown that the glycocalyx is significantly more expressed under atheroprotective condition, we hypothesized that this athero-resistant phenotype is established through glycocalyx acting as a physical protection barrier that prevents leukocyte adhesion, an early sign of atherosclerotic plaque formation. To test this hypothesis, we suppressed the expression of heparan sulfate via EXT1 siRNA. The siRNA silencing is followed by treatment with IL-1β (0.1 unit/mL) for 4 hours, then leukocyte adhesion assay. The data shows that when heparan-sulfate expression is suppressed by EXT1 siRNA, a higher number of leukocytes attached to both vehicle (PBS) treated or IL-1β activated endothelial cells (Figs. 4-1B, 4-1C). These data indicate that the EGL could act as a physical barrier against leukocyte adhesion.

4.3.3 Silencing of syndecan-1 does not affect shear-stress-induced KLF2, KLF4, or eNOS expression

Having established in our *in vitro* model that the EGL plays a role in protection against leukocyte adhesion, we further investigated the role of the EGL as a mechanosensor for shear-stress-

induced NO production. In chapter 3, we showed that heperan sulfate and its anchored protein, syndecan-1, are both much more expressed under atheroprotective flow condition. This observation leads to our hypothesis that the heparan-sulfate / syndecan-1 pair conducts flow-mediated mechanotranduction and leads to activation of signaling pathways that up-regulate eNOS gene expression. To test this hypothesis, HUVEC were transfected with control (non-target) shRNA or syndecan-1 shRNA (to silence syndecan-1 expression and atheroprotective-flow-induced heparan sulfate expression), and then exposed to atheroprotective shear stress for 7 days. After the 7-days flow exposure, RNA expressions of KLF2, KLF4, and eNOS were measured. The data (Fig. 4-2) revealed that atheroprotective flow significantly induces KLF2, KLF4, and eNOS expression. However, syndecan-1 silencing does not affect the shear-stress-induced expression of these genes. The mechanism of how the endothelial glycocalyx regulates NO production remains to be discovered.

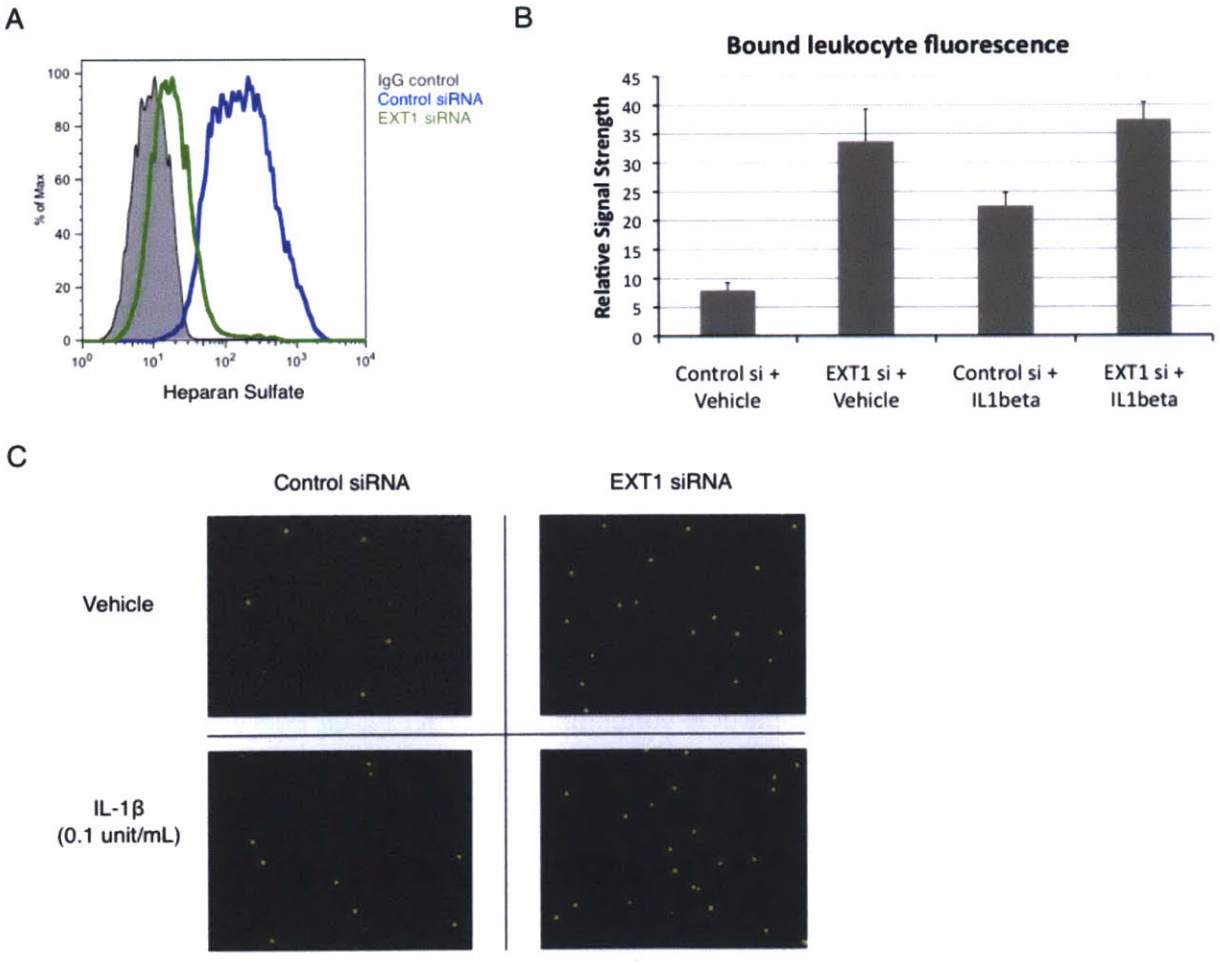

Fig. 4-1. EXT1 siRNA significantly suppresses the surface expression of heparan sulfate, and suppression of heparan sulfate surface expression increases leukocyte adhesion in endothelial cells treated with vehicle (PBS) or

activated with IL-1β (0.1 U/mL, 4 hr, 37°C). A) Representative flow cytometry histogram of heparan sulfate surface expression in endothelial cells 4 days after Control siRNA or EXT1 siRNA treatment. B) Quantitative analysis of HL-60 cells adhered to the monolayer from three independent experiments (*$p < 0.05$ vs. control siRNA + vehicle; #$p<0.05$ vs. control siRNA + IL-1β; N=3). C) Representative microscopic image of endothelial cells and bound HL-60 cells (yellow).

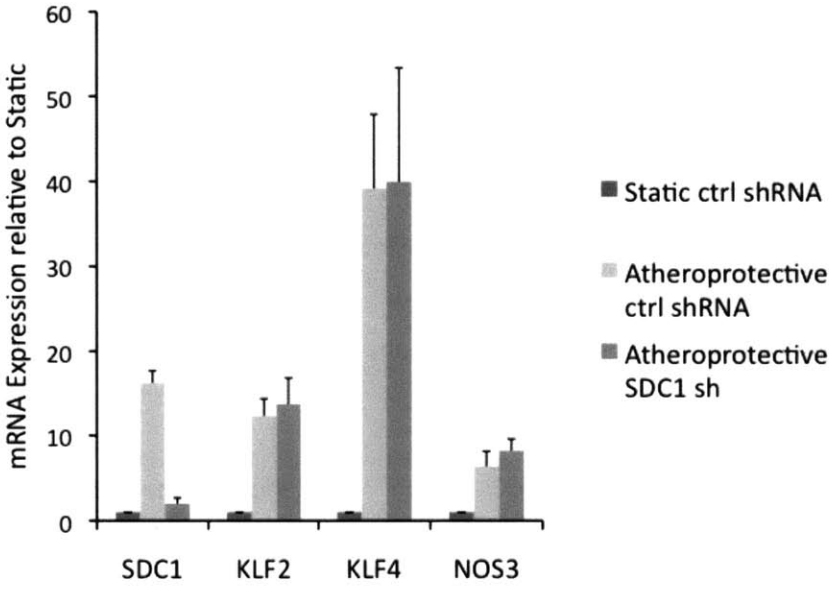

Fig. 4-2. Silencing syndecan-1 expression in endothelial cells does not affect atheroprotective-flow-induced KLF2, KLF4, and eNOS mRNA expression. The figure shows mRNA expression of syndecan-1 (SDC1), KLF2, KLF4, and NOS3 (eNOS) in cells treated with control (non-targeting) or syndecan-1 (SDC1) shRNA and then maintained under static conditions or exposed to atheroprotective flow for 7 days. (means ± SE; N=3).

4.3.4 Over-expression of KLF2 does not affect syndecan-1 or heparan sulfate expression

To further study whether there is a relationship between expression of KLF2 and components of the endothelial glycocalyx, we tested an alternative hypothesis that KLF2 plays an important role in up-regulating the expression of syndecan-1 and heparan sulfate. We tested this hypothesis by infecting HUVEC with adenoviral particle containing mouse KLF2-GFP to over-express KLF2. Surface expressions of syndecan-1 and heparan sulfate were assessed 48 hours and 72 hours after infection. Interestingly, these data demonstrated that KLF2 over-expression does not affect neither syndecan-1 nor heparan-sulfate expression, suggesting that KLF2 alone does not have a significant impact to glycocalyx expression.

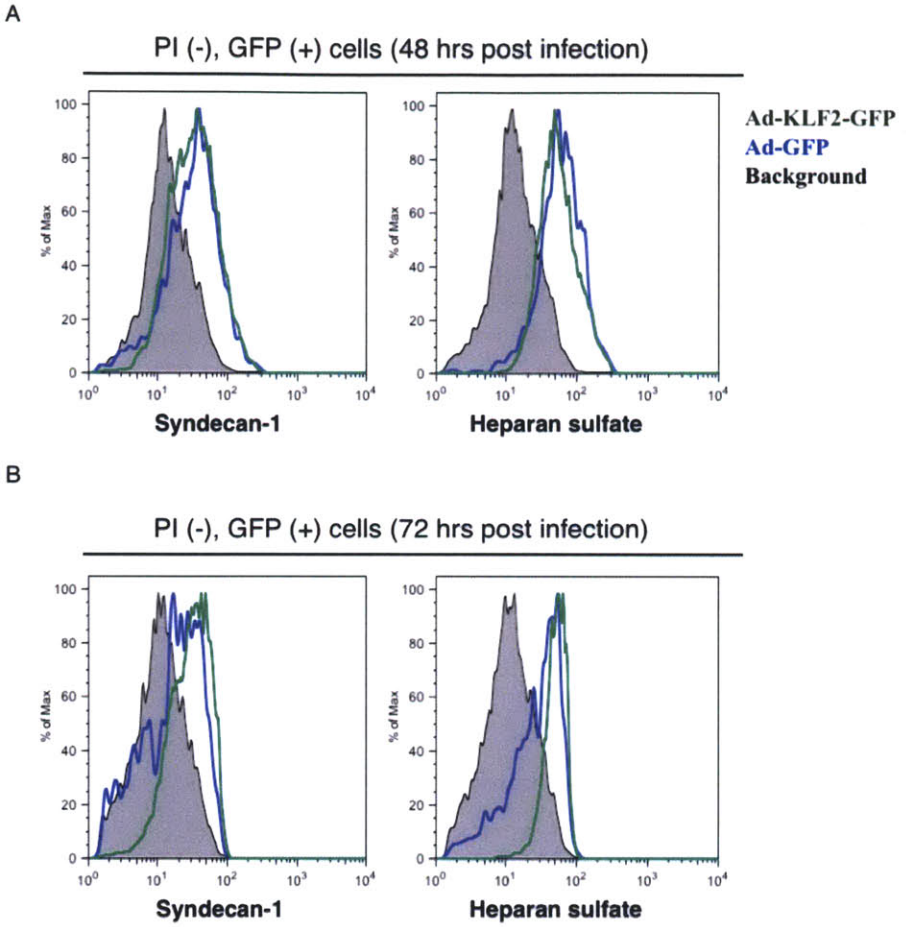

Fig. 4-3. Over-expressing KLF2 does not affect syndecan-1 or heparan sulfate expression. Flow cytometry histogram of cell surface syndecan-1 and heparan sulfate expression after being cultured with Ad-GFP or Ad-KLF2-GFP for A) 48 hours or B) 72 hours. Cells are gated to select for PI negative (alive) and GFP positive (virus infected) population.

4.4 Discussion and Conclusions

In the past decade, many researchers spent much effort on studying the function of the EGL. These experiments were typically done through enzymatic pre-treatment degrading the specific GAGs and then studying its effect under flow. In this chapter, we demonstrated an alternative siRNA approach by suppressing heparan sulfate biosynthesis, avoiding non-specific effect and allowing long-term study of the EGL function under shear stress conditions.

Heparan sulfate chain biosynthesis is a process involving multiple steps: First, a series of saccharides (N-acetylglucosaimne – glucuronic acid – galactose – galactose – xylose) are added onto the serine residue of the extracellular domain of syndecan or glypicans. Next, the elongation process starts with the polymerization reaction conducted by glycosyltransferase I, a protein dimer of exostosin-1 (EXT1) and exostosin-2 (EXT2). Finally, the elongated chain is deacetylated and sulfated by N-deacetylase/N-sulfotransferase (NDST). Previous experiments done by Busse *et al.* demonstrated that treating the HEK293 cells with EXT1 siRNA significantly decreases glycosyltransferase I activity and leads to a shorter heparan sulfate chain (1). Our results show that this EXT1 siRNA approach is equally efficient for HUVEC and can be used for *in vitro* study of the glycocalyx. The next question is if EXT1 siRNA can also be applied for *in vivo* study of the glycocalyx. It is known that mutation in both copies of the human EXT1 gene is lethal. Autosomal dominant mutation in EXT1 leads to hereditary multiple exostoses (HME) and osteochondroma (8). Similarly, homozygous EXT1 -/- knockout mice are embryonic lethal due to failure in gastrulation. Heterozygous EXT1 +/- mice have less than 50% heparan sulfate synthesis and may have shortened long bones (4). However, the vascular health of these heterozygous mice has not yet been assessed. In the future, it will be interesting to create endothelial specific EXT1 knockout mice to study the function of the glycocalyx *in vivo*.

In this chapter, EXT1 siRNA was used as a tool to study the effect of inhibiting heparan sulfate biosynthesis on leukocyte attachments. Suppressing heparan sulfate biosynthesis significantly decreases the cell surface expression of heparan sulfate and increases leukocyte attachments. The data from a control experiment showed that EXT1 siRNA does not induce inflammation response and up-regulation of cell adhesion molecules. Previously, Constantinescu *et al.* demonstrated that addition of Ox-LDL or enzymatic removal of mouse cremaster venules induces leukocyte adhesion. Perfusing the venules with heparan sulfate or heparin, however,

reverses this effect (2). Mulivor and Lipowsky *et al.* also found that chemoattractant fMLP leads to glycocalyx shedding and leukocytes attachment in the rat right internal juguar vein due to matrix metalloproteases (MMP) activation. Adding doxycycline, a MMP inhibitor, attenuates this process (6). These *in vivo* works and our *in vitro* study provide ample evidence that the overall integrity of the glycocalyx layer is critical for preventing leukocyte attachment.

Here we provide a theoretical explanation of the above-mentioned observations. We propose that while cell adhesion molecules increase the binding force between leukocytes and the endothelium, the glycocalyx layer acts as a spring repelling leukocytes from contacting the endothelial surface. In non-inflammatory state when there is few cell adhesion molecules expressed, this repulsion force is large enough to counter the adhesion force. However, under inflammatory condition when more cell adhesion molecules are expressed or the glycocalyx is compromised, the repulsion force is weaker than the adhesion force, resulting to leukocyte adhesion and trans-migration.

While the overall integrity of the glycocalyx is critical against leukocyte adhesion, its expression is tightly regulated by the specific shear stress waveform exposed to the endothelium. The data from this experiment indicates that the glycocalyx acts as a critical mediator between shear stress and atheroprotection.

One of the other mediator roles of the endothelial glycocalyx is acting as a mechano-sensor or mechano-amplifier. In our study, we also tested on the hypothesis that heparan-sulfate and its anchored protein syndecan-1 conduct flow-mediated mechanotranduction and lead to activation of signaling pathways that up-regulate eNOS gene expression. Even though the data is negative, it does not rule out several possibilities that the endothelial glycocalyx might play a role in shear-stress-induced nitric oxide production. One of such possibility is that the mechanotransduction pathways activated by the EGL regulates eNOS phosphorylation rather than eNOS transcription. It will be interesting in the future to silence individual components of the EGL and investigate how does it affect both the activating and inhibitory phosphorylation sites on eNOS under shear stress conditions. The second possibility is that silencing one individual component is insufficient: the EGL is a complex structure that even if one component is removed, the other components could still act as a functional mechano-sensor or mechano-amplifier. As silencing multiple genes at the same time is difficult, it might be necessary to first develop novel approaches to selectively remove multiple components of the endothelial

glycocalyx in order to advance our understanding of the mechanotransduction property of the glycocalyx.

On the other hand, our experiments also demonstrated that over-expressing KLF2 alone for 48 – 72 hours cannot promote syndecan-1 or heparan sulfate expression. It is possible that longer incubation time is required to observe a difference. It is also possible that activation of some other shear-stress-induced genes are required to act with KLF2 to co-promote endothelial glycoclayx expression. Finally, it is possible that glycocalyx production is completely independent of KLF2 expression.

In this chapter, we assessed several functional aspect of the endothelial glycocalyx. We have shown in our *in vitro* model that the EGL may play a role in protection against leukocyte adhesion. We also investigate one possible mechanism in which the endothelial glycocalyx regulates NO production and another mechanism in which endothelial glycocalyx expression is regulated. The data from these experiments can help us designing future experiments that will eventually bridge the pathways between the endothelial glycocalyx and shear-stress-mediated NO production.

4.5 References

1. **Busse M, Feta A, Presto J, Wilén M, Grønning M, Kjellén L, and Kusche-Gullberg M.** Contribution of EXT1, EXT2, and EXTL3 to heparan sulfate chain elongation. *J Biol Chem* 282: 32802-32810, 2007.
2. **Constantinescu AA, Vink H, and Spaan JA.** Endothelial cell glycocalyx modulates immobilization of leukocytes at the endothelial surface. *Arterioscler Thromb Vasc Biol* 23: 1541-1547, 2003.
3. **Gracia-Sancho J, Villarreal G, Zhang Y, Yu JX, Liu Y, Tullius SG, and García-Cardeña G.** Flow cessation triggers endothelial dysfunction during organ cold storage conditions: strategies for pharmacologic intervention. *Transplantation* 90: 142-149, 2010.
4. **Lin X.** Disruption of Gastrulation and Heparan Sulfate Biosynthesis in EXT1-Deficient Mice. *Dev Biol* 224: 299-311, 2000.
5. **McCormick C, Duncan G, Goutsos KT, and Tufaro F.** The putative tumor suppressors EXT1 and EXT2 form a stable complex that accumulates in the Golgi apparatus and catalyzes the synthesis of heparan sulfate. *Proc Natl Acad Sci USA* 97: 668-673, 2000.
6. **Mulivor A, and Lipowsky H.** Inhibition of Glycan Shedding and Leukocyte-Endothelial Adhesion in Postcapillary Venules by Suppression of Matrixmetalloprotease Activity with Doxycycline. *UMIC* 1-10, 2009.
7. **Parmar KM, Larman HB, Dai G, Zhang Y, Wang ET, Moorthy SN, Kratz JR, Lin Z, Jain MK, Gimbrone MA, and García-Cardeña G.** Integration of flow-dependent endothelial phenotypes by Kruppel-like factor 2. *J Clin Invest* 116: 49-58, 2006.
8. **SOLOMON L.** HEREDITARY MULTIPLE EXOSTOSIS. *Am J Hum Genet* 16: 351-363, 1964.

Chapter 5: Conclusions and Outlook

5.1 Summary of Findings

In this thesis, we constructed the first integrated model of shear-stress-induced NO production in endothelial cells. This system model captures the main events after the cells are exposed to fluid shear stress, describing the kinetics of all major pathways leading to eNOS activation, eNOS expression, and NO production. The integrated model is able to describe the experimentally observed change in NO production with time following the application of shear stress. This model can also be used to predict the specific effects to the system following interventional pharmacological or genetic changes. Importantly, this model reflects the up-to-date understanding of the NO system, providing a platform to aggregate information in an additive way. Unfortunately, the current model is still incomplete due to limitation of experimental data in several key pathways, including the KLF2 activation pathway and the pathways regulated by the endothelial glycocalyx.

To further improve the model, we conducted studies on the endothelial glycocalyx, seeking to establish the relationships between shear stress, glycocalyx expression, and atheroprotection. We first tested the hypothesis that the expression of components of the endothelial glycocalyx is differentially regulated by distinct hemodynamic environments. Our experiments revealed that heparan sulfate expression is higher and evenly distributed on the apical surface of endothelial cells exposed to the atheroprotective waveform, and is irregularly present in cells exposed to the atheroprone waveform. Furthermore, the expression of a heparan sulfate proteoglycan, syndecan-1, is also differentially regulated by the two waveforms, and its suppression mutes the atheroprotective-flow-induced cell surface expression of heparan sulfate. These data suggest that expression of components of the glycocalyx is regulated by the specific shear stress waveform and may be a novel mechanism behind flow-mediated atheroprotection

We further conducted several experiments to elucidate the functions of the endothelial glycocalyx and the mechanism of how the glycocalyx activates NO production. We have shown under static condition that there is increased leukocyte adhesion when heparan sulfate expression is suppressed by inhibiting its biosynthesis. Furthermore, we silenced syndecan-1 and measured how it affects KLF2, KLF4, and eNOS expression after 7 days of atheroprotective flow exposure. Even though expression of these transcription factors does not change under our tested

experimental conditions, it is possible that silencing multiple components of the glycocalyx is necessary to see an effect, or the endothelial glycocalyx affect other NO production mechanisms such as eNOS phosphosylration. Additional studies are required to understand the endothelial glycocalyx' function, downstream signaling pathways, and its connection to NO production.

5.2 Future Directions

The time of the graduate school is limited, but the knowledge to be discovered in the NO system and the endothelial glycocalyx seems infinite. I believe the following future experiments will be of great interests to investigators working on these fields:

- Assess whether flow-induced heparan sulfate expression leads to decrease in leukocyte adhesion. This can be achieved by suppressing shear-stress-induced heparan sulfate expression using SDC1 shRNA and conducting leukocyte adhesion assay after the cells are exposed to the atheroprotective flow for 7 days.
- Investigate how heparan-sulfate regulates NO production. One avenue is to suppress heparan sulfate expression through EXT1 siRNA or SDC1 shRNA and measure change in phosphorylation at various eNOS sites after onset of flow.
- Study the effect of syndecan-1/ heparan sulfate silencing on expression of vasoprotective genes. A gene expression microarray analysis can help us capturing all genes regulated by the endothelial glycocalyx under flow.
- Map signaling pathways down-stream of the endothelial glycocalyx. Once we know the set of genes regulated by the glycocalyx, it is possible to use bioinformatics tools to delineate the signaling pathways bridging the glycocalyx to those genes.
- Research the possible protective effect of syndecan-1 expression on the endothelium using endothelial-specific syndecan-1 knockout mice in a model of atherosclerosis.

As we increasingly understand the endothelium and the vascular system at the molecular level, I believe eventually we could use the systems biology approach to predict biology, and possibly develop therapeutics in a more rational, cost-effective, and efficient way.

"Much to learn you still have... This is just the beginning."

- Master Yoda

Star Wars: Episode II
Attack of the Clones (2002)